Study on Impurity Doped ZnO Terrace-truncated Nanocone Structures Grown by Advanced Spray Pyrolysis Deposition Technique

Doctoral Thesis

Study on Impurity Doped ZnO Terrace-truncated Nanocone Structures Grown by Advanced Spray Pyrolysis Deposition Technique.

Sameera Attanayake

Graduate School of Science and Technology

Department of Optoelectronics and Nanostructure Science

Shizuoka University

March 2019

I do hereby declare that the work reported in the thesis was exclusively carried out by me under the supervision of Prof. Kenji Murakami, Graduate School of Integrated Science and Technology, Shizuoka University. It describes the results of my own independent research except where due reference has been made in the text. No part of this thesis has been submitted earlier or concurrently for the same or any other degree.

This research work is dedicated to my beloved parents, Mr. Gunasekara Attanayake and Mrs. Sheela Attanayake.

Abstract

Investigations on semiconductor oxide materials, with high optical transmittance in the visible range and high electrical conductivity (Transparent conductive oxides - TCO), have gained the interest of researchers in last few decades. Due to their wide range of applications, still there is a great demand for new TCO materials. ZnO is known as an interesting semiconductor oxide material with unique physical and chemical properties such as direct wide band gap (3.37 eV), large exciting binding energy at room temperature (~60 meV), high thermal stability, radiation hardness, nontoxicity. In order to enhance the electrical conductivity and optical transparency, ZnO is dope with many impurities. Al and Ga are known as the most successful dopant due to its' compatible ionic and covalent radii with Zn. Few reports were found about the synthesize of ZnO nanocone structured thin films. We have investigated the structural properties of Al doped zinc oxide terrace-truncated nanocone structure which was grown by using advanced spray pyrolysis deposition method. The optimum growth temperature for Al doped ZnO was investigated in the range of 300 to 450 ºC. The major structural differences were found when changing the growth temperature. The optimum growth temperature was decided to be ~400 ºC with 40 nm, 290.10 per μm^2 and 80 % of average top diameter, average structure density and optical transparency in the visible range, respectively. Optimum Al doping ratio was found to be 2 at % of Al doping for optimum transparent conductive oxide properties. The spray angle is the crucial factor deciding the nano structure in spray pyrolysis deposition technique. This value was investigated in three ranges, ~15º, ~30º and ~45º. Properties of nanostructure highly depended on spraying angle. An excellent nanostructure with good separation, lowest number of structural defects was observed in ~15º of spraying angle. The differences of horizontal and vertical velocities of atomized particles in each spraying angle, were correspond to these structural changes. The lowest resistivity of 1.06×10^{-4} Ω.cm and highest optical transparency

of 80.3 % in the visible range were observed in Al doped ZnO sample, which was prepared at ~15º of spraying angle. However, the nanostructure was not clearly identified up to this stage. The spraying volume was increased from 100, 200 and 400 ml to identify the nano structure. The terraced truncated nanocone structure was confirmed at this stage. Due to the higher growth rate along the (002) direction increased the decay rate along the same direction and end up with terrace truncated nanostructure. Even though the top was decaying, the bottom of the nanostructure was narrow as the polar O^{2-} face tightly attached to the nucleation sites of the FTO glass substrate.

We have conducted research on Ga doped ZnO nanostructure using advanced spray pyrolysis method. The growth temperature was changed from 300 to 450 ºC and an excellent nanostructure of Ga doped ZnO was found in 400 ºC of growth temperature with 22.9 nm of average top diameter and 366 per μm^2 of average nanostructure density. Ga doping level was varied from 1 to 3 at %. The optimum nanostructure was found when sample was doped with 2 at % of Ga doping, average top diameter and average structure density were 37.0 nm and 230.4 per μm^2, respectively. All the Ga doped ZnO samples with varied Ga to Zn ratio, show high optical transmittance in the visible range. The spray angle dependence for the nanostructure growth was investigated in three different angles of ~15º, ~30º and ~45º. The ideal transparent conductive oxide properties with 82 % of optical transmittance in the visible range and 3.9×10^{-4} Ω.cm of low resistivity were grasped at ~15º of spraying angle. The average top diameter, average structure density and height were 22.8 nm, 195 per μm^2 and ~200 nm, respectively. The terrace-truncated nanocone structure was not confirmed until this stage. The spraying volume was changed 100, 200 and 400 ml to identify the nanostructure. Heights of the nanostructure were 200, ~380 and ~700 nm for 100, 200, and 400 ml volumes, respectively. The terraced truncated nanocone structure was found to be formed at this stage by FE-SEM images.

Acknowledgement

First, I would like to extend my sincere gratitude to Prof. Kenji Murakami, Graduate School of Integrated Science and Technology, Shizuoka University, for granting this valuable opportunity to undertake this research. Throughout the research, he gave me valuable knowledge, advice and encouragement for fulfillment of this endeavor. I would like to confer my beneficence to my co-supervisor, Associate Prof. Masayuki Okuya, Graduate School of Integrated Science and Technology, Shizuoka University for his succor in my research process. My special gratitude goes to Prof. Masaru Shimomura for his patronage, which was very important to come up with a solution. I am very grateful to Prof. R.M.G. Rajapakse, Department of Chemistry, University of Peradeniya for helping me in numerous ways during the entire period of this research. I am very thankful to Dr. Viraj Jayaweera of SPD laboratory, Hamamatsu for giving me guidance for my research even in his busy schedule. I also wish to convey my sincere thanks to all the members of the non-academic staff, lecturers and students of my laboratory who were supportive whenever necessary. I am grateful to all my colleagues for helping me in numerous ways during the entire period of this research. Finally, yet importantly, my thanks go out to my beloved parents for being with me in all the struggles that I faced and giving me a driving force to make this research a success.

List of Abbreviations

TCO	Transparent conductive oxide
SPD	Spray pyrolysis deposition
FE-SEM	Field emission scanning electron microscopy
XRD	X-ray diffraction
JCPDS	Joint Committee on Powder Diffraction Standards
HOMO	Higher occupied molecular orbital
LUMO	Lower unoccupied molecular orbital
AZO	Aluminum doped zinc oxide
GZO	Gallium doped ZnO

Contents

Chapter 1

Transparent conductive oxides, properties and deposition techniques.

1.1 Nanostructured thin films and deposition techniques

1.1.1 Introduction to deposition techniques

Two main technical methods available to construct thin films, which are chemical depositions and physical depositions. In general, chemical deposition techniques inaugurate with solutions, which reaches to the hot substrate and makes the thin film by a certain chemical reaction at the substrate. On the other hand, in physical vapor deposition techniques, the thin film deposition is conducting at the vapor phase. Various chemical and physical deposition methods have been reported for the production of thin films over past few decades.

- Pulsed Laser Deposition,
- Metal-Organic Chemical Vapor Deposition,
- Spray Pyrolysis,
- Sputtering,
- Chemical Bath Deposition,
- Molecular Beam Epitaxy,
- Arc Plasma Evaporation,
- Sol-gel,
- Dip Coating,
- Ion Planting.

Each of these deposition techniques have their own advantages and drawbacks [1-13]. Even though there are many thin film deposition techniques available, spray pyrolysis is known to be one of the most promising deposition technique. Chamberlin and Skarman did the initial work of spray pyrolysis deposition in 1966, which was cadmium sulfide films for solar cells.

Nowadays this technique is widely used due to its,

- Simplicity,
- Inherent suitability for large-scale production,
- No need of vacuumed condition,
- Possibility to operate at moderate temperature,
- High homogeneity.
- Easiness of doping,
- Low cost,
- Sensory activity,
- High productivity,

Over the last few decades, many thin films have been produced via this technique. Various metals and TCO materials (tin oxide, indium oxide, cadmium /Sn or In binary oxides, doped and undoped ZnO, oxide superconductors etc) were fabricated by using the spray pyrolysis deposition. This deposition technique involves a thermal stimulation process of chemical reaction. In this method, vapor particles, which reaches to the hot substrate, undergo an endothermic decomposition process and crystalline. Another merit of the hot substrate is the vaporization of other volatile by-products.

Table 1.1: Comparison of thin film deposition methods.

Process	Material	Uniformity	Impurity	Grain size	Film Density	Deposition rate	Substrate Temperature	Directional	Cost
Thermal Evaporation	Metal/low melting point materials	poor	High	10-100 nm	poor	1 - 20 Å/s	50-100 ºC	Yes	Very Low
E-beam Evaporation	Both metal & dielectrics	poor	Low	10-100 nm	poor	10 - 100 Å/s	50-100 ºC	Yes	High
Sputtering	Both metal & dielectrics	Very good	Low	~10 nm	Good	Metal: ~100 Å/s Dielectric: ~1-10 Å /s	~ 200 ºC	Some Degree	High
PECVD	Mainly dielectrics	Good	Very low	10-100 nm	Good	10 - 100 Å/s	200-300 ºC	Some Degree	Very High
LPCVD	Mainly dielectrics	Very good	Very low	1-10 nm	Excellent	10 - 100 Å/s	600-1200 ºC	Isotropic	Very High

Original source: P. French et al, MICROSYST. NANOENG. (2016) 2, 16048.

1.1.2 Normal Spray Pyrolysis Deposition Technique

Spray pyrolysis is very simple and cost-effective technique. Porous films, dense films and multilayered films could be synthesized by using this technique. Typical spray pyrolysis deposition technique constitutes of substrate heater, spray solution, spray nozzle, atomizer and a temperature controller. Fig 1.1 shows a schematic diagram of normal spray pyrolysis deposition technique. Normal SPD technique has one major drawback, which is an inability to disperse the particles while spraying. Due to this, lump-like structures are grown and the topography is not grow homogeneously, hence reduce the ability to use them as a transparent conductive oxide material.

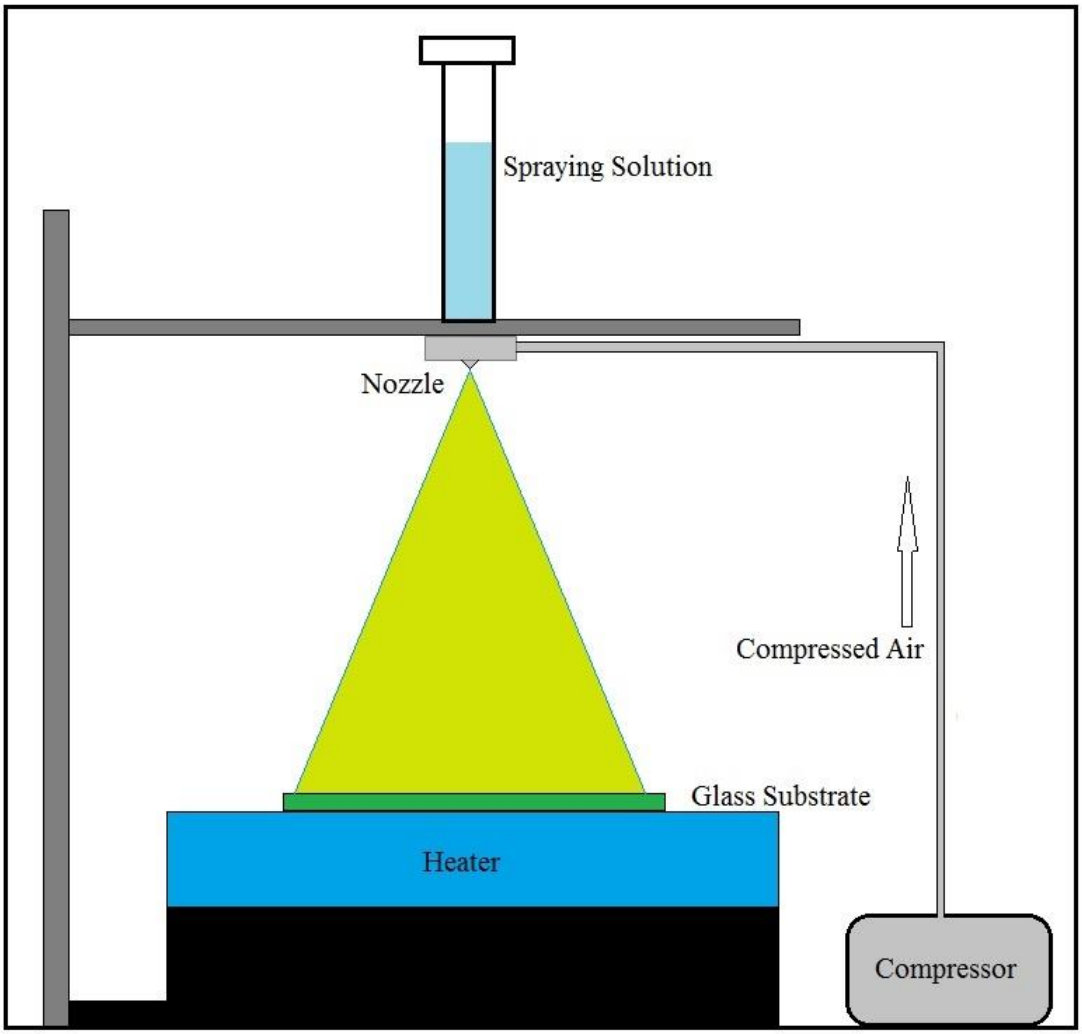

Fig. 1.1: The schematic diagram of normal spray pyrolysis deposition technique

Ultrasonic SPD technique is an improved version of SPD technique, which used to disperse agglomerated particles before spraying, to obtain a homogeneous structure. However, the ultrasonic spray pyrolysis deposition technique needs an extra energy and instrumentations. We have overcome these disadvantages and used a chamber to disperse the agglomerated particles by allowing them to hit into a Teflon sphere. This atomization process is happening inside the atomizing chamber, which does not need an extra power or special instruments. The schematic diagram of atomized spray pyrolysis deposition (ASPD) technique is shown in fig. 1.2.

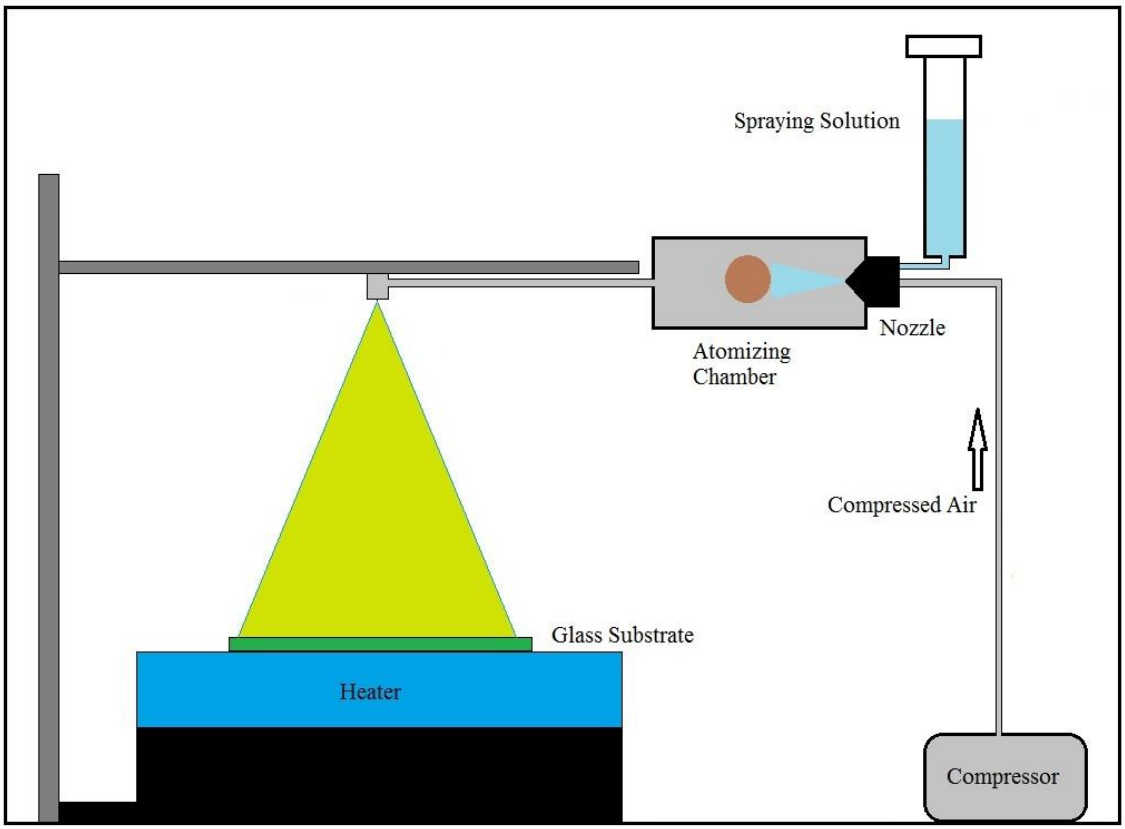

Fig. 1.2: Schematic Diagram of the Atomized Spray Pyrolysis Deposition Technique.

Atomized spray pyrolysis deposition technique has a major drawback, which is the drop of the temperature of the substrate due to the continuous spraying. To overcome this drawback, we have attached a microcontroller unit and the spraying was done as pulsed. In this case we kept time interval in between each pulse to regain the reduced temperature of the glass substrate.

This improved SPD instrumentation is known as Pulsed Atomized SPD technique. In order to grow more vertical aligned nanorod structure, it is important to keep the spraying aerosol stream along the substrate, which is horizontal direction [14]. Moreover, if the spray direction keep constant, the growth of the outlying nanorods could be diminished by the nanorods, which were already grown near the nozzle tip, as they disturb the propagation of aerosol stream. This phenomenon is known as the shadow effect. Because of that, the rotation of the nozzle tip was suggested, and the improved technique is known as Rotational, Pulsed and Atomized Spray Pyrolysis Deposition Technique, which is shown schematically in fig 1.3.

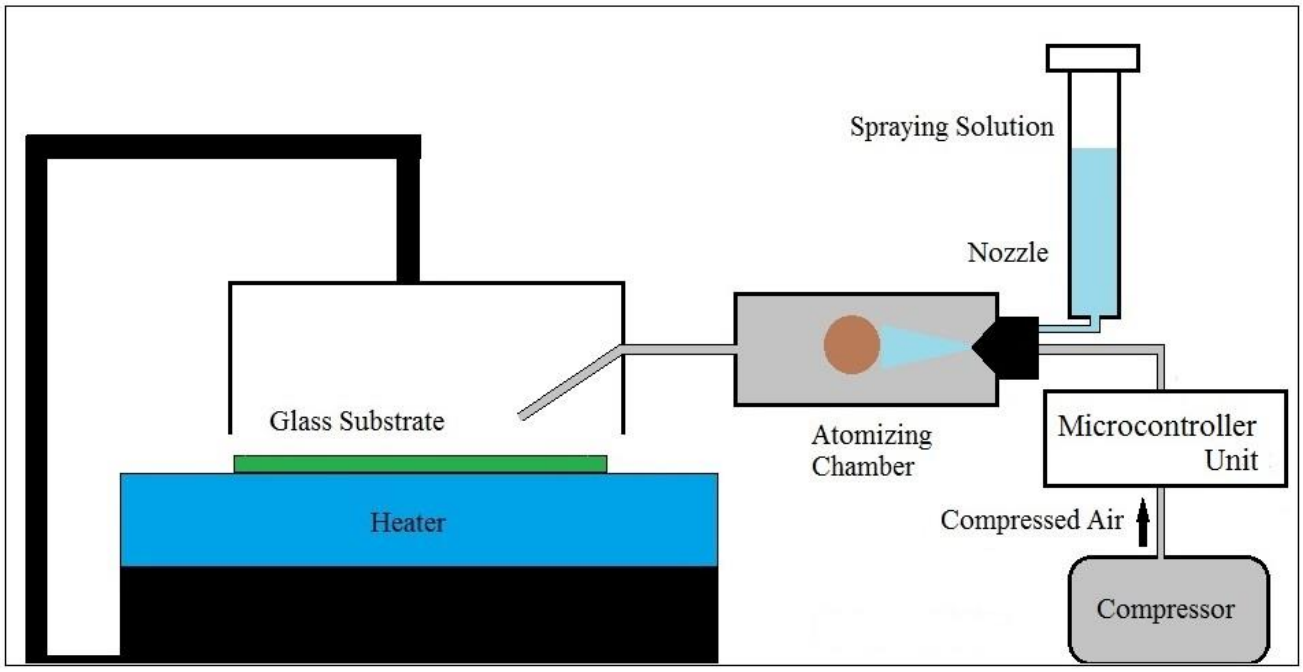

Fig. 1.3: Schematic Diagram of the Rotational, Pulsed and Atomized Spray Pyrolysis Deposition Technique.

Ajith et al has investigated about the spray angle dependence of for the growth of fluorine doped tin oxide 1-D nanostructure by using this SPD technique. They have found that, the spraying angle should be at a lower angle, to grow fluorine doped tin oxide 1-D nanorod structure, as it helps to swipe the aerosol particles along the glass substrate. Ajith et al found that, if the spray nozzle kept above 45º, FTO nano particles are formed, and the cross-linked

FTO 1-D nanorod structure was observed around 30º, while vertically aligned 1-D nanorod structure was formed at lower spray angle (below 15º). Another merit of RPASP deposition technique over other deposition techniques is, no need of a seed layer to grow the nano structure.

Fig. 1.4: Rotational, Pulsed and Atomized Spray Pyrolysis Deposition Technique.

1.2 Transparent Conductive Oxides and Material Selection

1.2.1 Introduction to transparent conductive oxide materials

The materials, which have an excellent electrical conductivity as well as high optical transparency, are known as transparent conductive oxide materials. Both of these phenomena is ought to be fulfill to consider as a successful TCO material, which can be described by band theory. Even though an isolated atom has a discrete energy levels, when two or more atoms are combined to form a compound, their energy levels simply overlap each other and end up with an energy band. Moreover, as there are no two electrons in same atoms with same quantum numbers with refer to the Pauli Exclusion Principle, the sea of atoms is end up with energy bands instead of energy level. In a semiconductor material highest occupied molecular orbital (HOMO) is the maximum of valence band, while the lowest unoccupied molecular orbital

(LUMO) is the minimum of the conduction band. For the electrical conductivity of a semiconductor material, the electrons at the valence band maximum must excite through the band gap to the minimum of the conduction band. One way of receiving the energy for this transition, is the absorption of photon. On the other hand, if the energy of a particular photon is not sufficient for this electron excitation, that light transmits through the material without absorbing. In general, the electrical conductivity and the optical transmittance of a transparent conductive oxide material should be over 10^3 Scm^{-1} and 80 % of an incident light. They should have resistivity lower than 10^{-4} Ω.cm-and the carrier concentration in the order of 10^{20} cm^{-3} with wide optical band gap (> 3 eV). Glass fibers are highly optical transmitters: but insulators. Silicon and compound semiconductors are optical resistors but dopant dependent electrical conductors. Transparent conductive oxide material should possess these two properties conjointly. These characteristics are impossible to obtain through an intrinsic stoichiometric oxide. Howbeit, this could be attained by impurity doping with an appropriate material. In 1907 Badeker observed that the CdO thin films which were created by the thermal oxidation of sputtered cadmium films, possess such characteristics. Afterwards, it was found that thin films of metals such as Fe, Ag, Cu, Mg and ZnO, SnO_2, In_2O_3 and their alloys also having similar characteristics[15-25].

1.2.2 Electrical properties

The conductivity of a TCO material is due to the oxygen vacancies or by extrinsic dopants. In general, the conductivity (σ) of the n-type semiconductor depends on the carrier concentration and their mobility. The conductivity is given by the following equation (1).

$$Conductivity\ (\sigma) = \mu ne \qquad (1)$$

Where μ is the mobility, n is the electron density and e is the electron charge.

Mobility (μ) is given by equation (2).

$$Mobility\ (\mu) = \frac{e\tau}{m^*} \qquad (2)$$

Where e is the electron charge, τ is the mean time and m^* is the effective electron mass. There are some limitations on enhancing the electrical conductivity. As an example, n and μ cannot be increased separately at higher doping levels (higher carrier concentrations) due to the limitations of ionized impurity scattering. While increasing the doping concentrations, the resistivity reaches to the minimum and could not decreased more. Bellingham et al initially mention this occurrence of limitation of resistivity at the higher carrier concentrations over 10^{20} cm^{-3} [26-31].

1.2.3 Optical properties

The optical properties of the transparent conductive oxides are decided by its reflection index n, extinction coefficient k, energy gap E_g and film structure (thickness, structural uniformity, thickness uniformity, surface roughness etc).

1.2.4 Applications of transparent conductive oxides

Due to the unique properties of transparent conductive oxide materials, they have been widely used in many commercial and academic industries [32-37].

- Smart devices (smart phone, smart devices etc),
- Flat panel displays
- Light emitting diodes
- Photovoltaic devices
- Liquid-crystal displays
- Polymer-based electronics
- OLEDs
- Touch screens
- Gas sensors
- Polymer-based electronics
- Electroluminescent

1.2.5 Different Types of Transparent Conductive Oxide Materials

Physicist Karl Baedeker did the first reported TCO material, by sputtering cadmium into a substrate to obtain cadmium oxide. Later in 1947, Harold McMaster invented a SnO_2 TCO material, by chemical vapor deposition on a glass substrate. In 1954, Rupprecht discovered ITO, which shows much better TCO behavior. There are two main types of TCO materials, which are n-type and p-type. n-type TCO materials are developed by choosing the doping impurity with higher valence such as Al:ZnO, Ga:ZnO, ITO, B:ZnO, In:CdO, Nb:TiO_2 etc. p-type semiconductor $CuAlO_2$ was reported in 1997 by Kawazoe et al. As many p-type TCO materials have been used in laboratory demonstration devices, further studies are needed to observe their optical and electrical properties. $CuBO_2$ and $CuGaO_2$ are examples of p-type TCO materials. Moreover, to compromise high optical transparency and electrical conductivity, some binary TCOs have been developed. ZnO-SnO_2, CdO-SnO_2, and ZnO-In_2O_3 are some examples of such binary TCO materials. In addition to these binary compounds, some ternary compounds are also used prior to 1980, such as, Cd_2SnO_4, $CdSnO_3$, and $CdIn_2O_4$. However, those ternary compounds have not been used widely. Even though there are many TCO materials, there is still a high demand for new TCO materials due to their wide range of applications in optoelectronic devices. In general, field of TCO material production could be improved by two methods, which are, by introducing a new TCO material or by improving/introducing deposition technique.

Table 1.2: Resistivity and Deposition Method of Reported Transparent Conducting Thin Films Composed of Ternary Compound TCO Materials.

Material	Resistivity (Ω cm)	Deposition Method
Zn_2SnO_4	1.7×10^{-2}	rf MSD*
$MgIn_2O_4$	4.3×10^{-3}	rf sputtering*
	7.9×10^{-4}	rf MSD (RT)
$GaInO_3$	2.7×10^{-3}	rf MSD*
$(Ga,In)_2O_3$	5.8×10^{-4}	dc MSD (RT)
$Zn_2In_2O_5$	3.9×10^{-4}	MSD (RT)
	2.9×10^{-4}	dc MSD (RT)
$In_4Sn_3O_{12}$	20×10^{-4}	dc MSD (350 ºC)

Note: MSD is magnetron sputtering deposition/ RT is room temperature. *Post annealed

Original source: Tadatsugu Minami, MRS BULLETIN/AUGUST 2000

Table 1.3: Widely used transparent conductive Oxides

TCO	Dopant Element
SnO2	Sb, F, As, Nb, Ta
ZnO	Al, Ga, B, In, Y, Sc, F, V, Si, Ge,Ti, Zr, Hf, Mg, As, H
$GaInO_3$	Sn, Ge
In_2O_3	Sn, Mo,Ta, W, Zr, F, Ge, Nb, Hf, Mg
$CdSb_2O_3$	Y
CdO	In, Sn

Among many TCOs, Indium doped tin oxide is the most widely used material, due to its high optical transmittance, conductivity, and wide band gap (>3.5 eV). However, as indium is

categorized as a rare metal, supply of In is unstable. Moreover, due to its scarcity, low-cost commercial production of ITO is still a challenge[38-43].

1.2.6 Zinc Oxide and its properties

Zinc Oxide (ZnO) has gained a lot of research interest as a future TCO material because of the shortcomings of ITO, which is high cost, scarcity and toxicity. ZnO is one of most attractive semiconductor oxide material due to its direct wide band gap (Eg =3.37 eV), large exciting energy of 60 meV, cheaper, non-toxicity, readily availability, high transparency, conductivity, piezoelectricity, good thermal stability, easy fabrication, and availability of many nanostructures[44-52]. Important properties of ZnO are tabulated in table 1.4.

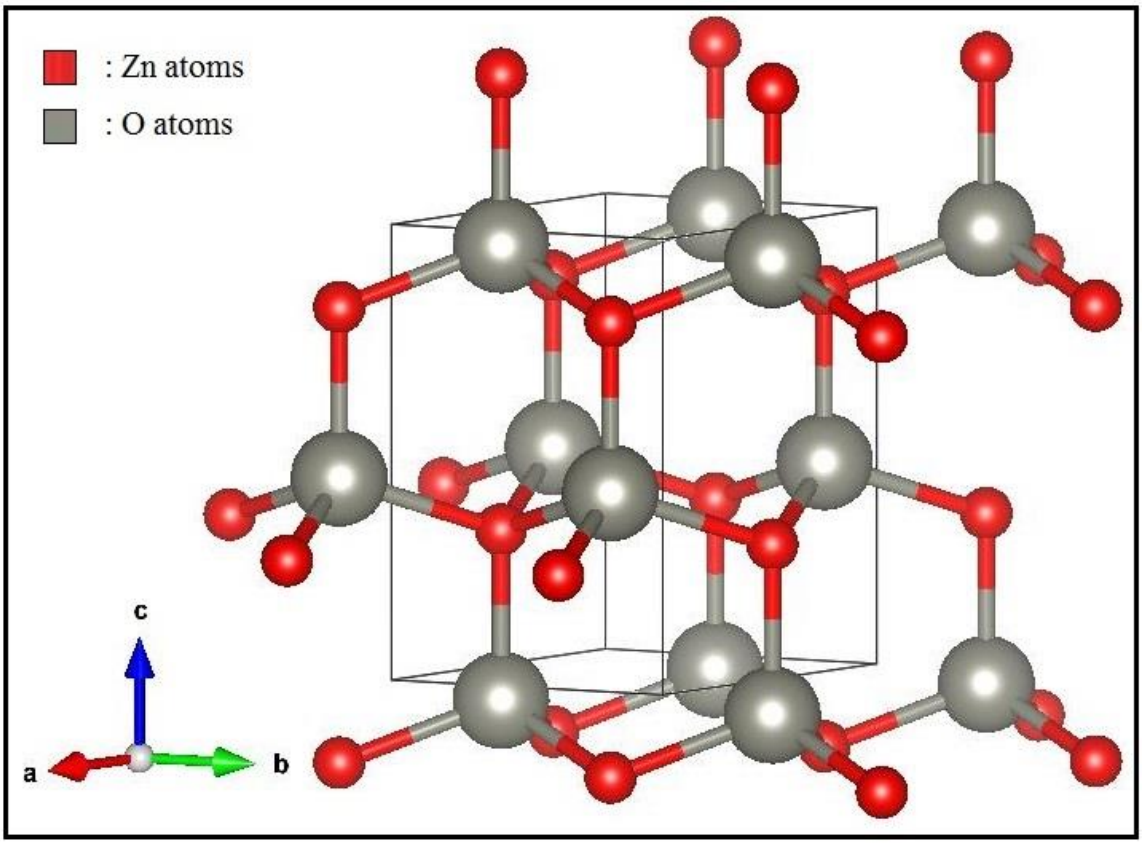

Fig. 1.5: Schematic diagram of hexagonal wurtzite structure of ZnO.

Table 1.4: Properties of ZnO	
Property	Value
Lattice parameters at 300 K: a c a/c	 0.32495 nm 0.52069 nm 1.602 (1.633 for ideal hexagonal structure)
Density	5.606 g/cm^3
Stable phase at 300 K	wurtzite
Melting point	1975 °C
Linear expansion coefficient (°C)	**a:** 6.5 x 10^{-6}, **c:** 3.0 x 10^{-6}
Static dielectric constant	8.656
Refractive index	2.008, 2.029
Energy gap	3.4 eV (direct)
Intrinsic carrier concentration	< 10^6 /cm^3
Exciton binding energy	60 meV
Electron effective mass	0.24
Electron Hall mobility at 300 K for low n-type conductivity	200 cm^2/V•s
Hole effective mass	0.59
Hole Hall mobility at 300 K for low p-type conductivity	5-50 cm^2/V•s

Original Source: D. P. Norton et al, ZnO: growth, doping & processing, materials today 2004, 34.

On behalf of improving optical transparency and electrical conductivity, ZnO could be doped with impurities such as, B, Al, Ga, Sn, Y, Sc, Ti or Zr. Among these dopants, Al, In and Ga are

considered as the most appropriate dopants due to its comparable ionic and covalent radii with Zn[53-57].

Table 1.5 Ionic radii, covalent radii, band lengths with O of Al, Ga and Zn

Element	Ionic Radius (Å)	Covalent Radius (Å)	Bond Length [X-O] (Å)
Zn	1.31	0.74	1.97
Al	1.18	0.53	2.7
Ga	1.26	0.62	1.92
In	1.44	0.80	2.1

Table 1.6 shows the properties of each dopants with ZnO.

Table 1.6 Resistivity, carrier concentration, and dopant content for ZnO films doped with various impurities.

Dopant	Doping Content (at %)	Resistivity (10^{-4} Ω cm)	Carrier Concentration (10^{20} cm^{-3})
Al	1.6–3.2	1.3	15.0
Ga	1.7–6.1	1.2	14.5
B	4.6	2.0	5.4
Y	2.2	7.9	5.8
In	1.2	8.1	3.9
Sc	2.5	3.1	6.7
Si	8.0	4.8	8.8
Ge	1.6	7.4	8.8

Ti	2.0	5.6	6.2
Zr	5.4	5.2	5.5
Hf	4.1	5.5	3.5
F	0.5	4.0	5.0

Original source: Tadatsugu Minami, MRS BULLETIN/AUGUST 2000

1.3 Truncated Nanocone structure of ZnO

There are many reports about formation of various kinds of ZnO nanostructures such as, nanorods, nanoflakes, nanoplates, nanodots, nanobridges, nanocone, nanotubes, nanowires, nanohelixes, nanobelts, nanonails, nanorings, polyhedral cages etc. 1-D nanorod structure is suitable for dye sensitized solar cell application due to its high surface-volume ratio. However, some researches have been reported about usage of ZnO nanocone structures, which could increase the light transmittance by reducing the photon scattering. Fig. 1.6 and fig. 1.7 shows the photon emission comparison of hexagonal nanorods with rough surfaced nanocone structures, respectively.

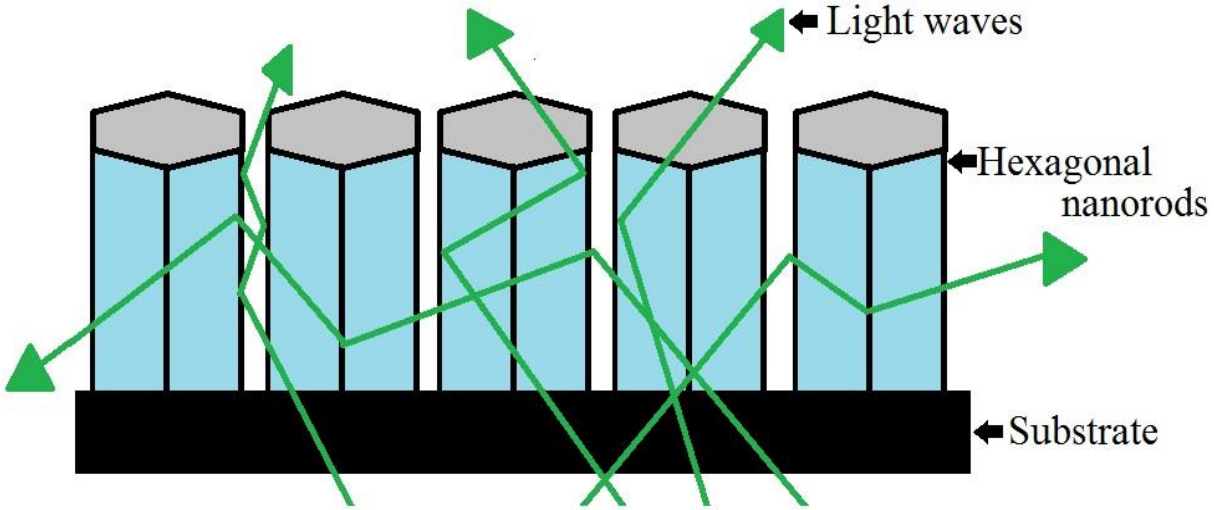

Fig. 1.6: Photon emission mechanism of hexagonal wurtzite nanorod structure.

Optical transmittance in the visible range might be higher in nanocone hexagonal structure, with respect to nanorod structure. Few reports have been found about constructing nanocone ZnO structure. These nanocone structures are consequential especially for light emitting diodes (LEDs) to increase their efficiency by decreasing the light extraction efficiency (LEE). Masui et al has reported, among the polygons, triangle shape has a least chance to trap the light. Yin et al reported that, rough-bevel, cone-shaped hexagonal nano structure of ZnO has higher LEE, with respect to hexagonal nanorods of ZnO.

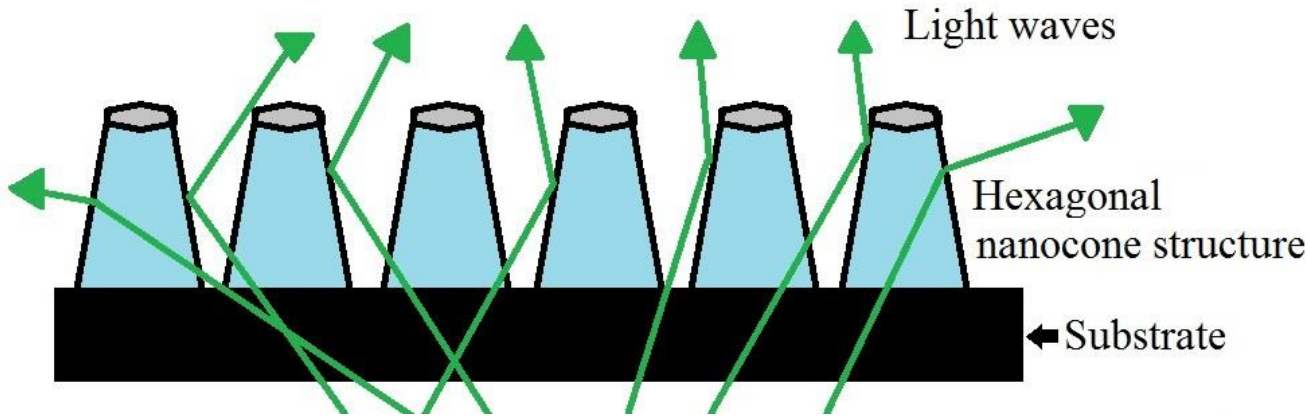

Fig. 1.7: Photon emission mechanism of hexagonal wurtzite nanocone structure.

There was no proper study was found on terrace-truncated nanocone structure of impurity doped ZnO by spray pyrolysis deposition technique. D. Visser et al has investigated about truncated ZnO structure by sol-gel method in 2017. They have grown a truncated nanocone structurer on c-Si substrate and obtained a structure with top diameter of 50 nm, bottom diameter between 50-500 nm and height between 500-1500 nm. FE-SEM image of their truncated nanocone structure is shown in fig. 1.8.

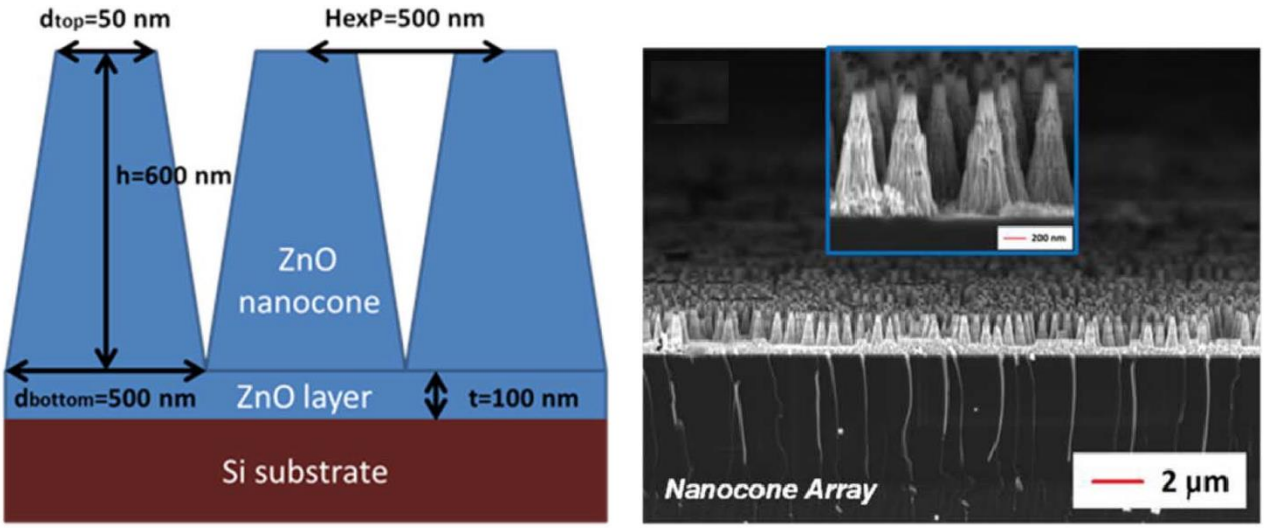

Fig. 1.8: Truncated nanocone arrays fabricated by D. Visser et al.

However, there are many studies have been performed about the importance of the nanocone structure of silicon by stating it is an excellent structure for optimum light harvesting due to superior antireflection properties [58-60].

1.4 Objectives of our study

One of our purpose in this study to investigate the spray angle dependence for the growth of terrace-truncated nanocone hexagonal structure, for an excellent transparent conductive oxide material, as our group investigated about the importance of lower spray angle for the growth of 1-D nanostructured fluorine doped tin oxide. To the best of our knowledge there was no proper study has been conducted on terrace–truncated nanocone structure of impurity doped ZnO as a transparent conductive oxide layer by spray pyrolysis deposition technique. Our final objective is to use this nanostructure as a working electrode to increase the efficiency of dye-sensitized solar cells (DSSCs). We believe the sinking of TiO_2 photo layer into the nanocone structure is higher than the hexagonal nanorod structure as illustrated in fig. 1.9.

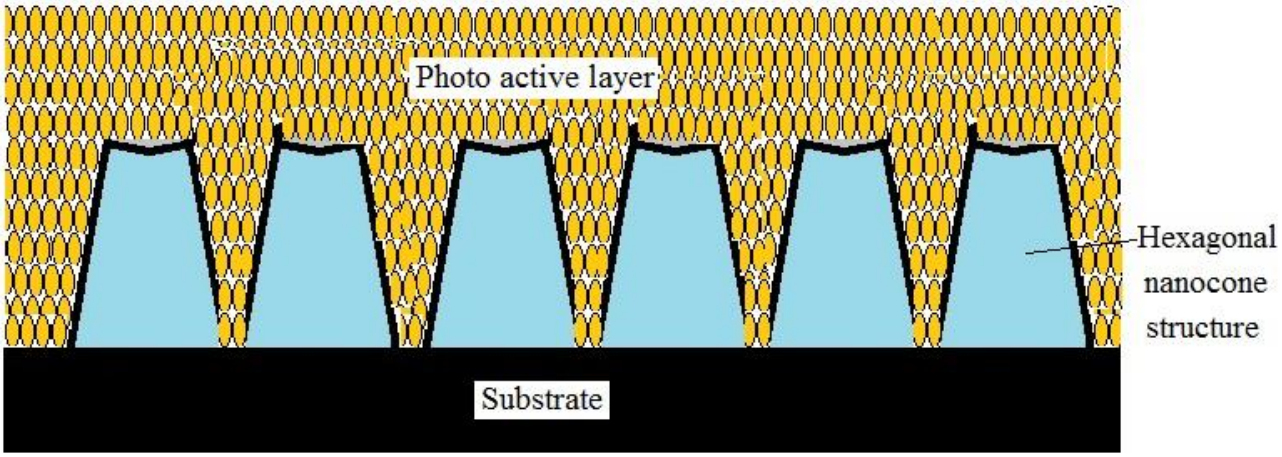

Fig. 1.9: Proposed Terrance-truncated nanocone structure for working electrode of DSSCs.

References:

1. T.B. Asafa, N. Tabet, S.A.M. Said, Neuro computing 2013, 106, 86.
2. D.K. Kim, H.B. Kim, Journal of Alloys and Compounds 2011, 509, 421.
3. A. Suzuki, T. Matsushita, N. Wada, Y. Sakamoto, M. Okuda, Jpn. J.Appl. Phys. 1996, 235, L56.
4. M. Miramatsu, K. Imeda, N. Horio, M. Nawata, J. Vac. Sci. Technol.A 1998, 16, 669.
5. K. Lin, P. Tsai, Mater. Sci. Eng. B-Solid 2007, 139, 81.
6. S.M. Rozati, Sh. Akesteh, Mater. Charact. 2007, 58, 319.
7. H. Go´mez, A. Maldonado, R. Castanedo-Pe´rez, G.Torres-Delgado, M. de la L. Olvera, Mater. Charact. 2007, 58, 708.
8. M. Ohyama, H. Kozuka, T. Yoko, S. Sakka, Ceram. Soc Jpn. 1996, 104, 296.
9. M. Ohyama, H. Kozuka, T. Yoko, Thin Solid Films 1997, 306, 78.
10. H. Li, J. Wang, H. Liu, C. Yang, H. Xu, X. Li, H. Cui, Vacuum 2004, 77, 57.
11. Y.S. Kim, W.P. Tai, S.J. Shu, Thin Solid Films 2005, 491, 153.
12. T. Pauporte, D. Lincot, Electrochim. Acta. 2000, 45, 3345.
13. D. Raviendra, J.K. Sharma, J. Appl. Phys. 1985, 58, 838.
14. A. Bandara, M. Okuya, M. Shimomura, K. Murakami, and R.M.G. Rajapakse, Journal of Advances in Physics, 2016, 12[1], 2347.
15. K. Baedeker, Ann. Phys. 1907, 22, 749.
16. K. Hayashi, S. Matsuishi, T. Kamiya, M. Hirano, H. Hosono, Nature 2002, 419, 462.
17. M. Ganose, D. O. Scanlon, J. Mater. Chem. C 2016, 4, 1467.
18. G. Haacke, Ann. Rev. Mater. Sci. 1977, 7, 7 3.
19. M. Hiramatsu, K. Imaeda, N. Horio, and M.Nawata, J. Vac. Sci. Technol. 1998, A 16 p. 669.
20. B.G. Lewis and D. C. Paine, Materials Research Society Bulletin, 2000, 25, pp.22.

21. G.J. Exarhos and X.D. Zhou, Thin Solid Films 2007, 515, 7025.

22. E. Fortunato, D. Ginley, H. Hosono, and D.C. Paine, MRS. BULLETIN. 2007, 32, pp.242.

23. P. P. Edwards, A. Porch, M. O. Jones, D. V. Morgan, R. M. Perks, Dalton Trans. 2004, 19, 2995.

24. https://en.wikipedia.org/wiki/Electronic_band_structure

25. https://en.wikipedia.org/wiki/Transparent_conducting_film

26. A. Stadler, Materials 2012, 5, 661.

27. H. Mizoguchi and P.M. Woodward, Chem. Mater. 2004, 16, 5233.

28. D.C. Look, B. Claflin, in: G.J. Brown, M.O. Manasreh, C. Gmachl, R.M. Biefeld, K. Unterrainer (Eds.), Progress in Compound Semiconductor Materials IV-Electronic and Optoelectronic Applications, Boston, U.S.A., 2004, Materials Research Society Symposium Proceedings, vol. 829, 2005, p. B8.6.1.

29. C.G. Van de Walle, Phys. Rev. Lett. 2000, 85, 1012.

30. C. Kiliç, A. Zunger, Phys. Rev. Lett. 2002, 88, 095501.

31. K. Ellmer, J. Appl. Phys. 2000, 33, R17.

32. D. S. Ginley and C. Bright, Mater. Res. Bull. 2000, 25, 15.

33. H. L. Hartnagel, A. L. Dawar, A. K. Jain, and C. Jagadish, Semiconducting Transparent Thin Films; Institute of Physics: Bristol, UK, 1995.

34. C. A. Pan and T. P. Ma, Appl. Phys. Lett. 1980, 37, 163.

35. Hamberg and C. G. Granqvist, J. Appl. Phys. 1986, 60, R123.

36. J.H. Lim, D.K. Hwang, H.S. Kim, J.Y. Oh, J.H. Yang, R. Navamathavan, S.J. Park, Appl. Phys. Lett. 2004, 85, 6191.

37. T. Minami, Mater. Res. Bull. 2000, 25, 38.

38. M. Hiramatsu, K. Imaeda, N. Horio, M. Nawata, J. Vac. Sci. Technol. A 1998, 16, p. 669.

39. K. Tominaga, T. Yuasa, M. Kume, and O. Tada, Jpn. J. Appl. Phys. 1985, 24, p. 994.

40. J.B. Webb, Thin Solid Films 1986, 136, p. 135.

41. T. Minami, H. Nanto, and S. Takata, Thin Solid Films 1988, 164, p. 275.

42. T. Minami, H. Sato, H. Imamoto, and S. Takata, Jpn. J. Appl. Phys., Part 2: Lett. 1992, 31, p. L257.

43. T. Minami, H. Sato, K. Ohashi, T. Tomofuji, S. Takata, J. Cryst. Growth 1992, 117, p. 370.

44. Q. Li, X. Li, J. Zhang, Microstructure, J. Alloys Comp. 2013, 572, 175.

45. X. Tian, Z. Pan, H. Zhang, H. Fan, X. Zeng, C. Xiao, G. Hu, Z. We, Ceram. Int. 2013, 39, 6497.

46. M. Caglar, S. Ilican, Y. Caglar, Thin Solid Films 2009, 517, 5023.

47. W. Water, S.-Y. Chu, Y.-D. Juang, S.-J. Wu, Mater. Lett. 2002, 57, 998.

48. A. Ahmad, J. Walsh, J. Mater. Sci. 2003, 38, 4325.

49. M. Caglar, Y. Caglar, S. Ilican, J. Optoelectron. Adv. Mater. 2006, 8 [4], 1410.

50. F. Yakuphanoglu, Y. Caglar, S. Ilican, M. Caglar, Physica B 2007, 394, 86.

51. Young Yi Kim, Si Woo Kang, Bo Hyun Kong, Hyung Koun Cho, Physica B 2007, 401, 408.

52. S. Ilican, Y. Caglar, M. Caglar, J. Optoelectron. Adv. Mater. 2008, 10, 2578.

53. W.Y. Zhang, D.K. He, Z.Z. Liu, L.J. Sun, Z.X. Fu, J. Optoelectron. Adv. Mater – Rapid Commun. 2010, 4 [11], 1651.

54. L.H. Van, M.H. Hong, J. Ding, J. Alloys Comp. 2008, 449 [1], 207.

55. H. Wang, M.-hui Xu, J.-wen Xu, M.-fang Ren, L. Yang, J. Mater. Sci. Mater. Electron. 2010, 21,pp. 589.

56. K. moh Lin, Y.Y. Chen, K.Y. Chou, J. Sol-Gel Sci. Technol. 2009, 49, pp. 238.

57. C. Major, A. Nemeth, G. Radnoczi, Zs. Czigany, M. Fried, Z. Labadi, I. Barsony, Applied Surface Science 2009, 255, pp. 8907.

58. P.X. Gao, W. Mai, and Z.L. Wang, Nano Lett. 2006, 6 [11], 2536.

59. S. Han, M.S. Akhtar, I. Jung, and O. Yang, Mater. Lett. 2018, 230, 92.

60. J. Y. Lao, J. Y. Huang, D. Z. Wang, and Z. F. Ren, Nano Lett. 2003, 3 [2], 235.

Chapter 2

Experimental procedure

2.1 Synthesis of Al doped ZnO nanostructure.

Zinc acetate dihydrate (Wako Pure Chemicals) was dissolved in 100 ml of 2-methoxyethanol (Wako Pure chemicals), and few drops of ethanolamine (Sigma Aldrich) was added as a stabilizer while stirring. $Al(NO_3)_3.9H_2O$ (Wako Pure Chemicals) was added for doping. The solution was stirred for 60 minutes at 70 ℃ and aged for 24 hours at room temperature. Commercially available FTO glasses (2.5 cm × 2.5 cm) were ultrasonically cleaned in a mixture of acetone, ethyl alcohol, and distilled water. Finally, precursor solution was deposited by using advanced spray pyrolysis deposition technique. The deposition temperature was changed from 300 ºC to 450 ℃. The distance between the nozzle tip and substrate was kept constant at 0.5 cm. spray pressure was set to 0.40 MPa. Spraying was continued for 2 s, with 12 s of time interval. Total spray time was 60 minutes.

2.2 Synthesis of Ga doped ZnO nanostructure

Zinc acetate dihydrate (Wako Pure Chemicals) was dissolved in 100 ml of 2-methoxyethanol (Wako Pure chemicals), and few drops of ethanolamine (Sigma Aldrich) was added as a stabilizer while stirring. $Ga(NO_3)_3.XH_2O$ (Wako Pure Chemicals) was added for doping. The solution was stirred for 60 minutes at 70 ℃ and aged for 24 hours at room temperature. Commercially available FTO glasses (2.5 cm × 2.5 cm) were ultrasonically cleaned in a mixture of acetone, ethyl alcohol, and distilled water. Finally, precursor solution was deposited by using advanced spray pyrolysis deposition technique. The deposition temperature was changed from 300 ºC to 450 ℃. The distance between the nozzle tip and substrate was kept

constant at 0.5 cm. spray pressure was set to 0.40 MPa. Spraying was continued for 2 s, with 12 s of time interval. Total spray time was 60 minutes. The growth temperature, doping concentration, spray angle and the volume of Ga doped ZnO samples were changed as shown in table 3.5 in each experimental section.

2.3 Characterization

The crystal structure was characterized by X-ray diffraction patterns (Rigaku RINT Ultima-III at 40 kV with Cu K_α radiation $\lambda = 1.541836$ Å). XRD patterns were taken in the range of 30º - 80º. Surface morphology was examined by field emission scanning electron microscope/FE-SEM (JEOL JSM-6320F) with an acceleration voltage of 15 keV, with accompanying energy dispersive X-ray spectroscopy. Atomic force microscopy images were taken by (XE-Series, XE-70, Park system) in 1 μm × 1 μm scan size. The layer thickness was measured by cross-sectional images. The UV/visible transmittance spectra were obtained by JASCO V-630 spectrometer in the wavelength range of 300 –800 nm. Electrical studies of prepared samples were carried- out by four probe method-Hall effect measurement system, HMS-3000. ImageJ software was used to measure and characterise FE-SEM images. AutoCAD software was used for the simulations.

2.3.1 Investigations of the electrical conductivity by four probe method

In this study,measuring of the electrical study is challenging, as we have to measure the conductivity of two layerd structure by four probe method. Fig. 2.1 shows the electrical conductivity measuring technique of four probe method, and fig. 2.2 shows the four probe measuring technique on proposed impurity doped ZnO nanostructure.

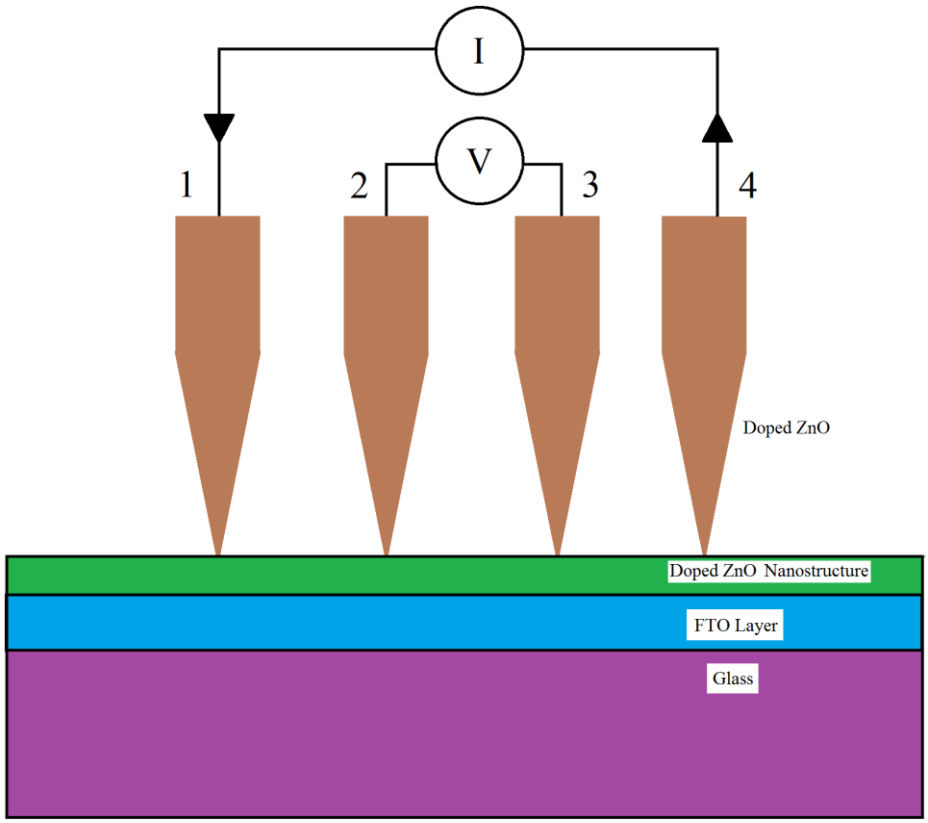

Fig.2.1: Electrical conductivity measuring technique of four probe method.

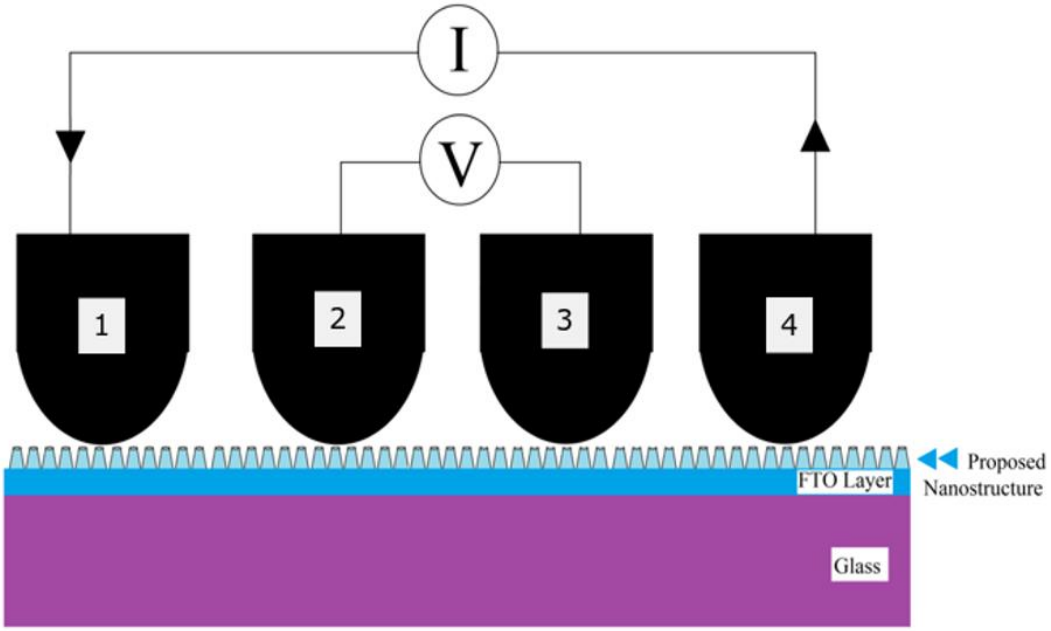

Fig.2.2: Electrical conductivity measuring using four probe method on proposed nanostructure.

2.3.2 Importance of the FTO glass substrate

In this study, impurity doped ZnO terrace-truncated nanocone structure was grown on FTO glass substrate to achieve main three targets which are,

1. *To measure the electrical conductivity,*

   As described in the fig 2.1 & 2.2, when measuring the electrical conductivity of the nanostructure, the electrons are propagating from the 1^{st} probe to the 4^{th} probe by completing the circuit, and the voltage difference is measure in between the 2^{nd} and the 3^{rd} probe. In this case, the horizontal propagation of the electrons (1^{st} probe to the 4^{th} probe) is compulsory to complete the circuit and cannot fulfilled without having the FTO layer.

2. *To increase the electrical conductivity,*

   FTO glass substrates were used to increase the electrical conductivity of the whole structure by increasing the electron propagation.

3. *To make a suitable substrate for the growth of terrace-truncated nanocone structure,*

   It is well-known factor, that the growth of a nanostructure is stabilized by having an excellent rough substrate such as FTO/ZnO. However, in this research we only concern about the growth and the growth mechanism of the terrace-truncated nanocone structure, and we have used an FTO glass substrate which can improve the growth of nanostructure by providing an excellent growth substrate.

Chapter 3

Synthesis of Al doped ZnO Nanocone Structure

- *In this chapter detailed discussion was done about the synthesis of Al doped ZnO terrace-truncated nanocone structure by using advanced spray pyrolysis deposition technique.*
- *In the first section of this chapter, we have investigated the optimum temperature for the deposition of Al doped ZnO nanostructure.*
- *In the second part we have investigated about the optimum doping concentration with Al. We have changed the Al to Zn ratio and obtained the optimized results.*
- *In the third part, we have changed the spraying angle and obtained the results. The core of the research is in this part, as the spray angle is the critical factor for the growth of an excellent transparent conductive oxide properties.*
- *Last part of this chapter is also an important part. In this part we have increased the spraying volume to investigate about the synthesized structure. It was found that, terrace-truncated nanocone structured Al doped ZnO was grown successfully.*
- *Prepared samples were characterized by using FE-SEM images, X-ray diffraction patterns and UV-visible spectroscopy, atomic force microscopy and obtained the results. Electrical studies were done by four probe method.*

3.1. Al doped ZnO nanostructure at different growth temperatures.

3.1.1. Introduction

ZnO is an attractive semiconductor oxide material with wide band gap (3.37 eV), large exciting binding energy at room temperature (~60 meV), excellent thermal stability, splendid electron mobility and nontoxicity. ZnO is doped with impurities in order to improve the electrical conductivity and optical transmittance in the visible range. Al is widely used as a dopant of ZnO, due to its compatible ionic radius (0.05 nm) with the ionic radius of Zn (0.074 nm)[1-14]. Moreover, as the ionic radius of Al is smaller than Zn, the lattice distortion would be low when doping into ZnO. The growth temperature is a crucial factor, which determines the properties and structure quality of a nanostructure. Even though there are many techniques available to make impurity-doped ZnO nanostructures, we have used advanced spray pyrolysis deposition technique with rotational, pulsed and atomized function[15-23].

3.1.2. Experimental

Al doped ZnO samples were fabricated as described in section 2.1. The sample nomenclature of prepared Al doped ZnO samples at different growth temperature is shown in the table 3.1.

Table 3.1. Sample preparations at different growth temperatures.

Sample	Growth Temperature (ºC)
Al 300 ºC	300
Al 350 ºC	350
Al 400 ºC	400
Al 450 ºC	450

X-ray diffraction patterns, field emission scanning electron microscope images and optical transmittance data were used to characterize the prepared Al doped ZnO samples as described in section 2.3.

3.1.3. Results and discussion

Figure 3.1 shows the obtained XRD spectra of Al doped ZnO samples prepared at different growth temperatures. Significant peak around 34.37º in all samples, shows the growth of the nanostructure favoured in (002) direction of hexagonal wurtzite ZnO phase (JCPDS card No. 36-1451), which is along the c-axis, perpendicular to the glass substrate. All the other peaks are corresponding to FTO layer. The crystallite sizes were calculated by using Debye-Scherrer's formula, which is shown in Eq.1, based on (002) peak.

$$D = \frac{0.94\lambda}{\beta \cos\theta} \qquad (1)$$

Where D is the crystallite size, β is the peak broadening (FWHM), Θ is the Bragg's diffraction angle and λ is the wavelength of CuK_α radiation (λ= 1.5406 Å). Crystallite sizes are 27.4 nm, 26.7 nm, 27.9 nm, and 21.8 nm and FWHMs are 0.277, 0.284, 0.272, and 0.264 for Al 300 °C, Al 350 °C, Al 400 °C and Al 450 °C samples, respectively.

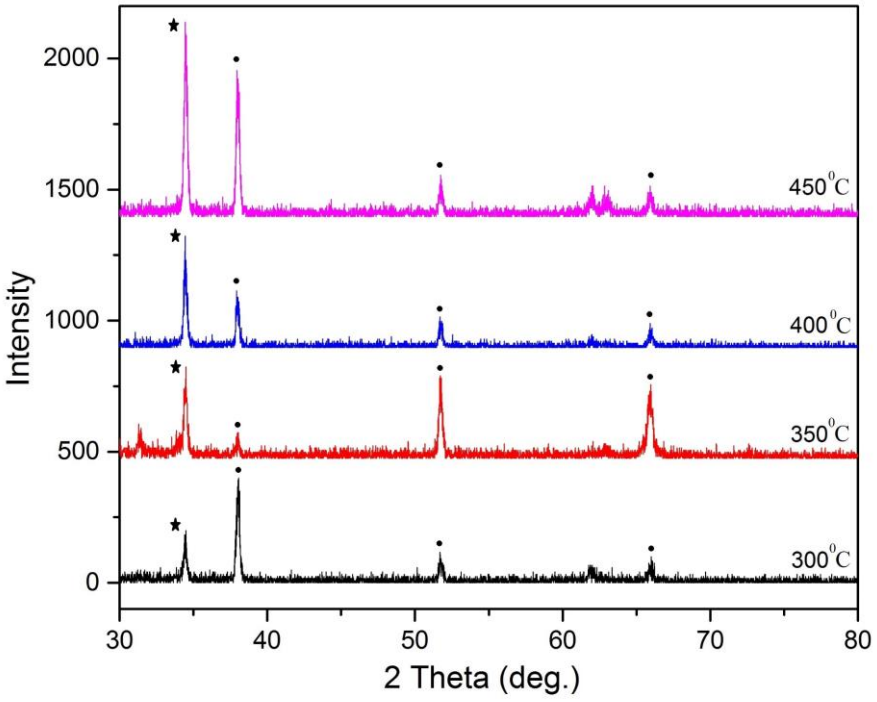

• : Peaks correpond to FTO layer ★ : Peaks correspond to Al - ZnO

Fig.3.1: X-ray diffractogram for Al doped ZnO samples at different growth temperatures.

Figure 3.2 shows the FE-SEM image of Al 300°C sample. The top diameter of the nanostructure is very low. There are many structural defects found (as shown in red color), as the growth temperature is not optimized. Moreover, the low diameter of nanostructure, allow them to grow, as they have much space in between them.

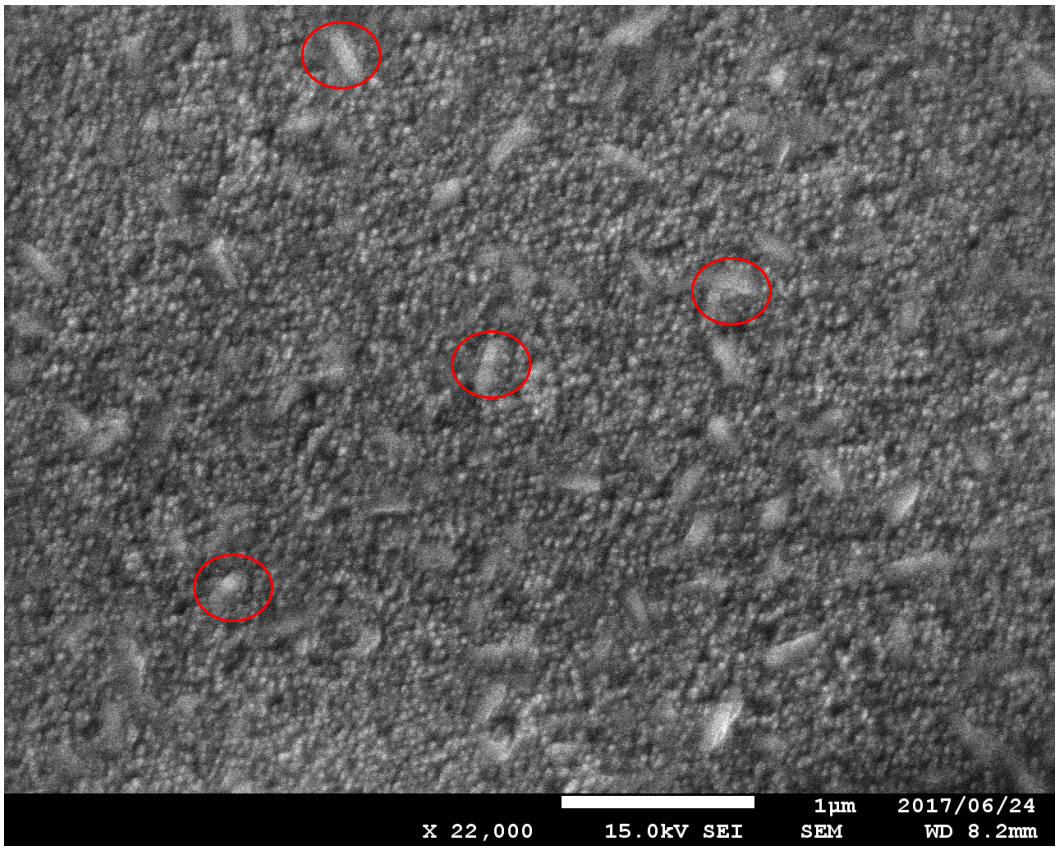

Fig.3.2: FE-SEM image of Al 300 °C sample.

Figure 3.3 shows the FE-SEM image of Al 350 ºC. Nanostructure diameter and density were ~ 40 nm and 381.4 per μm^2, respectively. However, agglomerated structures were identified (as shown in red color) in many regions. Figure 3.4 shows the FE-SEM image of Al doped ZnO prepared at 400 ºC. Nanostructure density was reduced with respect to 300 ºC and 350 ºC as the agglomerated structures were disappeared.

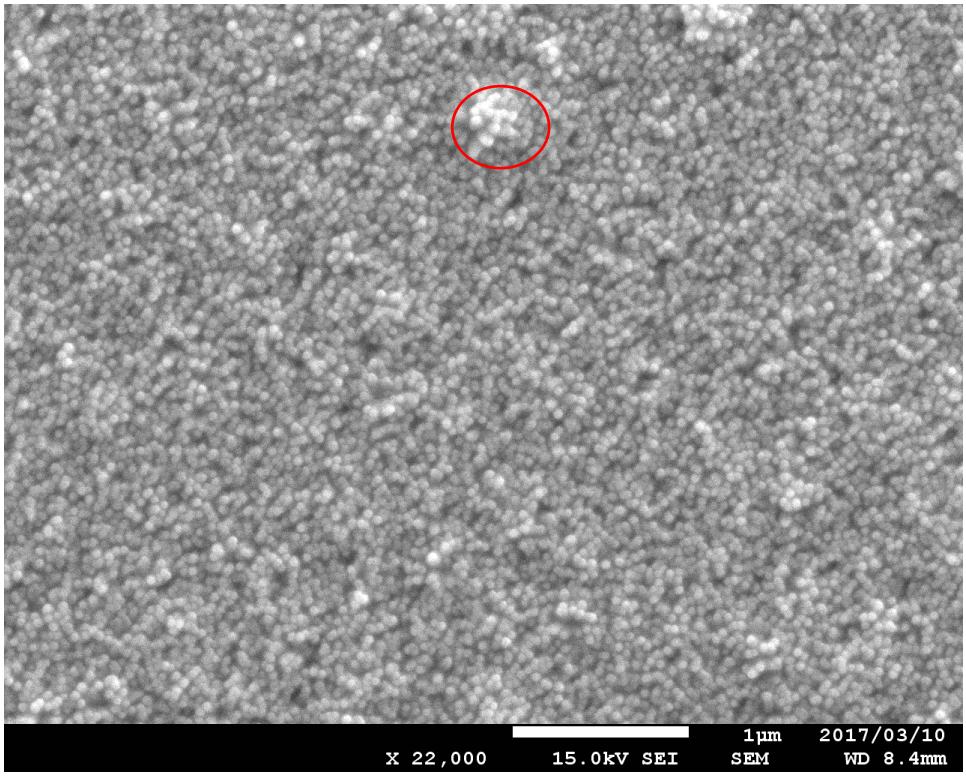

Fig. 3.3: FE-SEM image of Al 350 ºC sample.

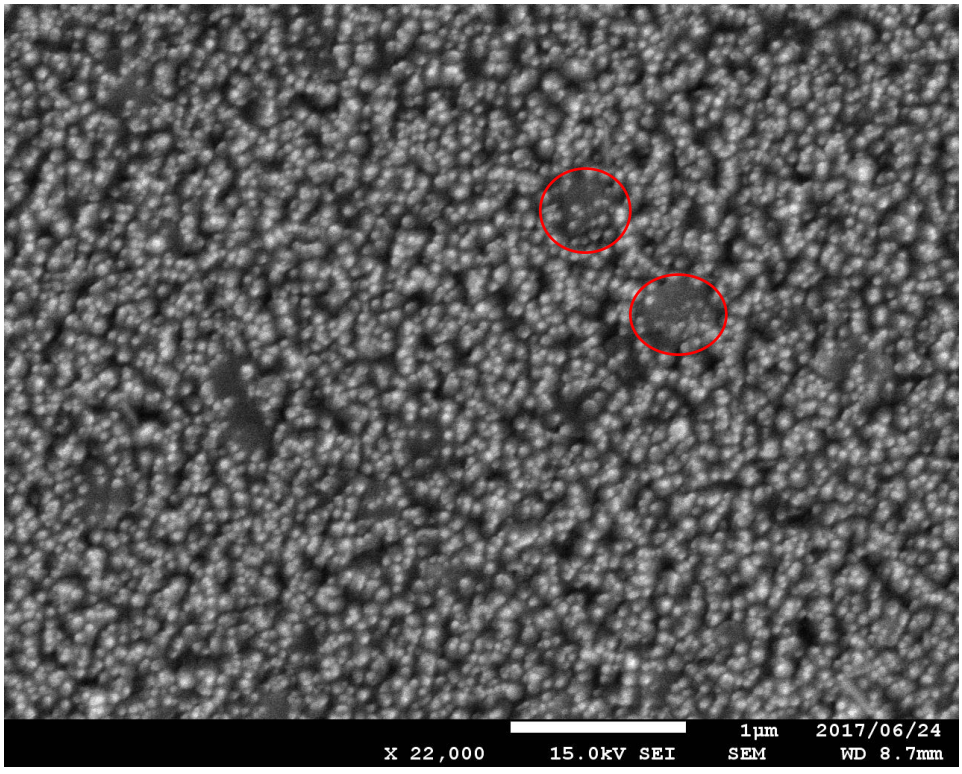

Fig.3.4: FE-SEM image of Al 400 ºC sample.

Top diameter was constant around 40 nm as obtained at Al 350 ºC sample, while the structure density reduced to 290.1 per μm^2. Plate-like structural defects were identified (as shown in red color) in some regions. Previous researches also have obtained same results of structural defects, when doping ZnO with Al. Figure 3.5 shows the FE-SEM images of Al doped ZnO nanostructure prepared at 450 ºC. Top diameter was increased up to 80 nm while the structure density reduced to 38.2 per μm^2. The top of the nanostructure seems to be sharpened. Many regions have plate-like structure (as shown in red color). Because of that, the nanostructure density is further decreases.

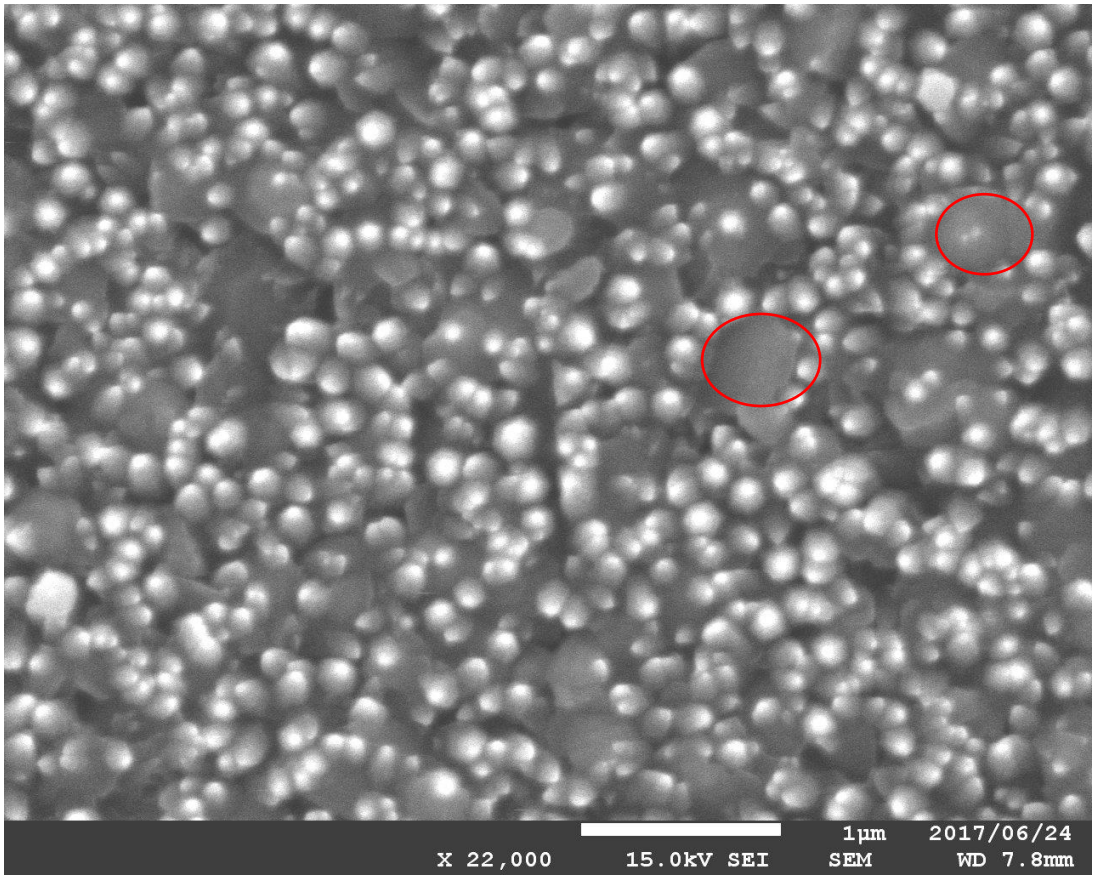

Fig. 3.5: FE-SEM image of Al 450 ºC sample.

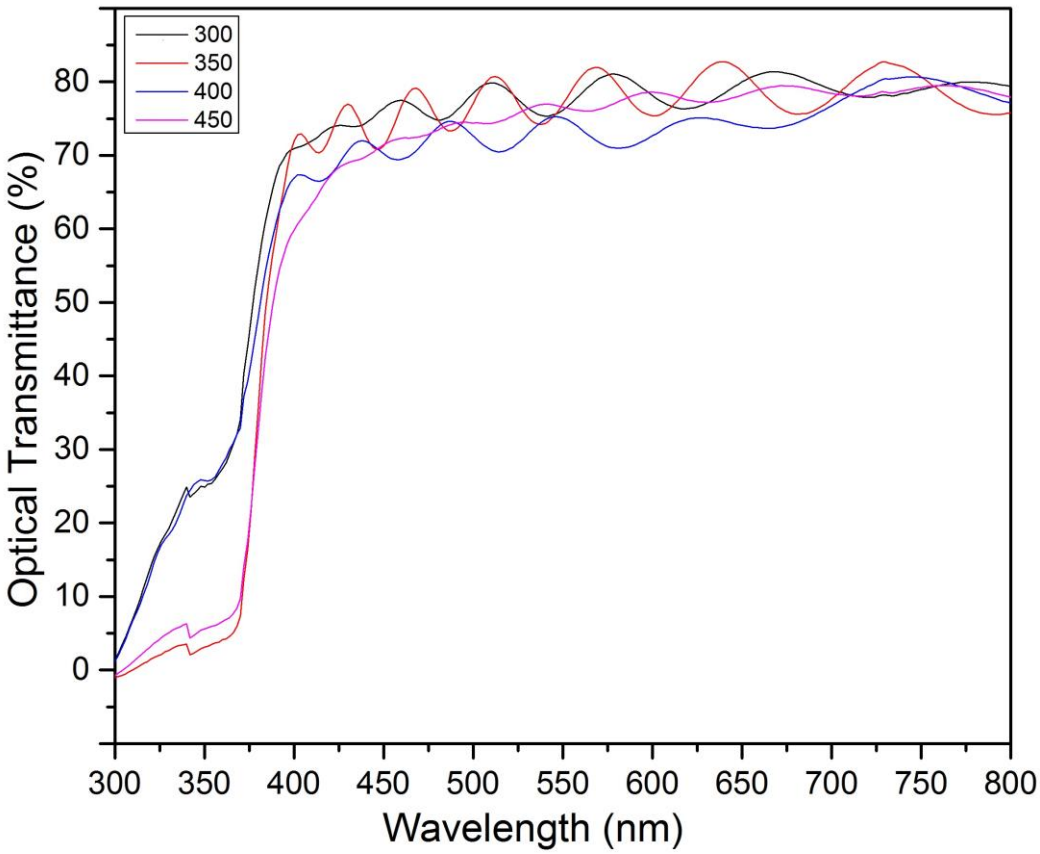

Fig. 3.6: Transmittance of the Al doped ZnO samples prepared at different growth temperatures.

Figure 3.6 shows the transmittance of Al doped ZnO at all different growth temperatures. All the samples show average optical transmittance around ~80 % in the visible range. There is a peak around 350 nm due to the change of the lamp of the UV-visible spectrometer, from deuterium to halogen. Below 370 nm of wavelength, the energy of the light is sufficient to overcome the band gap. Therefore, the light is not transmitted below 370 nm. On the other hand, the energy of the light is not sufficient to cross the energy gap at higher wavelengths (<370 nm). Because of that, the light is transmitting through the structure, without absorbing in higher wavelengths.

Conclusion

Properties of the Al doped ZnO nanostructures were severely dependent on the growth temperature. Crystallite size is fluctuating and the highest crystallinity was obtained at 400 ºC. The top diameter and average structure density were changed from ~40 nm and 381.4 per μm^2, ~ 40 nm and 290.1 per μm^2, 80 nm and 38.2 per μm^2 at 350 ºC, 400 ºC and 450 ºC, respectively. At 300 ºC and 450 ºC of growth temperature, plate-like structures were formed. When the growth temperature was 350 ºC, nanostructures were agglomerated. An excellent nanostructure with low structural defects with well separation was identified in the Al doped ZnO sample which was grown at 400 ºC. All the samples indicated high optical transmittance of ~ 80 %, in the visible range. Optimum transparent conductive properties were obtained for Al doped ZnO nanostructure grown at 400 ºC.

References

1. H. Cao, J. Y. Xu, D. Z. Zhang, S. H. Chang, S. T. Ho, E. W. Seeling, X. Liu,R. P. H. Chang,Phys. Rev. Lett. 2000, 84, 5584.
2. D. M. Bagnall, Y. F. Chen, Z. Zhu, T. Yao, S. Koyama, M. Y. Shen, T. Goto,Appl. Phys. Lett.1997, 70, 2230.
3. D. Canteli, S. Fernandez, C. Molpeceres, I. Torres, J. J. Ganda, Appl. Surf. Sci. 2012, 258, 9447-9451.
4. Y.H. Kima, J. Jeong, K.S. Lee, B. Cheong, T.Y. Seong, W.M. Kim, Applied Surface Science, 2010, 257, 109.
5. . Kima, J. Jeong, K.S. Lee, B. Cheong, T.Y. Seong, W.M. Kim, Applied Surface Science 2010, 257, 109.
6. K.C. Lai, C.C. Liu, C. Lu, C.H. Yeh, M.P. Houng, Solar Energy Materials and Solar Cells. 2010, 94, 397.
7. B. Rech, T. Repmann, S. Wieder, M. Ruske, U. Stephan, Thin Solid Films. 2006, 502, 300.
8. W.J. Jeong, S.K. Kim, G.C. Park, Thin Solid Films. 2006, 180, 506.
9. M. Benetti, D. Cannatá, F. Di Pietrantonio, E. Verona, P. Verardi, N. Scarisoreanu, D. Matei, G. Dinescu, A. Moldovan, M. Dinescu, Superlattices and Microstructures. 2006, 39, 366.
10. H. Xu, X. Liu, D. Cui, M. Li, M. Jiang, Sensors and Actuators B. 2006, 114, 301.
11. T. Mizuta, T. Ishibashi, T. Minemoto, H. Takakura, Y. Hamakawa, Thin Solid Films. 2006, 515, 2458.
12. Ü. Özgür, Ya.I. Alivov, C. Liu, A. Teke, M.A. Reshchikov, S. Dogan, ˘ V. Avrutin, S.J. Cho, H. Morkoc¸ , Journal of Applied Physics, 2005, 98, 041301.
13. L.J. Mandalapu, F.X. Xiu, Z. Yang, J.L. Liu, Solid-State Electronics.2007, 51, 1014.
14. B.D. Ahn, S.H. Oh, D.U. Hong, D.H. Shin, A. Moujoud, H.J. Kim, Journal of Crystal Growth. 2008, 310, 3303.
15. H.C. Park, D. Byun, B. Angadi, D.H. Park, W.K. Choi, J.W. Choi, Y.S. Jung, Journal of Applied Physics.2007, 102, 073114.

16. V. Assuncao, E. Fortunato, A. Marques, H. Aguas, I. Ferreira, M.E.V. Costa, R. Martins, Thin Solid Films. 2003, 427, 401.
17. S. Fay, U. Kroll, C. Bucher, E. Vallat-Sauvain, A. Shah, Solar Energy Materials and Solar Cells. 2005, 86, 385.
18. J.H. Kim, B.D. Ahn, C.H. Lee, K.A. Jeon, H.S. Kang, S.Y. Lee, Journal of Applied Physics. 2006, 100, 113515.
19. N. Bouhssira, S. Abed, E. Tomasella, J. Cellier, A. Mosbah, M.S. Aida, M. Jacquet, Applied Surface Science. 2006, 252, 5594.
20. S.H. Mohamed, R. Drese, Thin Solid Films. 2006, 513, 64.
21. B. Joseph, P.K. Manoj, V.K. Vaidyan, Ceramics International. 2006, 32, 487.
22. A.R.Babar, P.R. Deshamukh,R.J. Deokate, D.Haranath,C.H.Bhosale,K.Y.Rajpure, Journal of Physics D: Applied Physics. 2008, 41, 135404.
23. T. Prasada Rao, M.C. Santhosh Kumar, Journal of Alloys and Compounds. 2010, 506, 788.

3.2. Al doped ZnO nanostructure with different doping concentrations.

3.2.1 Introduction

Even though ZnO has unique properties to use as transparent conductive oxide (TCO) material, impurity doped ZnO is vastly used in many researches to improve the electrical conductivity and optical transparency in the visible range[1-12]. Al is a major dopant for ZnO due to its' compatible ionic and covalent radii with Zn. When doping, Al is substituted for Zn atoms in hexagonal wurtzite nanostructure. Every substituted Al atom gives extra free electrons to the conduction band, which reduce the electrical resistivity. In general, the high conductivity of Al doped ZnO is attribute to Al^{3+} ions in substitutional sites and interstitial sites of zinc sites and oxygen vacancies. Moreover, the optical transparency increased due to the optical bandgap change which could be described by Burstein-Moss effect. Al is mostly used as a dopant to obtain an excellent stability at high temperature, transparency and conductivity, non-toxicity and high availability[13-39]. The bond energy of Zn-O and Al-O are 159 ± 4 kJ and 511 ± 3 kJ, respectively[40]. Al doped ZnO was synthesized by various types of deposition techniques. Many researchers have reported that the properties of Al doped ZnO is highly dependent on the deposition technique[41-50]. In this part we are investigating about optimum doping concentration of Al with ZnO.

3.2.2. Experimental

Al doped ZnO samples were fabricated as described in section 2.1. The sample nomenclature of prepared Al doped ZnO samples at different doping concentrations is shown in table 3.2.

Table 3.2. Sample preparations with different doping concentrations.

Sample	Growth Temperature (ºC)	Al to Zn Ratio
Al (400 ºC) 1%	400	1:99
Al (400 ºC) 2%	400	2:98
Al (400 ºC) 3%	400	3:97
Al (400 ºC) 4%	400	4:96

X-ray diffraction patterns, field emission scanning electron microscope images and optical transmittance data were used for characterization of prepared Al doped ZnO samples as described in section 2.3.

3.2.3 Results and discussion

Figure 3.7 shows the obtained XRD patterns of Al doped ZnO samples prepared at different doping concentrations. Significant peak around 34.37º in all samples shows the growth of nanostructure favoured in (002) direction of hexagonal wurtzite ZnO phase (JCPDS card No. 36-1451), which is along the c-axis, perpendicular to the substrate. All other peaks correspond to FTO layer. The crystallite sizes are calculated from using Debye- Scherrer's formula, as shown in Eq.1, based on (002) peak.

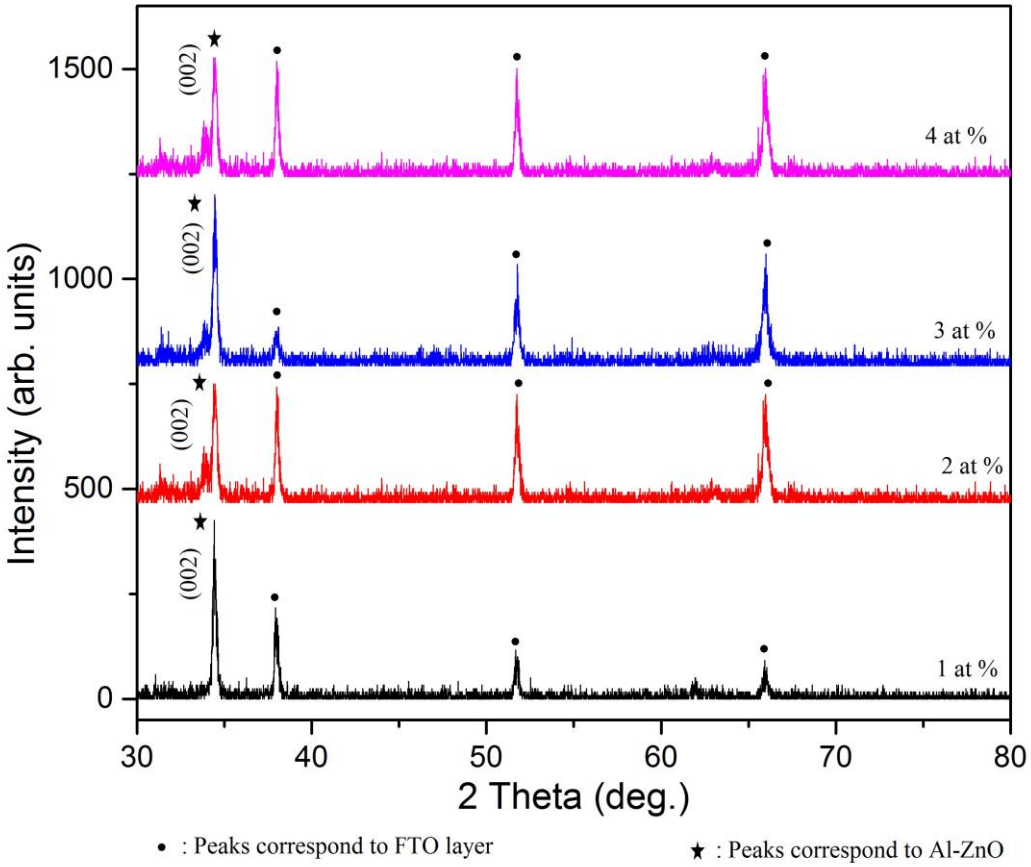

Fig.3.7: X-ray diffractogram for Al doped ZnO samples at different doping concentrations.

Calculated crystallite sizes were 30.6, 28.5, 27.8 and 26.8 nm and FWHMs were 0.272, 0.292, 0.300 and 0.313 for Al (400 ºC) 1%, Al (400 ºC) 2%, Al (400 ºC) 3% and Al (400 ºC) 4% samples, respectively. Figure 3.8 shows the FE-SEM image of Al (400 ºC) 1% sample. The

average top diameter and average structure density were ~ 40 nm and 290.1 per μm^2. There are many plate-like structural defects found in between nanostructures (as discussed in chapter 3.1-fig 3.4). Figure 3.9 shows the FE-SEM image of Al (400 ºC) 2% sample. Nanostructure with low structural defects was observed at this doping level. Average top diameter was 66.2 nm while the average nanostructure density was 250.9 per μm^2. Enlargement of structure density was observed as a result of increase of number of nucleation sites when adding more Al atoms.

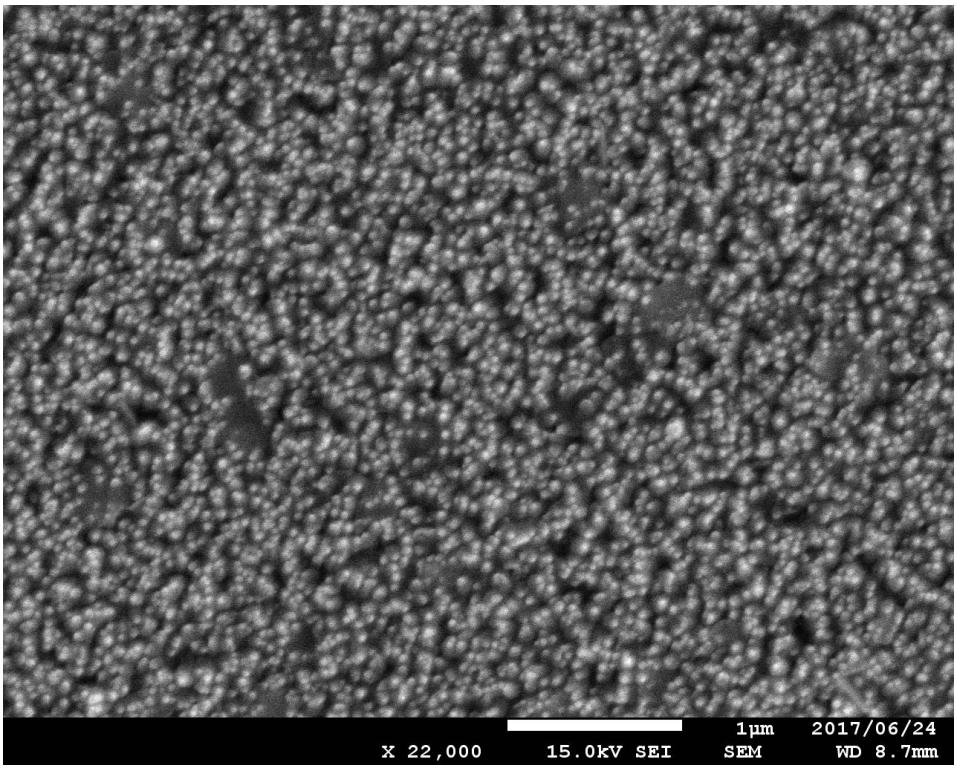

Fig. 3.8: FE-SEM image of Al (400 ºC) 1% sample.

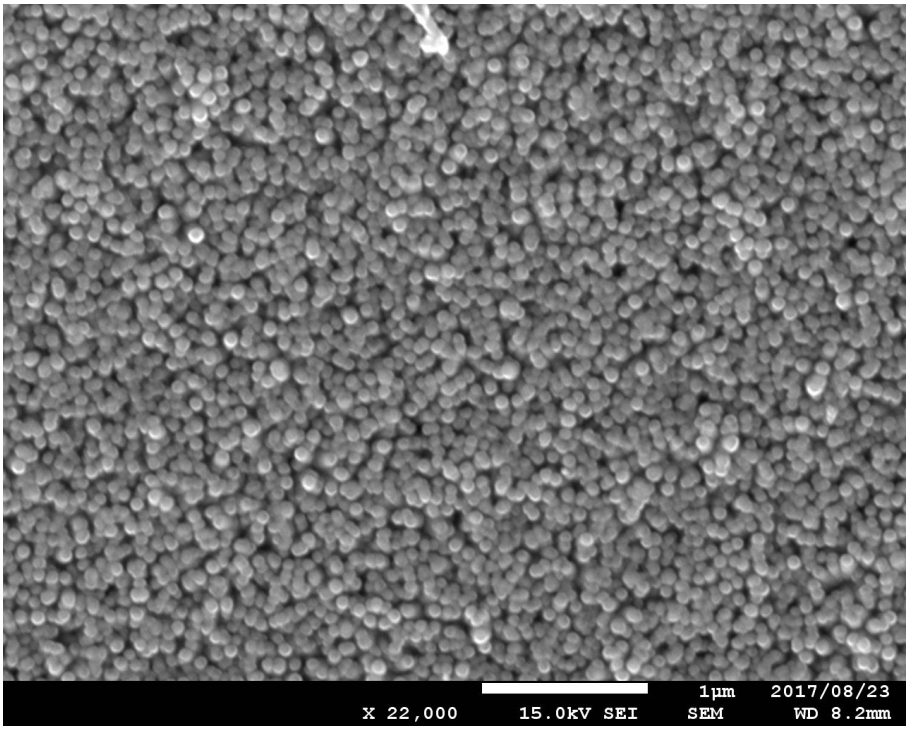

Fig. 3.9: FE-SEM image of Al (400 ºC) 2% sample.

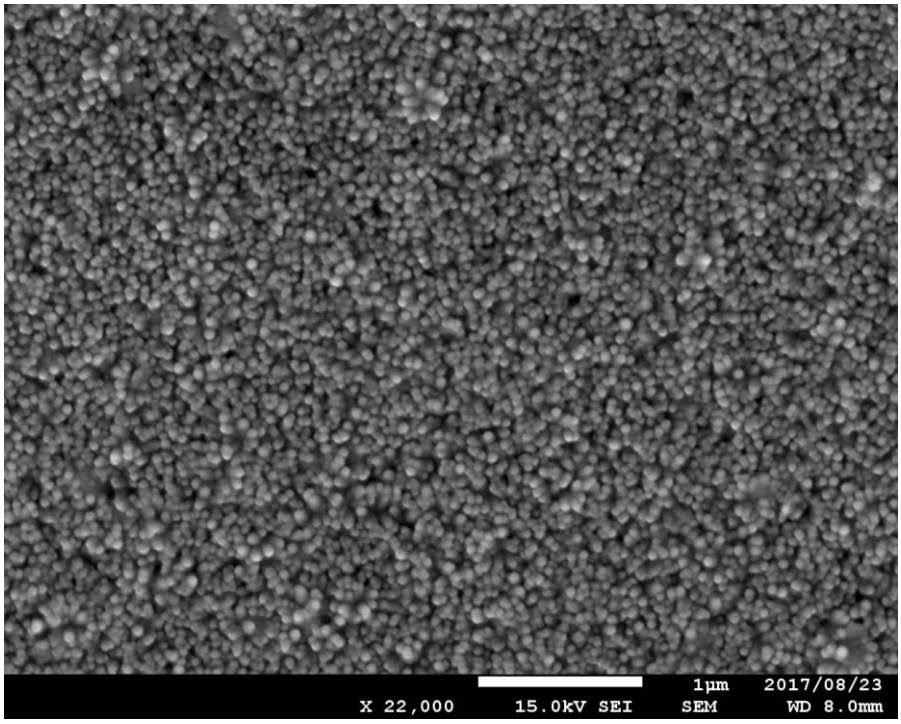

Fig. 3.10: FE-SEM image of Al (400 ºC) 3% sample.

Figure 3.10 shows the FE-SEM image of Al (400 ºC) 3% sample. Agglomerated nanostructures were started to increase. Average top diameter was reduced to 49.2 nm while average structure

density was increased up to 390.3 per μm^2. Figure 3.11 shows the FE-SEM images of Al (400 ºC) 4% sample. Nanostructures were highly agglomerated (as shown in red circles) with each other due to high doping concentration. Average top diameter was reduced to ~30 nm.

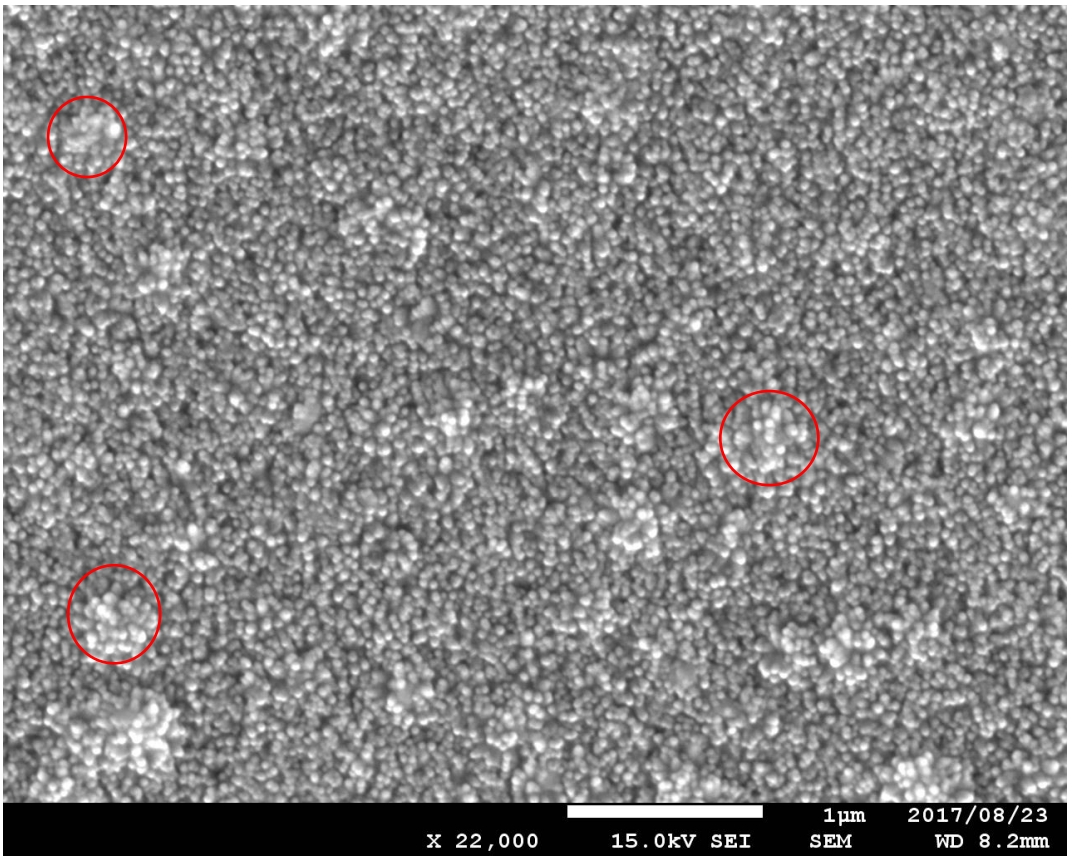

Fig. 3.11: FE-SEM image of Al (400 ºC) 4% sample.

Figure 3.12 shows the UV-visible spectra of Al doped ZnO at all different Al concentrations. 74.2, 78.8, 78.0 and 78.8 % of optical transmittance in the visible range were shown in Al (400 ºC) 1%, Al (400 ºC) 2%, Al (400 ºC) 3% and Al (400 ºC) 4% samples, respectively. Around 350 nm absorption edges were obtained as the light source of UV-visible spectrometer was change from deuterium (185 – 400 nm), to halogen (Tungstein: 350 – 3000 nm). When Al doped to ZnO, the band gap is increases according to the Burstien-Moss effect as shown in fig. 3.12. As the band gap is increases, transparency is increasing.

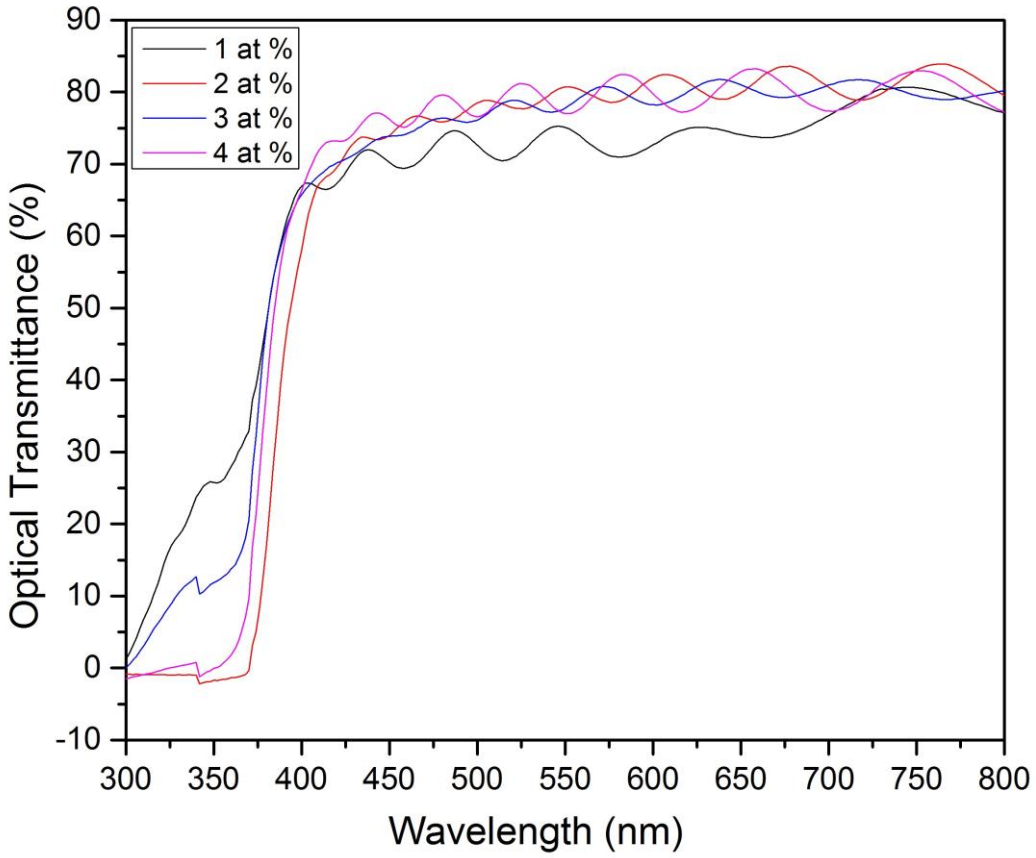

Fig. 3.12: UV-Visible spectra of Al doped ZnO at all different Al concentrations.

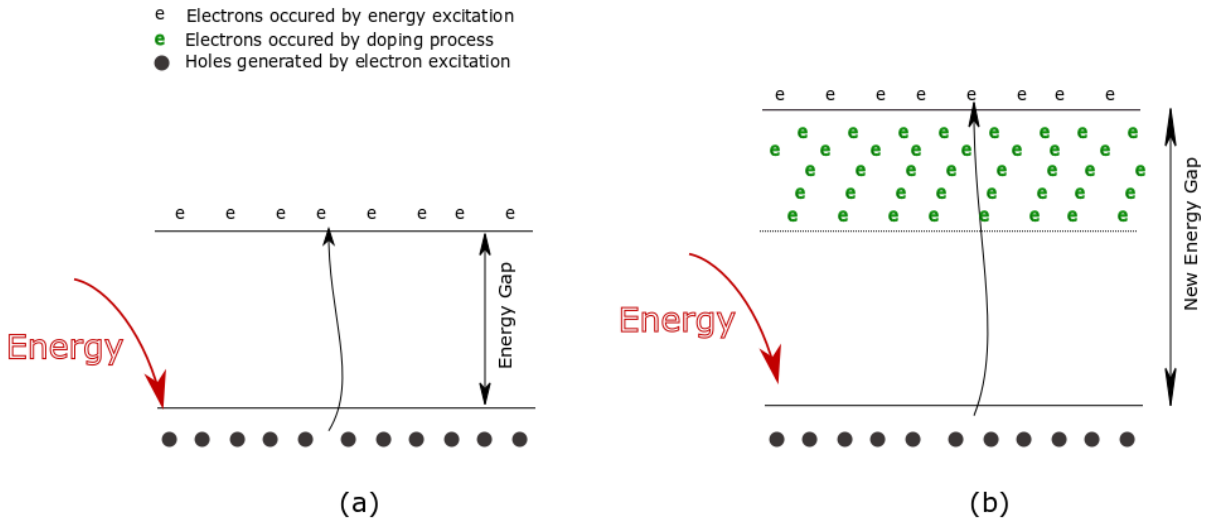

3.13: Burstein-Moss effect (a) before doping, (b) After doping.

Conclusion

The properties of the Al doped ZnO nanostructures were vastly dependent on the doping concentration. The average top diameters were ~40, 66.2, 49.2 and ~ 30 nm for 1 at %, 2 at %, 3 at % and 4 at % of Al to Zn ratio, respectively. The highest nanostructure density was obtained at 4 at % of Al doping while the lowest value was obtained in 2 at % of Al doping. An excellent nanostructure with lowest number of structural defects was obtained at 2 at % of Al doping. Highest optical transmittance in the visible range was also found when Al to Zn ratio changed to 2 at %.

References

1. J. Bao, M. A. Zimmler, F. Capasso, X. Wang, Z. F. Ren, Nano Lett. 2006, 6, 1719.
2. H. C. Cheng, C. F. Chen and C. Y. Tsay, Appl. Phys. Lett. 2007, 90, 012113.
3. P. P. Sahay and R. K. Nath, Sens. Actuators B 2008, 133, 222.
4. J. Xu, C. Yuping, L. Yadong and S. Jianian, J. Mater. Sci. 2005, 40, 2919.
5. Mahroug A, Boudjadar S, Hamrit S and Guerbous L, Mater. Lett. 2014, 134, 248.
6. Selmi M, Chaabouni F, Abaab M, Rezig B, Superlattices and Microstructures 2008, 44, 268.
7. Jang K, Park H, Jung S, Duy NV, Kim Y, et al. Thin Solid Films 2010, 518, 2808.
8. Kluth, B. Rech, L. Houben, S. Wieder, G. Scho¨pe, C. Beneking, H. Wagner, A. Lo¨ffl, H.W. Schock, Thin Solid Films 1999, 351, 247.
9. Z.-C. Jin, I. Hamberg, C.G. Granqvist, B.E. Sernelius, K.-F. Berggren, Thin Solid Films 1988, 164, 381.
10. J. Yoo, J. Lee, S. Kim, K. Yoon, I. Jun Park, S.K. Dhungel, B. Karunagaran, D. Mangalaraj, Y. Junsin, Thin Solid Films 2005, 480–481, 213.
11. T. Shiosaki, M. Adachi, A. Kawabata, Thin Solid Films 1982, 96, 129.
12. T. Sergiu, S. Teodor, I. Shishiyanu, Oleg Lupan, Sens. Actuators B 2005, 107, 379.
13. M. Jin, Ji Feng, Ma Hong-lei, Li Shu-ying, Solar energy materials & Solar Cells 2010, 60, 341.
14. S.S. Lina, J.L. Huanga, P. Sajgalik, Surface & Coatings Technology 2005, 190, 39.
15. N. Gupta, G.F. Alapatt, R. Podila, R. Singh, K.F. Poole, Int. J. Photoenergy, 2009, 10, 1155.
16. F. Maldonado, A. Stashans, J. Phys. Chem. Solids 2010,71, 784.
17. P. Raghu, N. Srinatha, C.S. Naveen, H.M. Mahesh, B. Angadi, J. Alloys Compd. 2017, 694, 68.

18. H. Serier, M. Gaudon, M. Menetrier, Solid State Sci. 2009, 11, 1192.
19. A. Verma, F. Khan, D. Kar, B. C. Chakravarty, S. N. Singh, M. Husain, Thin Solid Films 2010, 518, 2649.
20. T. Ogi, D. Hidayat, F. Iskandar, A. Purwanto and K. Okuyama, Adv Powder Technol. 2009, 20, 203.
21. E. Hamarberg, A. P. Schwab and C. Feldmann, J. Colloid. Interface Sci. 2009, 334, 29.
22. B. Baruwati, D. K. Kumar, S. V. Manorama, Sens. Actuators B 2006, 19, 676.
23. K. V. Gurav, V. J. Fulari, U. M. Patil, C. D. Lokhande, O. Joo, Appl. Surf. Sci. 2010, 256, 2680.
24. S. H. Jeong, B. N. Park, D. G. Yoo, J. H. Boo, J. Korean Phys. Soc. 2007, 50, 622.
25. J. Nishino, S. Ohshio, K. Kamata, J. Am. Ceram. Soc. 1992, 75, 3469.
26. B. Chatpong, C. Krisana, P. Wisanu, T. Wicharn, Sains Malaysiana, 2013, 42(2), 239.
27. Li Q. H, Zhu D, Liu W, Liu Y, Ma X. C, Appl. Surface Sci. 2008, 254, 2922.
28. H. Kim, J. S. Horwitz, G.P. Kushto, Z. H. Kafa, D. B. Chrisey, Appl. Phys. Lett. 2001, 79, 284.
29. J.H. Lee, B. O. Park, Mater. Sci. Eng. B 2004, 106, 242.
30. K. Ellmer, F. Kudella, R. Mientus, R. Schieck, S. Fiechter, Thin Solid Films 1994, 247, 15.
31. J.H. Lee, B. O. Park, Thin Solid Films 2003, 426, 94.
32. E.M. Wong, P.C. Season, Appl. Phys. Lett. 1999, 74, 2939.
33. A. Leenheer, J. Perkins, M. van Hest, J. Berry, R. O'Hayre, D. Ginley, Phys. Rev. B 2008 77, 115215.
34. Bhosle V, Tiwari A, Narayan J, Appl. Phys. Lett. 2006, 88, 032106.
35. D. Kim, I. Yun, H. Kim, Curr. Appl. Phys. 2010, 10, S459.

36. J. Steinhauser, S. Faÿ, N. Oliveira, E. Vallat-Sauvain, C. Ballif, Appl. Phys. Lett. 2007, 90, 142107.

37. Q.Y. Fu, S. Hao, B. Shen et al, Res. Chem. Intermed. 2013, 39, 527.

38. B. Benhaoua, A. Rahal, S. Benramache, Superlattice Microst. 2014, 68, 38.

39. M.H. Mamat, M.Z. Zahdan, S. Amizam, H. A. Rafaie, Z. Khusaimi, M. Rusop, J. CERAM. SOC. JPN. 2009, 117 (11), 1263.

40. Tanusevskia A, Georgieva V, Appl Surface Sci. 2010, 19964.

41. J. Hüpkes, B. Rech, S. Calnan, O. Kluth, U. Zastrow, H. Siekmann, M. Wuttig, Thin Solid Films 2006, 502, 286.

42. J.L. Zhao, X.M. Li, J.M. Bian, W.D. Yu, X.D. Gao, Structural, J. Cryst. Growth 2005, 276, 507.

43. K.E. Lee, M. Wang, E.J. Kim, S.H. Hahn, Curr. Appl. Phys. 2009, 9, 683.

44. D. Kim, I. Yun, H. Kim, Curr. Appl. Phys. 2010, 10, S459.

45. R. Ayouchi, D. Leinen, F. Martin, M. Gabas, E. Dalchiele, J.R. Ramos-Barrado, Thin Solid Films 2003, 426, 68.

46. Y.H. Kim, K. Lee, T.S. Lee, B.k. Cheong, T.Y. Seong, W.M. Kim, Curr. Appl. Phys. 2010, 10, S278.

47. D.J. Kwak, J.H. Kim, B.W. Park, Y.M. Sung, M.W. Park, Y.B. Choo, Curr. Appl. Phys. 2010, 10, S282.

48. S.H. Lee, J.H. Jung, S.H. Kim, D.K. Lee, C.W. Jeon, Curr. Appl. Phys. 2010, 10, S286.

49. K.U. Sim, S.W. Shin, A.V. Moholkar, J.H. Yun, J.H. Moon, J.H. Kim, Curr. Appl. Phys. 2010, 10, S463.

50. J. Kim, M.C. Kim, J. Yu, K. Park, Curr. Appl. Phys. 2010, 10, S495.

3.3 Al doped ZnO nanostructure at different spray angles.

3.3.1 Introduction

Studies on TCO materials have attracted many research groups due to their wide range of applications in research and industrial fields such as solar cells, liquid crystal displays (LCDs), light emitting diodes (LEDs) and organic photovoltaics (OPVs) and display devices. Several researches have been conducted on deposition of Al-doped ZnO by various deposition techniques, such as chemical bath, spray pyrolysis, magnetron sputtering, chemical vapor deposition, molecular beam epitaxy and pulsed laser deposition[1-21]. Among them, the spray pyrolysis deposition technique is attractive due to its simplicity, low cost, no need of vacuumed environment and high productivity on large scale[22,23]. In this research, we have used advanced spray pyrolysis deposition technique of rotational, pulsed and atomized (RPASP). Few researches have been conducted about the spray angle dependence for the growth of nanostructure. However, there was no proper study has explained the growth and growth mechanism while changing the spray angle. In this chapter we investigate about the spray angle dependence for the growth of Al doped ZnO nanostructure with high TCO properties.

3.3.2. Experimental

Al doped ZnO samples were fabricated as described in section 2.1. The sample nomenclature of prepared Al doped ZnO samples at different spraying angles is shown in table 3.3.

Table 3.3. Spraying angles of Al-doped ZnO samples

Sample	Growth Temperature (ºC)	Al:Zn Ratio	Spraying Angle
Al (400 ºC/2%) 15º	400	2:98	15º
Al (400 ºC/2%) 30º	400	2:98	30º
Al (400 ºC/2%) 45º	400	2:98	45º

X-ray diffraction patterns, field emission scanning electron microscope images, optical transmittance spectra, atomic force microscopy images, and hall mobility values were used to characterize the prepared Al doped ZnO samples as described in section 2.3.

3.3.3 RESULTS AND DISCUSSION

Figure 3.14 shows the XRD patterns of Al-doped ZnO samples at different spraying angles. The significant peak around 34.37° evidenced for the growth of nanostructure was along the (002) direction (JCPDS card No. 36-1451) of hexagonal wurtzite structure, which is along the c-axis, perpendicular to the glass substrate. The peaks correspond to FTO layer are shown by "•". Crystallite sizes were calculated by Debye-scherre's formula, which are shown in Eq.1. FWHM, crystallite sizes for each sample, are tabulated in Table 3.4. Minimum crystallite size was observed in Al (400 ºC/2%) 30º sample. There was no significant difference of crystallite sizes in Al (400 ºC/2%) 15º and Al (400 ºC/2%) 45º samples.

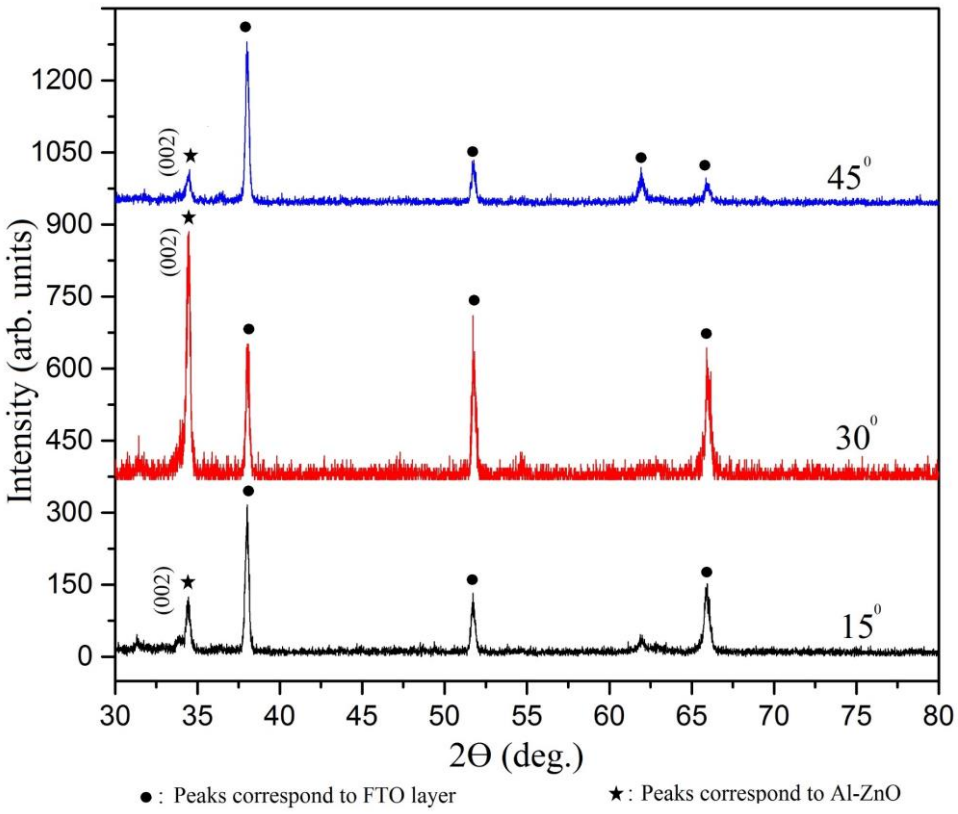

Fig. 3.14: X-ray diffraction patterns of Al-ZnO samples at different spraying angles.

Figure 3.15(a) shows the FE-SEM image of Al (400 ºC/2%) 45º sample with typical hexagonal shaped nanostructure. The average top diameter and average structure density were 31.1 nm and 78 per μm^2 respectively. Plate-like structural defects (shown by red color circles) could be identified in in some regions, which covers the nanostructures. These plate structures might reduce the optical transmittance as they disturb the propagation of the photon. On the other hand, it might increase the electrical conductivity as it increases the horizontal propagation of electrons. Figure 3.15 (b) shows the FE-SEM images obtained on Al (400 ºC/2%) 30º sample. The nanostructure was improved when decreasing the spray angle as the structural defects were reduced. However, flower-like structures and some agglomerated nanostructures (shown by red color circles) are hackneyed in the thin film. The average top diameter was 34.0 nm and the average structure density were 55.4 per μm^2.

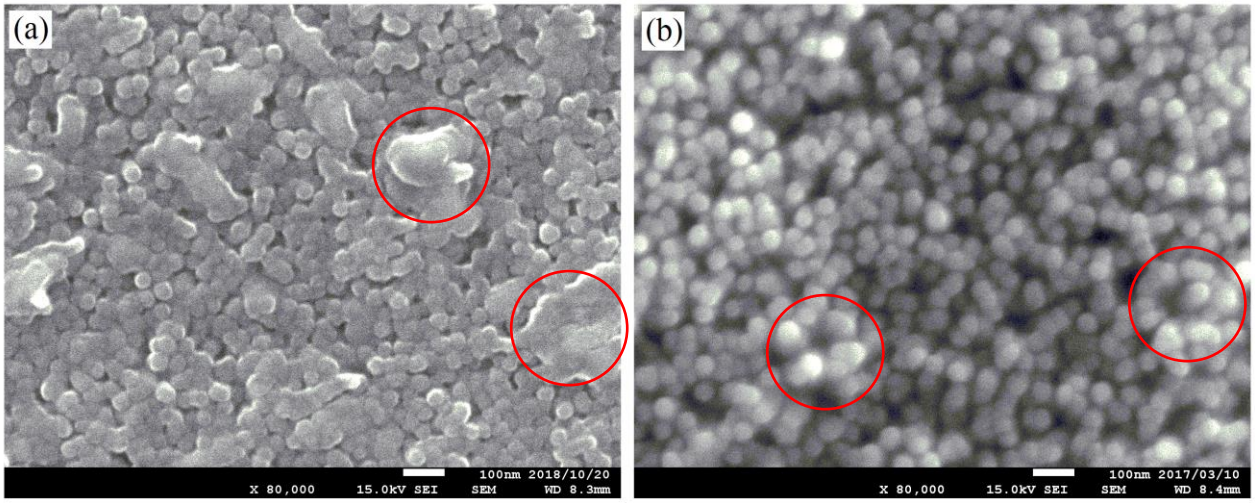

Fig. 3.15: FE-SEM images of, (a) Al (400 ºC/2%) 45º, (b) Al (400 ºC/2%) 30º.

Table 3.4. Calculated crystal size, and FWHM for Al-doped ZnO thin films

Sample	Crystallite Size (nm)	FWHM
Al (400 ºC/2%) 15º	31.16	0.267
Al (400 ºC/2%) 30º	28.44	0.292
Al (400 ºC/2%) 45º	31.61	0.263

Figure 3.16 shows the FE-SEM image of Al (400 ºC/2%) 15º sample, which has hexagonal wurtzite nanostructure. The average top diameter and the average structure density were 29.9 nm and 86.2 per μm^2, respectively. According to the FE-SEM images, an excellent nanostructure with high homogeneity and low structural defects were obtained, when spraying angle was posed at the minimum value.

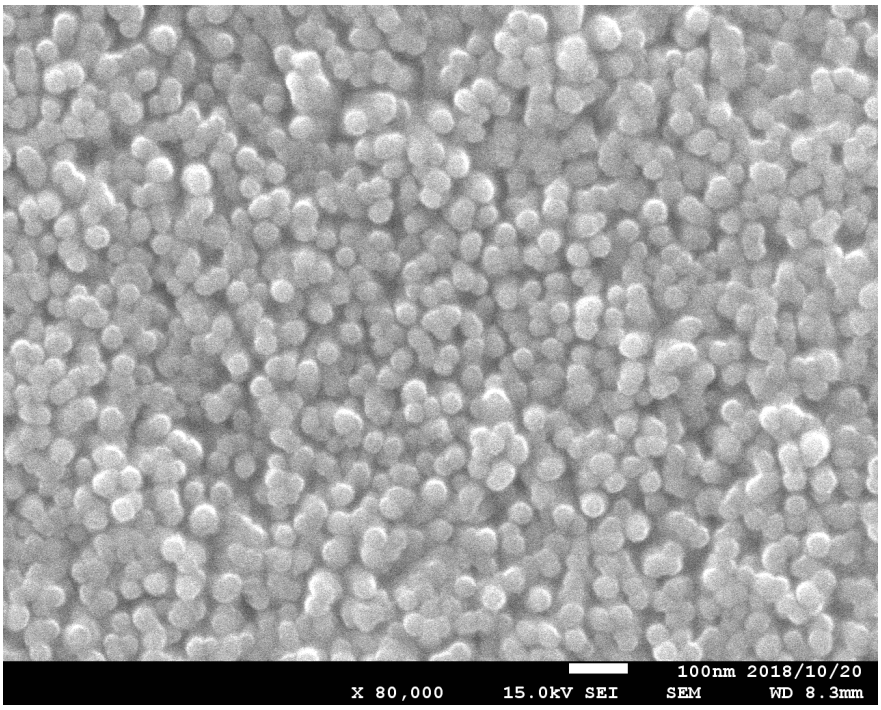

Fig. 3.16: FE-SEM images of Al-doped ZnO thin films at the spray angle of 15º.

Many structural differences of Al doped ZnO samples were found, by changing the spraying angle. This happens due to the changes of horizontal and vertical component of velocity in each spraying angle. Fig 3.17 illustrates the projectile of a particle at each spraying angle. At lower spraying angles particles travels longer distance horizontally direction and shorter vertically. Because of this phenomenon, particles disperse and spread all over the glass substrate and finally come up with a good homogeneous structure. On the other hand, at higher spraying angles particles travels longer distance vertically and shorter distance horizontally, and spraying area become narrow. The vaporized particles drop on each other and finally make plate like structures at the top. According to the FE-SEM images of Al (400 ºC/2%) 45º sample, these plate-like structure can be identified clearly.

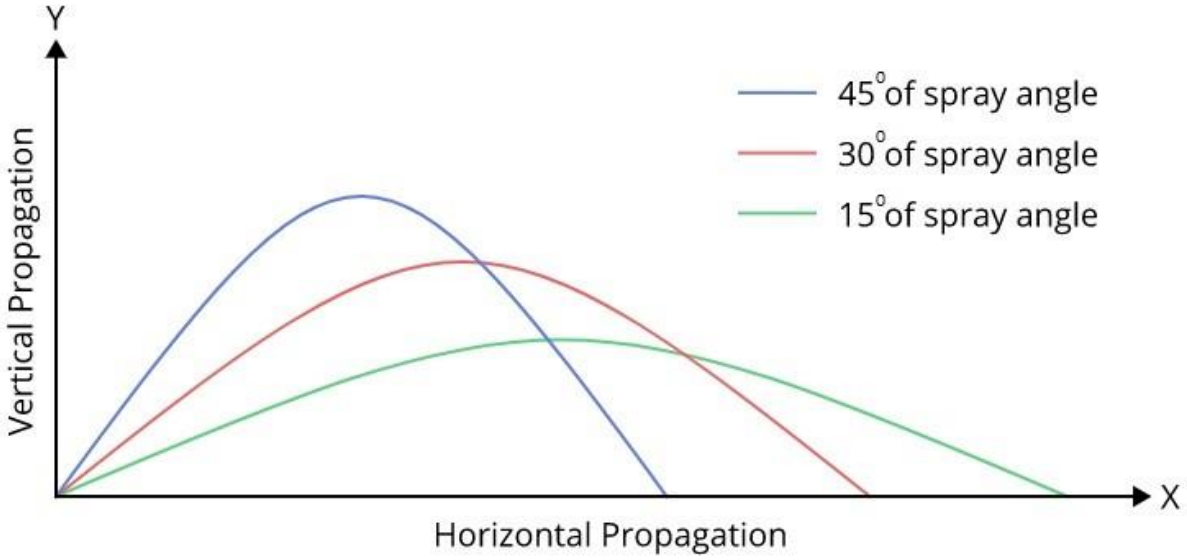

Fig. 3.17: The projectile movement of a particle at each spraying angle

However, the nanostructure couldn't be clarified by SEM images at this stage of the research as the height of the nanostructure is low. Figure 3.18 shows the EDX spectrum of Al (400 ºC/2%) 15º sample. Zn L_α peak at 1.012 keV, Zn K_α peak at 8.637 keV, Sn L_α peak at 3.444 keV, O K_α peak at 0.525 keV and Al K_α peak at 1.486 keV were found in EDX spectrum. The peak at 1.486 keV evidenced the successful doping of Al into ZnO crystal structure.

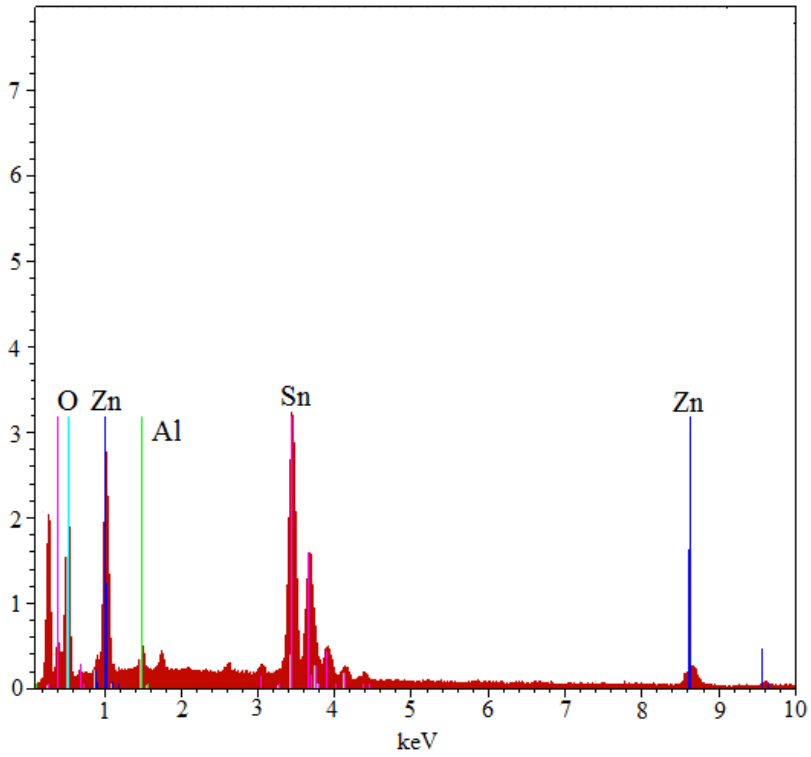

Fig. 3.18: EDX spectrum of Al (400 ºC/2%) 15º.

Figure 3.19 (a) shows the AFM images taken on Al (400 ºC/2%) 15º sample. Line profile and line histogram are shown in fig. 3.19 (b) and 3.19 (c), respectively. The surface roughness and the mean height was 57.9 and 175.5 nm, respectively.

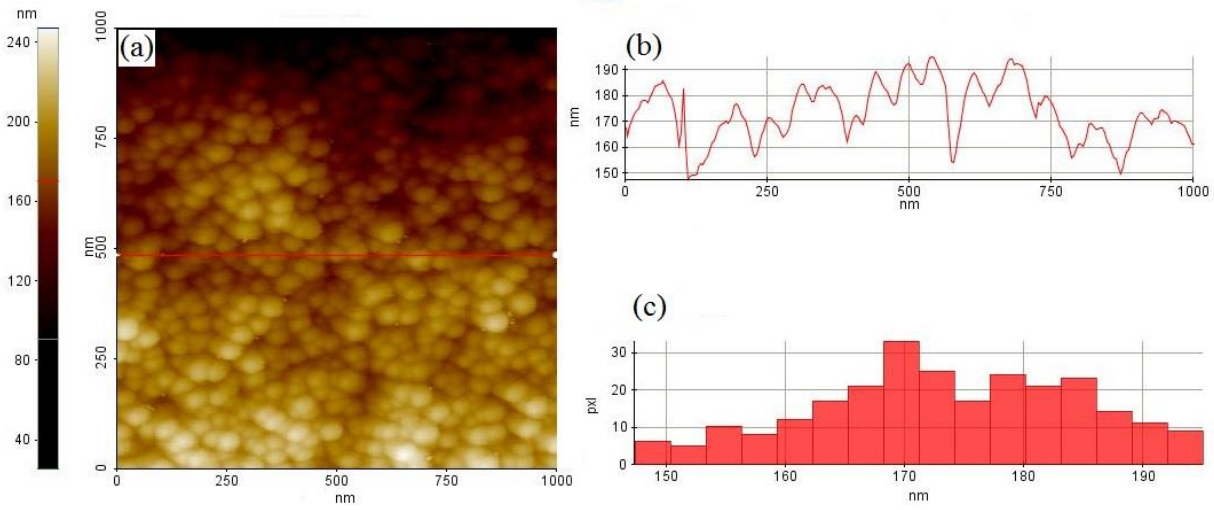

Fig. 3.19: (a) AFM image, (b) Line profile, (c) Line histogram, Al (400 ºC/2%) 15º sample.

Figure 3.20 shows the UV visible spectra, examined 300-800 nm. 80.3 %, 78.8 % and 78.1 % of optical transmittance were obtained for Al (400 ºC/2%) 15º, Al (400 ºC/2%) 30º and Al (400 ºC/2%) 45º samples, respectively. Due to structural defects and highly compact nanostructure, the optical transmittance was found to be minimum in Al (400 ºC/2%) 45º sample as expected. On the other hand, the highest transmittance at visible range was obtained in Al (400 ºC/2%) 15º sample, at 15° spray angle, with smooth nanostructure. Al (400 ºC/2%) 30º sample shows lower optical transmittance due to lower grain sizes, which could be increased the scattering at grain boundaries.

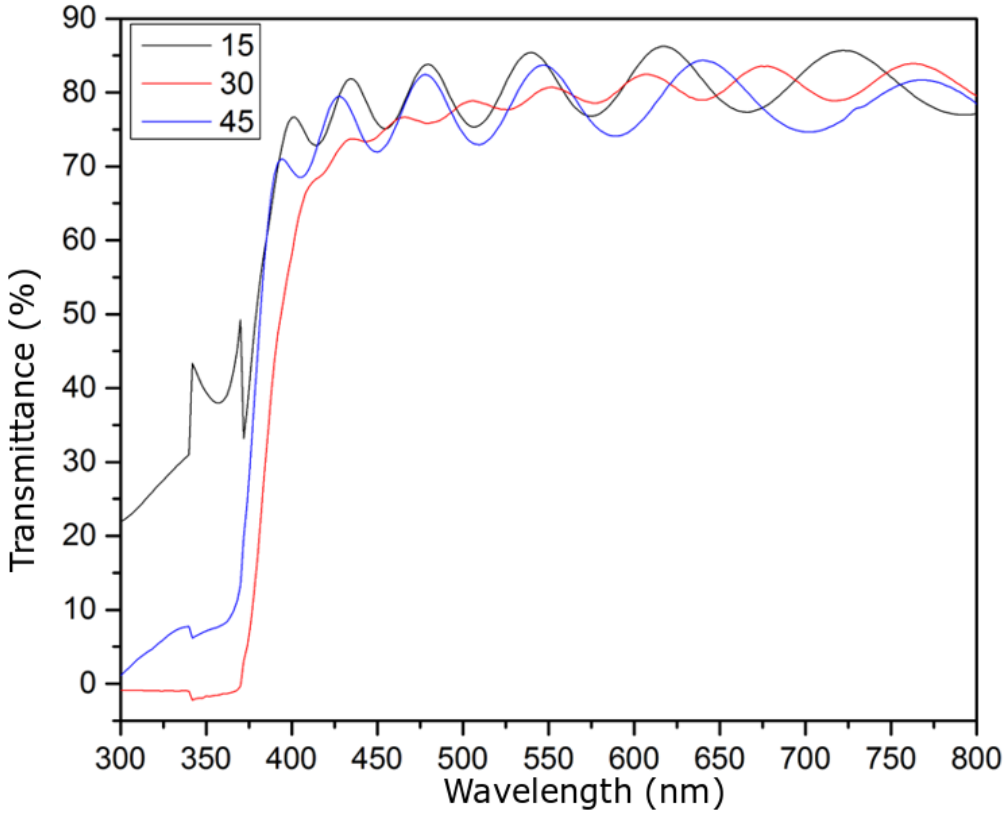

Fig. 3.20: Transmittance of Al doped ZnO thin films at different spray angles.

The electrical conductivity of the Al-doped ZnO samples were measured by using the four-probe method (described in section 3.3.1). The resistivity values were 1.06×10^{-4}, 1.39×10^{-4}, and 1.05×10^{-4} Ωcm for Al (400 ºC/2%) 15º Al (400 ºC/2%) 30º, Al (400 ºC/2%) 45º, samples respectively. The lowest resistivity was obtained in Al (400 ºC/2%) 45º sample, while the

highest resistivity was in Al (400 ºC/2%) 30º sample. The resistivity of Al (400 ºC/2%) 45º sample was increased as the mobility increased due to the reduction of grain boundary scattering. Moreover, the plate-like structures help to increase the electron propagation in horizontal direction and hence increase the conductivity. Higher grain size is influence for the decrease of grain boundary scattering as numbers of grain boundaries decreased in Al (400 ºC/2%) 45º sample, which were confirmed by XRD patterns. However, there was no significant difference of electrical conductivity in between Al (400 ºC/2%) 15º sample and Al (400 ºC/2%) 45º samples.

CONCLUSION

We have prepared Al-doped ZnO nanostructure using rotational, pulsed and atomized spray pyrolysis deposition technique with 2 at % of Al doping at 400 ºC of growth temperature. The average top diameters and the average structure densities were 29.9 nm and 86.2 per μm^2, 34.0 nm and 55.4per μm^2, 31.1 nm and 78.0 per μm^2, respectively for 15º, 30º and 45º of spray angles. An excellent nanostructure with high homogeneity and minimal structural defects were obtained at the lowest spray angle of 15º. Optimum transparent conducting oxide properties of 80.3 % of optical transmittance in the visible range and 1.06×10^{-4} of resistivity was obtained in Al-doped ZnO samples prepared at lower spraying angles.

References

1. Huiyong Liu, V. Avrutin, N. Izyumskaya, Ü. Özgür, H. Morkoç, Superlattices Microstruct.; 2010, 48, 458-484.
2. Rakesh A. Afre, Nallin Sharma, Maheshwar Sharon and Madhuri Sharon, Rev.Adv. Mater. Sci.; 2018, 53, 79-89.
3. C.G. Granqvist, Sol. Energy Mater. Sol. Cells; 2007, 91, 1529–1598.
4. Ki Cheol Park, Dae Young Ma, Kun Ho Kim, Thin solid Films; 1997, 305, 201-209.
5. Gurpreet Kaur, Anirban Mitra, K.L.Yadav, PRO NAT SCI-MATER.; 2015, 25, 12-21.
6. M. U. Shahid, K. M. Deen, A. Ahmad, M. A. Akram, M. Aslam, W. Akhtar, Appl. Nanosci.; 2016 6, 235-241.
7. Chih-Cheng Lin, Yuan-Yao Li, Mater. Chem. Phys.; 2009, 113, 334-337.
8. D.C. Look, Mater. Sci. Eng. B; 2001, 80, 383-387.
9. Kyung Ho Kim, Zhuguang Jin, Yoshio Abe, Midori Kawamura, Superlattices Microstruct.; 2014, 75, 455-460.
10. Shahzad Salam, Mohammad Islam, Aftab Akram, 2013, 529, 242-247.
11. Sung-Hak Yi, Seung-Kyu Choi, Jae-Min Jang, Jung-A Kim, Woo-Gwang Jung, J. Colloid Interface Sci.; 2007, 313, 705-710.
12. Chien-Yie Tsay, Kai-Shiung Fan, Yu-Wu Wang, Chi-Jung Chang, Yung-Kuan Tseng, Chung-Kwei Lin, CERAM INT.; 2010, 36, 1791-1795.
13. Major S, Banerjee A, Chopra K.L., Thin Solid Films; 1985, 125, 179-185.
14. Xudong Wang, Jinhui Song, Christopher J. Summers, Jae Hyun Ryou, Peng Li, Russell D. Dupuis, Zhong L. Wang, J. Phys. Chem. B; 2006, 110, 7720-7724.
15. Deniz Kadir Takci, Ebru Senadim Tuzemen, Kamuran Kara, Sadi Yilmaz, Ramazan Esen, Ozge Baglayan, J Mater Sci: Mater Electron.; 2014, 25, 2078-2085.

16. J. Hüpkes, B. Rech, S. Calnan, O. Kluth, U. Zastrow, H. Siekmann, M. Wuttig, Thin Solid Films; 2006, 502, 286-291.
17. J.L. Zhao, X.M. Li, J.M. Bian, W.D. Yu, X.D. Gao, J. Cryst. Growth; 2005, 276, 507-512.
18. D. Kim, I. Yun, H. Kim, Curr. Appl. Phys.; 2010, 10, S459-S462.
19. K.E. Lee, M. Wang, E.J. Kim, S.H. Hahn, Curr. Appl. Phys.; 2009, 9, 683-687.
20. R. Ayouchi, D. Leinen, F. Martin, M. Gabas, E. Dalchiele, J.R. Ramos-Barrado, Thin Solid Films; 2003, 426, 68-77.
21. Y.H. Kim, K. Lee, T.S. Lee, B.k. Cheong, T.Y. Seong, W.M. Kim, Curr. Appl. Phys.; 2010, 10, S278-S281.
22. M.A. Mahadik, S.S. Shinde, K.Y. Rajpure, C.H. Bhosale, Mater. Res. Bull.; 2013, 48, 4058-4065.
23. Y.Belghazi, M.AitAouaj, M.ElYadari, G.Schmerber, C.Ulhaq-Bouillet, C.Leuvrey, S.Colis, M. Abd-lefdil, A.Berrada, A.Dinia, Microelectron. J.; 2009, 40, 265-267.

3.4 Al doped ZnO nanostructure by using different volumes.

3.4.1 Introduction

Impurity doped Zinc oxide widely are used as transparent conductive oxide material (TCO) in many industries such as solar cells, organic photovoltaics (OPVs) and display devices, sensors, liquid crystal displays (LCDs) and light emitting diodes (LEDs). In order to increase the electrical and optical properties, ZnO is doped with impurities. [1-11)] The dopant and the doping concentration highly decide the structure and characteristics of ZnO lattice. [12-17)] The doping level should possess at relatively low value to avoid the lattice distortion, due to the difference of ionic radii of Zn and impurity atoms. However, when Al or Ga used as a dopant with Zn, lattice distortions are minimized, even at higher doping concentrations, due to their compatibility of ionic and covalent radii with native Zn atoms. [1, 18, 19)] There are many reports on formation of various kinds of ZnO nanostructures such as, rods, plates, bridges, cones, nanotubes etc. 1-D nanorod structure is suitable for photovoltaic applications due to its high surface-volume ratio. [20-24)] However, some researches have been reported about usage of ZnO nanocone structure, which could increase the light transparency by reducing the photon scattering. [25-30)] In this section, we increase the spraying volume of Al doped ZnO solution, to identify the crystal structure.

3.4.2. Experimental

Al doped ZnO samples were fabricated as described in section 2.1. The sample nomenclature of prepared Al doped ZnO samples with different volumes is shown in table 3.5.

Table 3.5. Spray volumes of Al-doped ZnO samples

Sample	Growth Temperature (ºC)	Al:Zn Ratio	Spraying Angle	Spraying Volume (ml)
Al-ZnO (400 ºC/ 2%/15º) 100	400	2:98	15º	100
Al-ZnO (400 ºC/ 2%/15º) 200	400	2:98	15º	200
Al-ZnO (400 ºC/ 2%/15º) 400	400	2:98	15º	400

X-ray diffraction patterns, field emission scanning electron microscope images and optical transmittance data were used to characterize the prepared Al doped ZnO samples as described in section 2.3.

3.4.3 Results and discussion

Figure 3.21 shows the obtained XRD images of Al doped ZnO samples prepared at different temperatures. Significant peak around 34.37º in all samples, shows the growth of nanostructure favoured in (002) direction of hexagonal wurtzite ZnO phase (JCPDS card No. 36-1451), which is along the c-axis, perpendicular to the substrate. All other peaks are for FTO layer. The crystallite sizes are calculated from using Debye-Scherrer's formula, which is shown in Eq.1, based on (002) peak. Crystallite sizes were 31.1nm, 28.1 nm, 30.6 nm and FWHMs were 0.27, 0.30, 0.27 for Al-ZnO (400 ºC/ 2%/15º) 100, Al-ZnO (400 ºC/ 2%/15º) 200 and Al-ZnO (400 ºC/ 2%/15º) 400 samples respectively. Figure 3.22 shows a FE-SEM image of Al-ZnO (400 ºC/ 2%/15º) 100 sample, which has hexagonal wurtzite nanostructure at the top. The average diameter and the average structure density were 29.9 nm and 86.2 per μm^2 respectively.

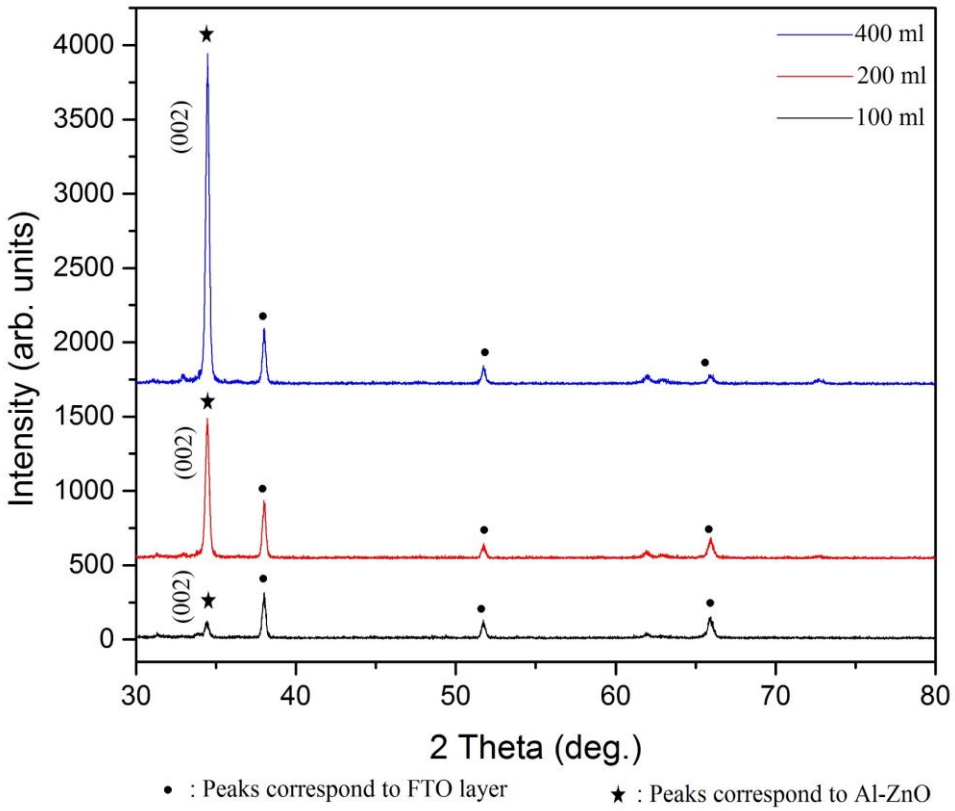

Fig 3.21: X-ray diffractogram for Al doped ZnO samples at different growth temperatures.

Figure 3.23 shows the FE-SEM image of Al-ZnO (400 ºC/ 2%/15º) 200 sample. Nanostructure density was reduced. An excellent nanostructure with average top diameter of 38.6 nm and the

average structure density of 67.9 per μm^2 was observed. Nanostructure was well separated. Figure 3.23 shows the FE-SEM image of Al-ZnO (400 ºC/ 2%/15º) 400 sample.

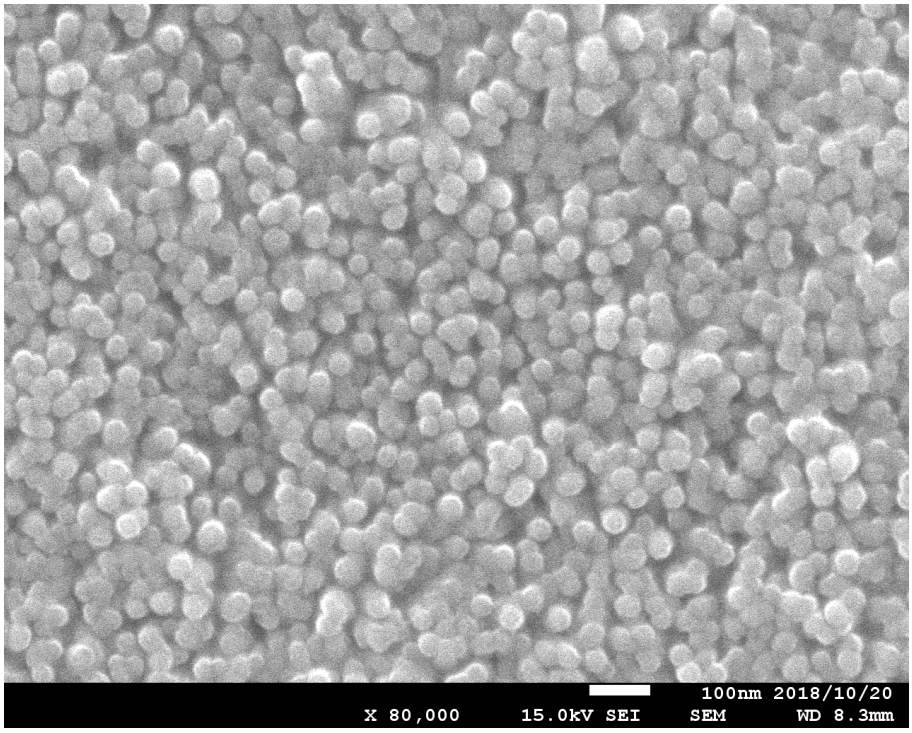

Fig. 3.22: FE-SEM image of Al doped ZnO with spray volume of 100 ml.

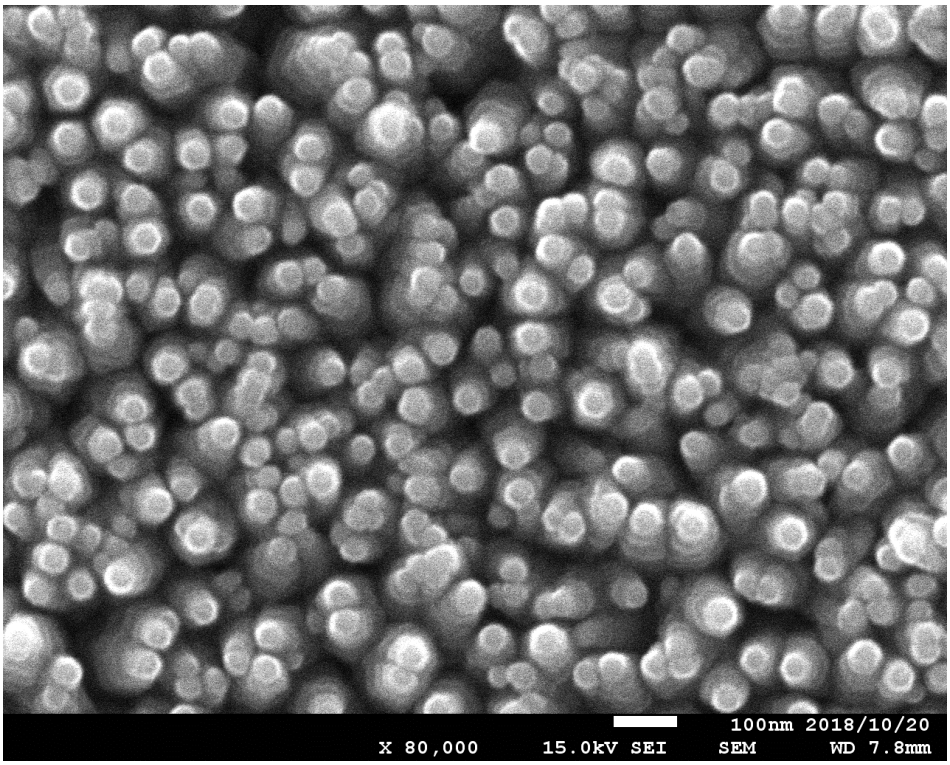

Fig. 3.23: FE-SEM image of Al-ZnO (400 ºC/ 2%/15º) 200.

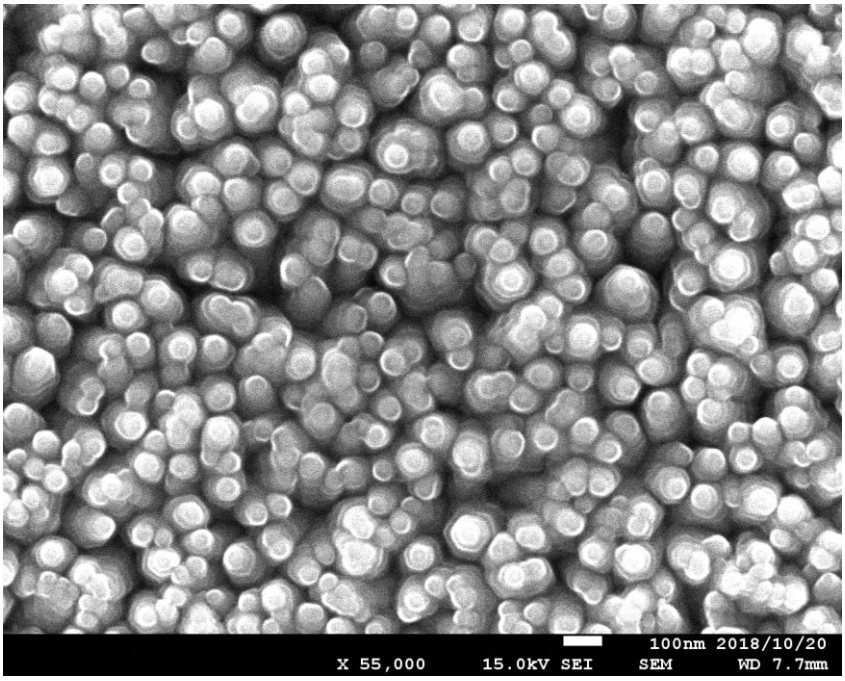

Fig. 3.24: FE-SEM image of Al-ZnO (400 ºC/ 2%/15º) 400.

Fig. 3.25 shows the FE-SEM images of Al-ZnO (400 ºC/ 2%/15º) 400 sample at higher magnification. The nanostructure is clearly visible at this stage. Terrace-truncated nanocone structure was confirmed by SEM images in fig. 3.25. The average top diameter and the height of the nanostructure is 35-40 and 600-650 nm.

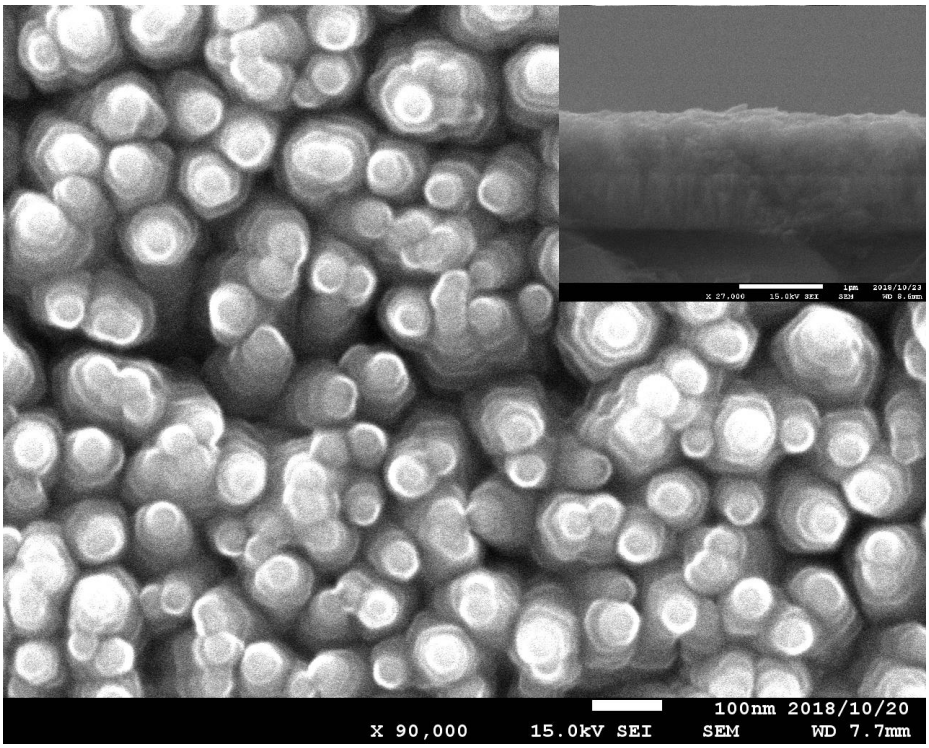

Fig. 3.25: FE-SEM image of Al-ZnO (400 ºC/ 2%/15º) 400 at higher magnification.

The simulated terrace-truncated nanocone structure is shown in fig. 3.26, which was developed as a result of high growth rate along the (002) direction.

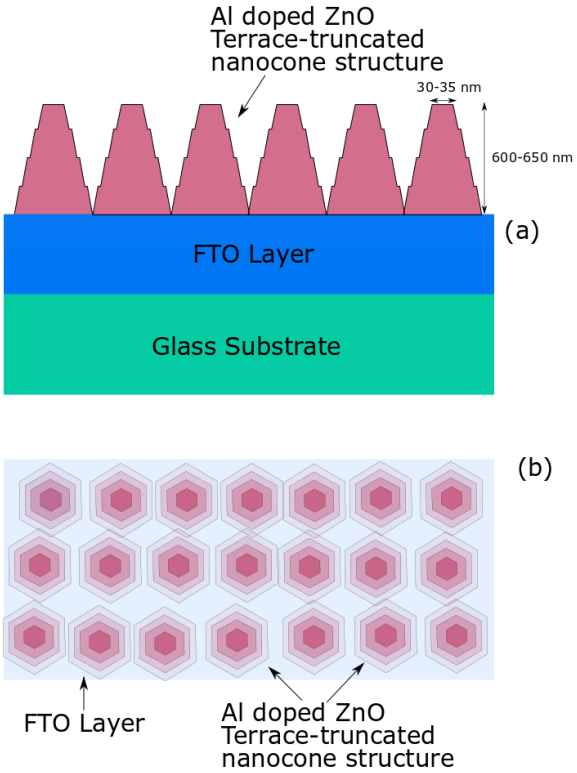

Fig.3.26. Simulated terrace-truncated nanocone structure of Al doped ZnO, (a). Cross section (b). Top view.

In our deposition method, the total spray time was 5.3 hours. However, among this total spray time, 4.5 hours are spraying intervals. The spraying was continued only for 45 minutes. As the structure was grown along the c-axis by high growth rate, the decay rate (of the crystal) is also high along the same direction. As a result, the hexagonal nanorod structure was end up as terrace truncated nanocone structure which was illustrated in fig.3.27. However, the bottom of the crystal structure was wide even though the top is decaying. This phenomenon might be occurred due to two main reasons which are,

- Decay rate along $(00\bar{2})$ direction of ZnO crystal structure is slow, as the growth rate along that direction is also slow.
- The bottom face of ZnO crystal structure (polar O^{2-} face) is tightly attached to the nucleation sites of the FTO glass substrate, which disturbs the decaying.

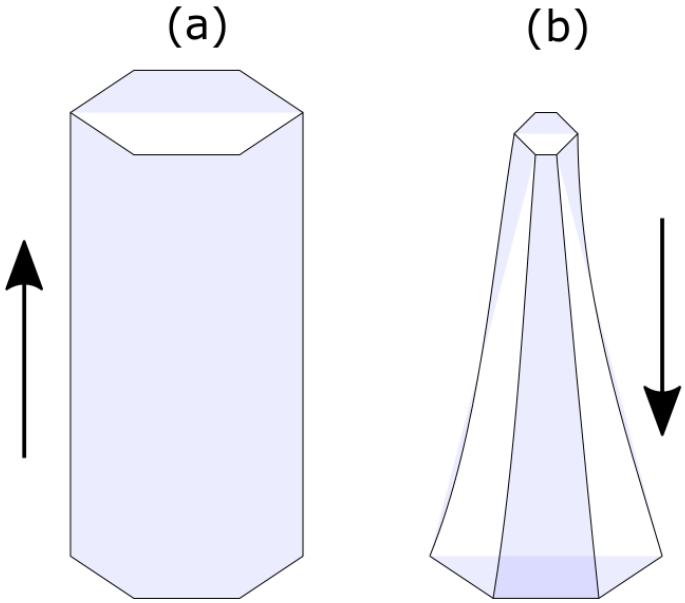

Fig.3.27. (a). Growth direction, (b). Decay direction of Al doped ZnO crystal structure.

The decaying of the structure is happening while it is growing and the removed particles are brushed off by the air flow of the system. Figure 3.28 shows a simulated 3-D image of doped ZnO. While decaying, the side walls of the crystal is become rough, and as a result, a terrace structure is formed.

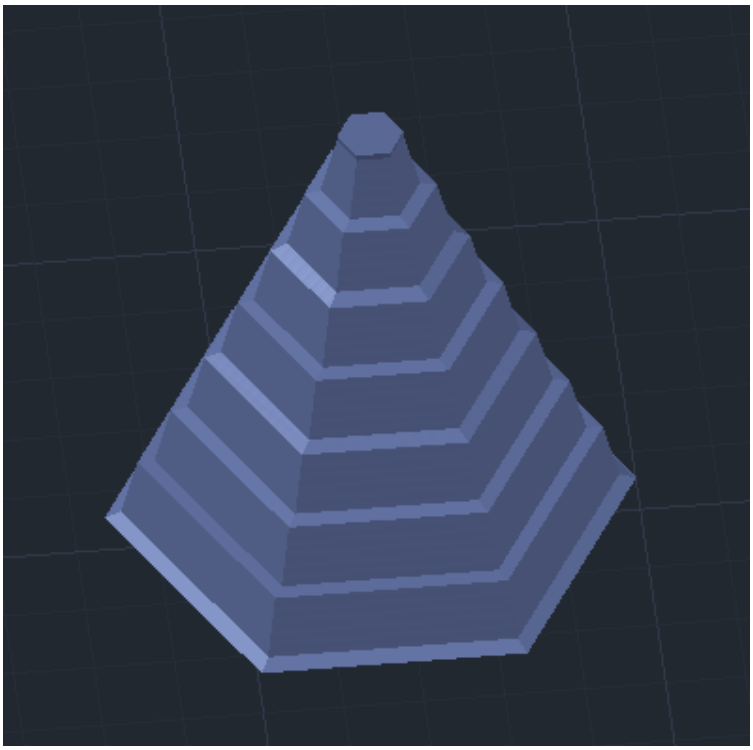

Fig.3.28. 3-D simulation of Terrace-truncated nanocone structure of impurity doped ZnO.

Figure 3.29 shows the AFM images of Al-ZnO (400 ºC/ 2%/15º) 400 sample. Triangular shape is visible in the 3-D AFM images. However, the nanocone structure could not be confirmed by 3-D AFM images. Surface roughness was 57.9 nm, 151.0 nm for Al-ZnO (400 ºC/ 2%/15º) 100, Al-ZnO (400 ºC/ 2%/15º) 400, respectively.

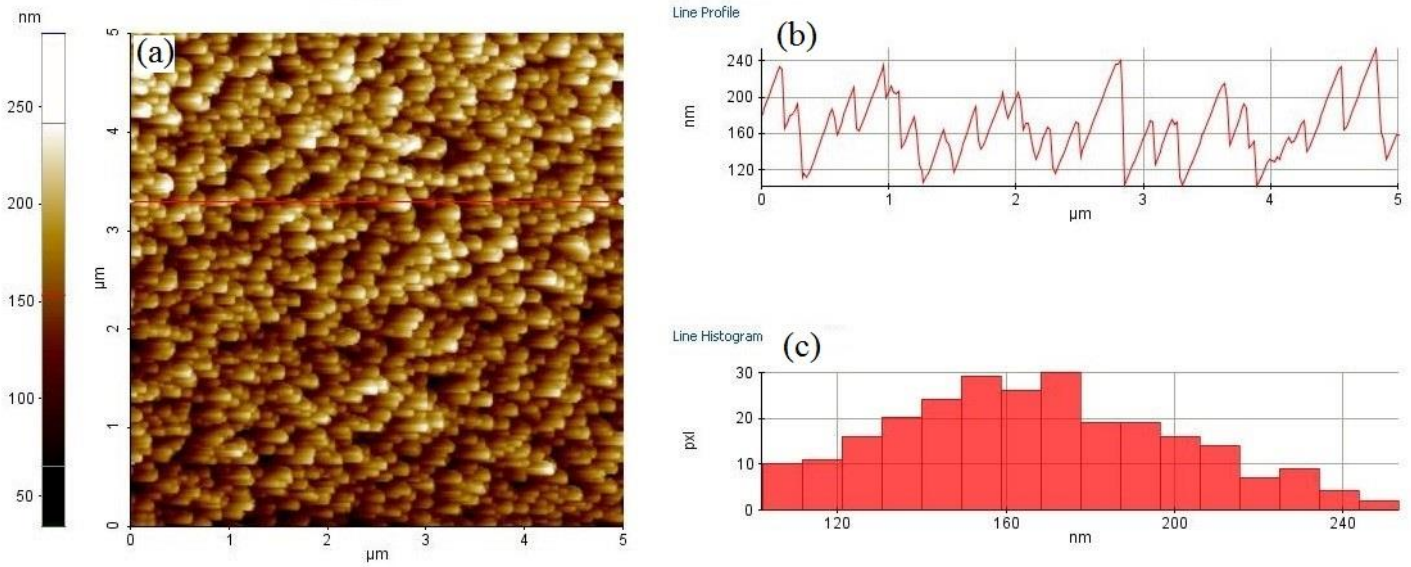

Fig. 3.29: (a) AFM image, (b) Line profile, (c) Line histogram, Al-ZnO (400 ºC/ 2%/15º) 400 sample.

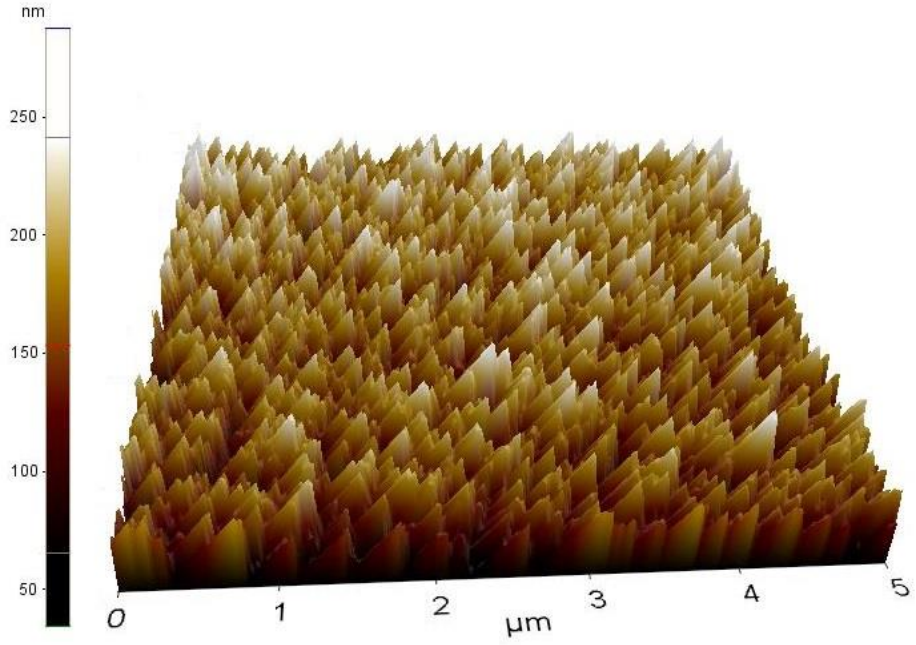

Fig. 3.30: 3-D AFM image of Al-ZnO (400 ºC/ 2%/15º) 400 sample.

Figure 3.31 shows the UV-visible spectra of Al doped ZnO with different volumes. Optical transmittance in the visible range were 80.3, 80.5 and 80.0 %, respectively. Optimum optical

transmittance value was obtained in Al-ZnO (400 ºC/ 2%/15º) 200 sample due to its' excellent nanostructure. Due to the terrace-truncated nanocone structure light harvesting is optimized as it has excellent antireflection properties. [31,32)]

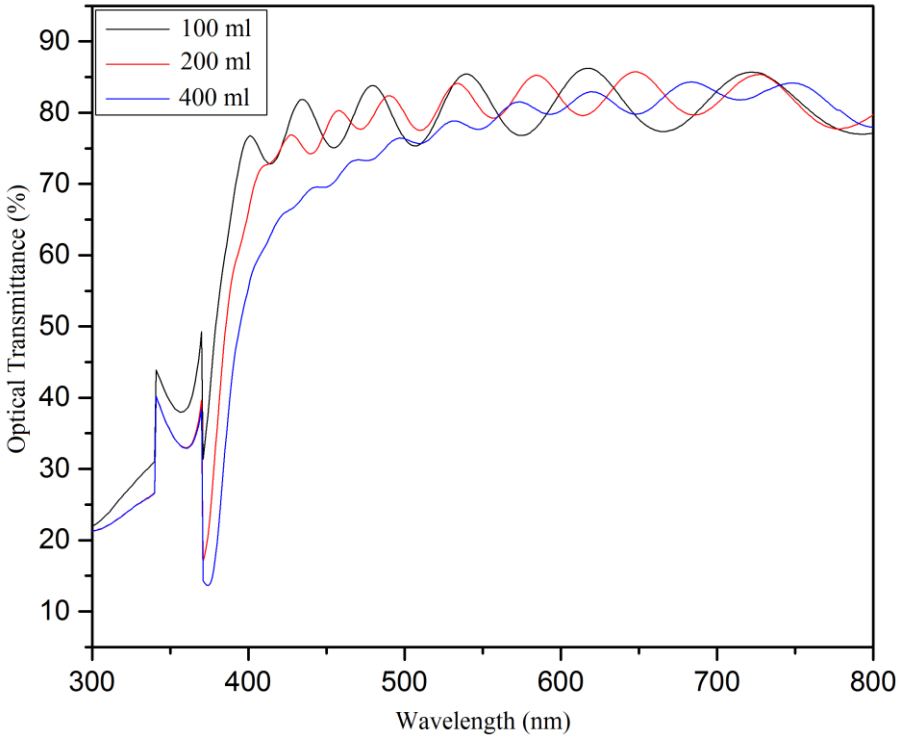

Fig. 3.31: UV- visible spectra of Al-doped ZnO with different volumes.

Moreover, narrow top of the synthesized structure helps to increase the light transparency by decreasing the light scattering as shown in fig.3.32.

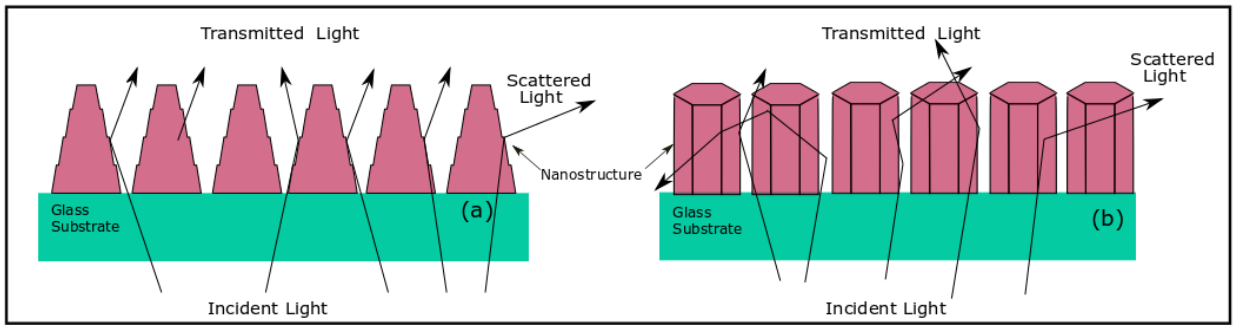

Fig. 3.32: Comparison of light transmittance, scattering of (a). Terrace-truncated nanocone structure (b) Hexagonal nanorod structure.

Strange absorption peak around 350 nm is observed due to the light source change. However, the optical transparency as not high as we expected due to the two layered (FTO & AZO-*see*

fig. 3.26(a)) structure. Even though the light scattering by the nanostructure is reduced by terrace-truncated nanocone structure, the light scattering at the layer boundaries was increased and hence reduce the photon transmittance.

Conclusion

Properties of Al doped ZnO nanostructure was changed with the spraying volume. The average top diameter was 29.9, 38.6 and 58.5 nm for Al doped ZnO samples with 100, 200 and 400 ml, respectively. The average structure densities were decreased due to the reduction of average diameter of nanostructures from 86.2 per μm^2, 67.9 per μm^2 and 32.9 per μm^2 for Al doped ZnO samples with 100 ml, 200 ml and 400 ml samples, respectively. Surface roughness was 57.9 nm, 151.0 nm for Al doped ZnO samples with 100 ml and 400 ml, respectively. The optical transmittance in the visible range, were 80.3 %, 80.5 %, and 80.0 % for Al doped sample with 100, 200 and 400 ml, respectively. Terrace-truncated nanocone structured Al doped ZnO was successfully grown as identified by FE-SEM images. The high growth rate along the (002) direction which leads to a high decay along the same direction is responsible for the growth of Terrace-truncated nanocone structure.

References

1. D.C. Look, Mat. Sci. Eng. B 2001, 80, 382.
2. P. Ynag, H. Yan, S. Mao, R. Russo, J. Johnson, S. Richard, N. Morris, J. Pham, R. He, H.J. Choi, Adv. Func. Mater. 2002, 12, 323.
3. B. Ismail, M. Abaab, B. Rezig, Thin Solid Films 2001, 383, 92.
4. G. H. Lee, Y. Yamamoto, M. Kourogi, M. Ohtsu, Thin Solid Films 2001, 386, 117.
5. C. Shaoqiang, Z. Jian, F. Xiao, W. Xiaohua, L. Laiqiang, S. Yanling, X., S.J. pearton, D.P. Norton, K. Ip, Y.W. Heo, T. Steiner, Prog. Mater. Sci. 2005, 50, 293.
6. Qingsong, W. Chang, Z. Jianzhong, Z. Ziqiang, Appl. Surf. Sci. 2005, 241, 384.
7. Z. Ye, G. Yuan, B. Li, L. Zhu, B. Zhao, J. Huang, Mater. Chem. Phys. 2005, 93, 170.
8. M. Zamfirescu, A. Kavokin, B. Gil, G. Malpuech, M. Kaliteevski, Phys. Rev. B 2002, 65, 161205.
9. R. Ghosh, B. Mallik, S. Fujihara, D. Basak, Chem. Phys. Lett. 2005, 403, 415.
10. T. Makino, C.H. Chia, Nguen T. Tuan, Y. Segawa, M. Kawasaki, A. Ohtomo, K. Tamura, H. Koinuma, Appl. Phys. Lett. 2000, 77, 975.
11. R.K. Shukla, A.Srivastava, A.Srivastava, K.C.Dubey, J.Cryst.Growth 2006, 294, 427.
12. B.K. Sharma, N.Khare, D.Haranath, Solid State Commun. 2010, 150, 2341.
13. X.Y. Li, H.J. Li, Z.J. Wang, H. Xia, Z.Y. Xiong, J.X. Wang, B.C. Yang, Opt. Commun. 2009, 282, 247.
14. H.W. Lee, S.P. Lau, Y.G. Wang, K.Y. Tse, H.H. Hng, B.K. Tay, J. Cryst. Growth 2004, 268, 596.
15. E.B. Pollock, R.J.Lad, J. Vac. Sci. Technol. 2014, A32, 041516.
16. D.J. Lee, H.M. Kim, J.Y. Kwon, H. Choi, S.H. Kim, K.B. Kim, Adv. Funct. Mater. 2011, 21, 448.
17. F.S.S. Chien, C.R. Wang, Y.L. Chan, H.L. Lin, M.H. Chen, R.J. Wu, Sens. Actuators B: Chem 2010, 144, 120.
18. X. Zhang, X. Han, J. Su, Q. Zhang, Y. Gao, Appl. Phys. A 2012, 107, 255.
19. S. Dhara, P.K. Giri, Nanoscale Res. Lett. 2011, 6, 504.
20. X.Y. Liu, C.X. Shan, S.P. Wang, Z.Z. Zhang, D.Z. Shen, Nanoscale 2012, 4, 2843.

21. M.H. Huang, S. Mao, H. Feick, H. Yan, Y. Wu, H. Kind, E. Weber, R. Russo, P. Yang, Science 2001, 292, 1897.
22. Z.H. Chen, Y.B. Tang, Y. Liu, G.D. Yuan, W.F. Zhang, J.A. Zapien, I. Bello, W.J. Zhang, C.S. Lee, S.T. Lee, J. Appl. Phys. 2009, 106, 064303.
23. M. Seol, E. Ramasamy, J. Lee, K. Yong, J. Phys. Chem. 2011, 115, 22018.
24. J.W. Chen, D.C. Perng, J.F. Fang, Sol. Energy Mater. Sol. Cells 2011, 95, 2471.
25. J. Zhang, W. Que, F. Shen, Y. Liao, Sol. Energy Mater. Sol. Cells 2012, 103, 30.
26. S.H. Lee, S.H. Han, H.S. Jung, H. Shin, J. Lee, J.H. Noh, S. Lee, I.S. Cho, J.K. Lee, J. Kim, H. Shin, J. Phys. Chem. C 2010, 114, 7185.
27. L. Wang, D. Zhao, Z. Su, D. Shen, Nanoscale Res. Lett. 2012, 7, 106.
28. Z.L. Wang, J. Song, Science 2006, 312, 242.
29. J. Conradt, J. Sartor, C. Thiele, F.M. Flaig, J. Fallert, H. Kalt, R. Schneider, M. Fotouhi, P. Pfundstein, V. Zibat, D, Gerthsen, J. Phys. Chem. C 2011, 115, 3539.
30. D. Calestani, F. Pattini, F. Bissoli, E. Gilioli, M. Villani, A. Zappettini, Nanotechnology 2012, 23, 194008.

Chapter 4

Synthesis of Ga Doped ZnO Nanocone Structure.

- *In this chapter we have synthesized Ga doped ZnO terrace truncated nanocone structure by using advanced spray pyrolysis deposition technique.*
- *In the first part of this chapter, we have investigated about the optimum temperature for the deposition of Ga doped ZnO nanostructure.*
- *The second part of this chapter we have investigated about the optimum doping concentration of Ga. We have changed the Ga to Zn ratio and obtained the optimum concentration.*
- *In the third part we have changed the spraying angle and obtained the results. The core of the research is in this research part as the spray angle is a critical factor for the growth of an excellent transparent conductive oxide properties.*
- *Last part of this chapter, we have increased the spraying volume to investigate about the synthesized structure. It was found that, terrace-truncated nanocone structured Ga doped ZnO was grown successfully.*
- *Prepared samples were characterized by using FE-SEM images, x-ray diffraction patterns and UV-visible spectroscopy, atomic force microscopy and obtained the results. Electrical studies were done by four probe method.*

4.1 Ga doped ZnO nanostructure at different growth temperatures.

4.1.1 Introduction

ZnO is an excellent semiconductor oxide material with unique properties and numerous applications[1-14]. Even though there are many dopants, which can doped with ZnO, Ga has gained the attraction of researchers, as it has many advantages over other dopants[15-19]. Nanostructures of impurity doped ZnO has developed by many deposition methods[20-26]. We have used advanced spray pyrolysis deposition technique of rotational, pulsed and atomized to obtain well-vertically aligned nanostructure. In many deposition methods, deposition temperature plays a major role which decides the structural properties of impurity doped ZnO nano structure.

4.1.2 Experimental

Ga doped ZnO samples were fabricated as described in section 2.2. The sample nomenclature of prepared Ga doped ZnO samples at different growth temperature is shown in table 4.1.

Table 4.1. Sample preparation temperatures

Sample	Growth temperature(ºC)
Ga 300 ºC	300
Ga 350 ºC	350
Ga 400 ºC	400
Ga 450 ºC	450

X-ray diffraction patterns, field emission scanning electron microscope images and optical transmittance data were used for the characterization of prepared Ga doped ZnO samples as described in section 2.3.

4.1.3 Results and discussion

Figure 4.1 shows the obtained XRD images of Ga doped ZnO samples prepared at different growth temperatures. The significant peak around 34.37º, shows the growth of the structure is favoured in (002) direction of hexagonal wurtzite ZnO phase (JCPDS card No. 36-1451), which is along the c-axis, perpendicular to the substrate. All the other peaks are for FTO layer. The crystallite sizes were calculated by using Debye- Scherrer's formula, which is shown in Eq.1, based on (002) peak. Crystallite sizes are 15.8, 19.1 nm, and FWHMs were 0.53, 0.44 for Ga 400 ºC, Ga 450 ºC samples, respectively. Ga 300 ºC and Ga 300 ºC samples did not show a significant peak of (002), which may be due to the low crystallinity.

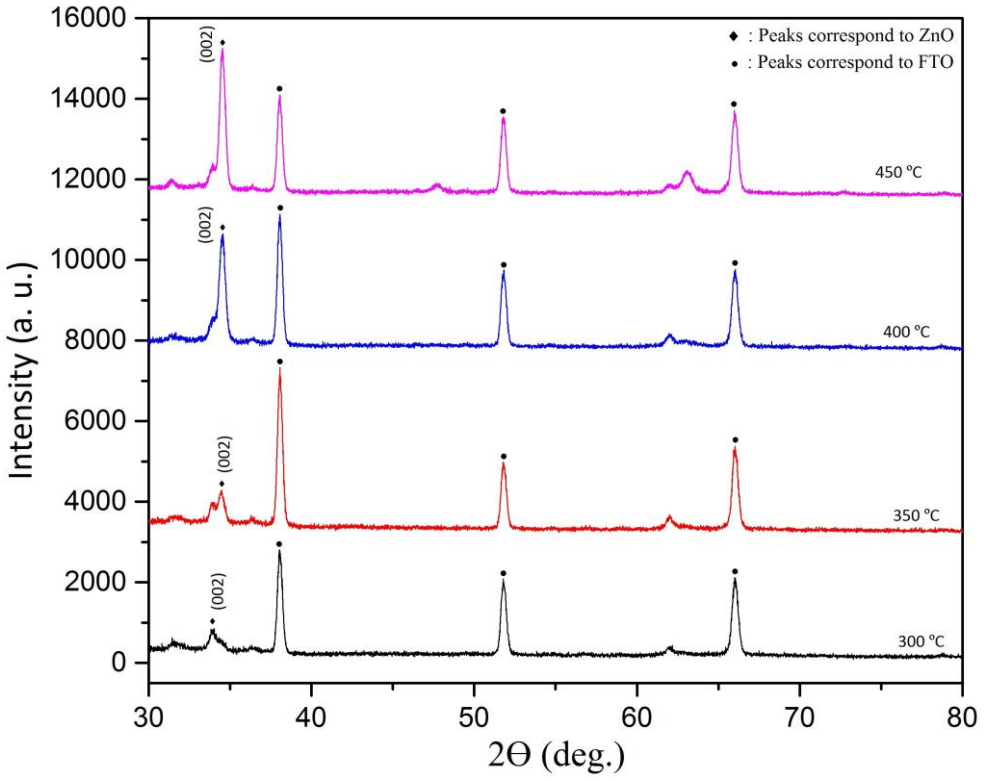

Fig.4.1: X-ray diffractogram for Ga doped ZnO samples at different growth temperatures.

Due to the much lower crystallinity in Ga 300 ºC and Ga 350 ºC samples, perpendicular growth of nanostructure was not observed by FE-SEM images. Ga doped ZnO nanostructure needs

high temperature to grow along vertical direction, even though Al doped ZnO nanostructure shows vertical nanostructure at lower temperatures. Figure 4.2 shows the FE-SEM image of Ga 400 ºC sample, and an excellent, well-separated nanostructure was found. Moreover, the nanostructure was homogenously spread all over the FTO substrate. The average top diameter and the average nanostructure density were 22.9 nm and 366 per μm^2. However, unlike the aluminum doped ZnO, Ga doped ZnO does not show structural defects such as nano flowers, nano flakes or nano plates.

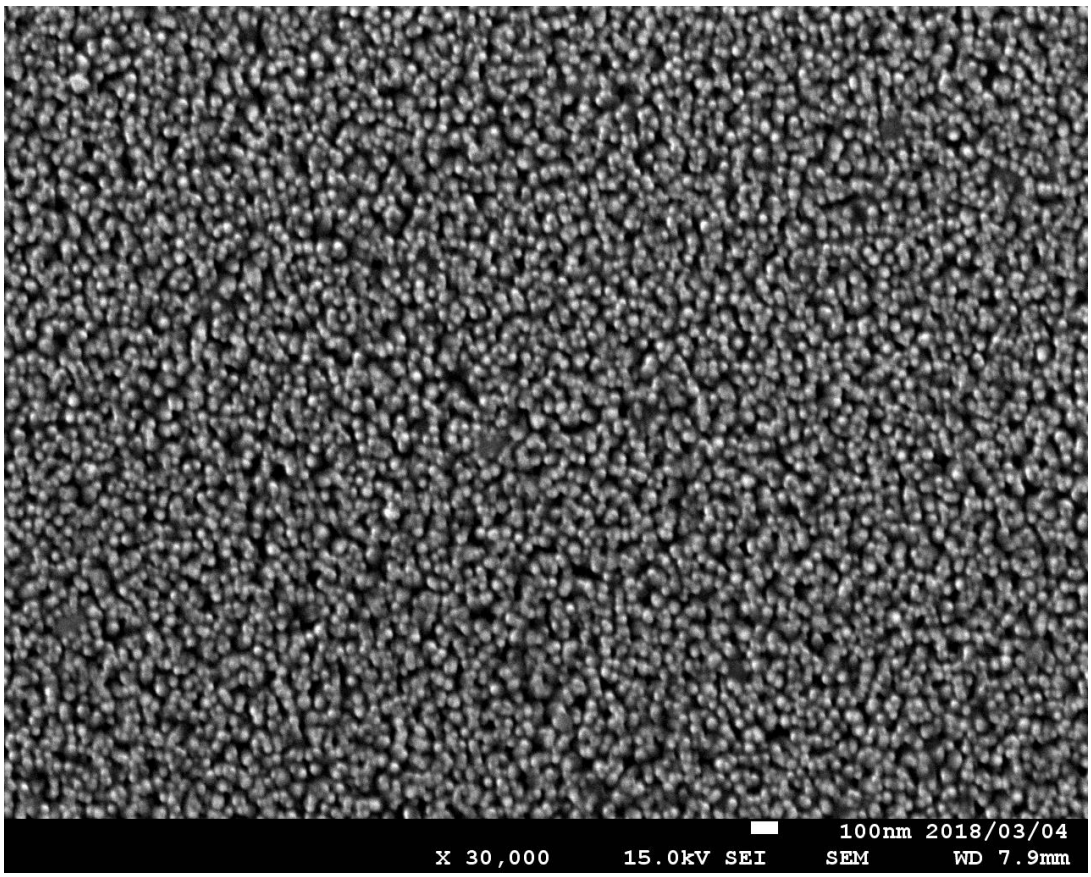

Fig. 4.2: FE-SEM image of Ga 400 ºC sample.

Figure 4.3 shows the FE-SEM image of Ga 450 ºC sample. The nanostructure is not clear in FE-SEM images. However, rice-shaped structure can be identified in some regions. Due to the high temperature, there were many structural defects all over the substrate. When ZnO based structure was grown over 419.5 ºC, this phenomenon is occurred as the melting point of Zn is

419.5 ºC. Over this temperature, ZnO structure is melting due to the high substrate temperature and deposit randomly, while cooling. In this temperature average top diameter is 48.6 nm and average nanostructure density were 51 per μm^2. When increasing the growth temperature of each Ga doped ZnO sample, top diameter is increasing, while decreasing the average structure density. It is obvious to reduce the average nanostructure density as the diameter increased and structural defects were formed.

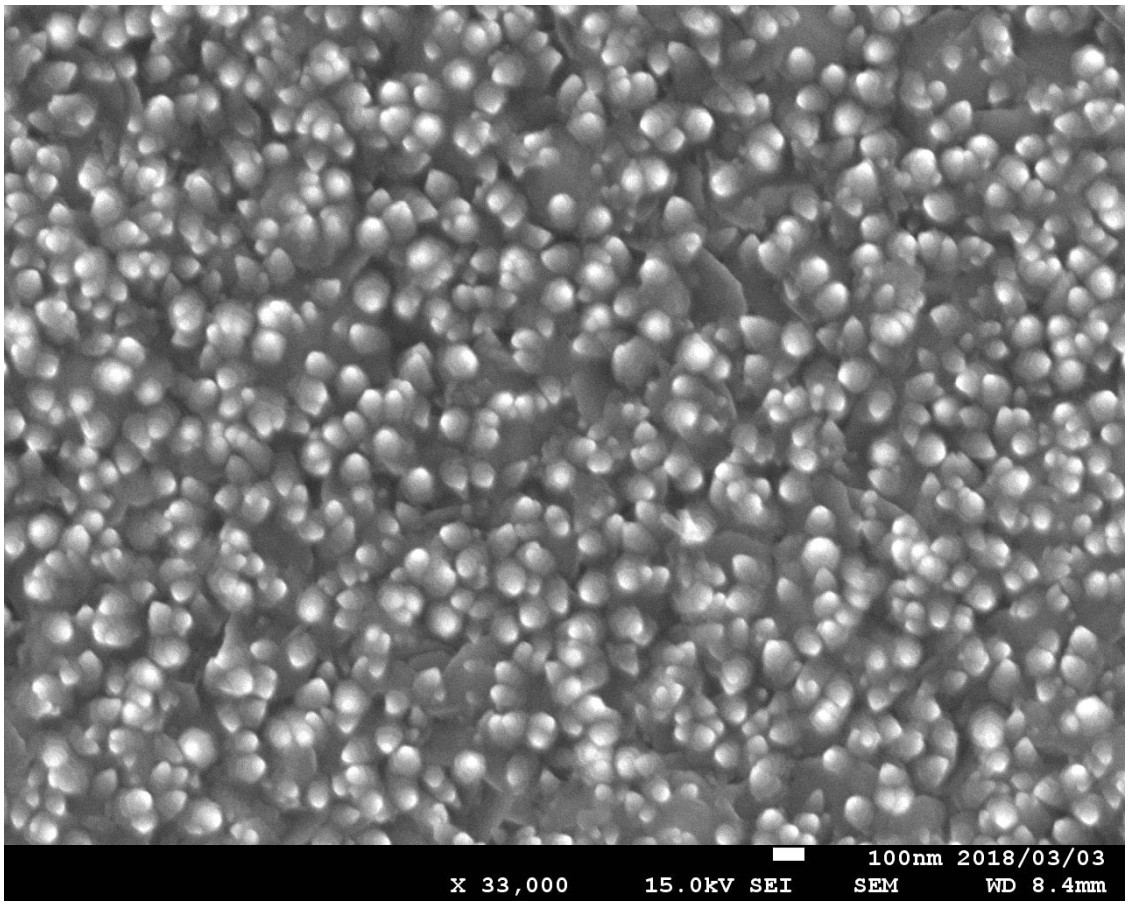

Fig. 4.3: FE-SEM image of Ga 450 ºC sample.

Conclusion

Ga doped ZnO sample prepared at 400 ºC shows vertically aligned nanostructure. Properties of nanostructure were highly dependent on the growth temperature. Crystallite size was increased with growth temperature and the highest crystallinity was obtained at 450 ºC. The diameter and theaverage structure density were changed from 22.9 nm and 366 per μm^2, 48.6 nm and 51 per μm^2 for Ga doped ZnO nanostructure grown at 400 ºC and 450 ºC, respectively. At 450 ºC, plate-like structures were observed. An excellent nanostructure with low structural defects with well separation and high vertical alignment was observed in the Ga doped ZnO sample grown at 400 ºC.

References

1. K. Ellmer, J. Phys. D: Appl. Phys. 2001, 34, 3097.
2. A. Janotti, C.G. Van de Walle, Rep. Prog. Phys. 2009, 72, 126501.
3. F.Z. Bedia, A. Bedia, N. Maloufi, M. Aillerie, F. Genty, B. Benyoucef, J. Alloys Compd. 2014, 616, 312.
4. M.M. Islam, S. Ishizuka, A. Yamada, K. Matsubara, S. Niki, T. Sakurai, K. Akimoto, Appl. Surf. Sci. 2011, 257, 4026.
5. Q.B. Ma, Z.Z. Ye, H.P. He, L.P. Zhu, J.Y. Huang, Y.Z. Zhang, B.H. Zhao, Scr. Mater. 2008, 58, 21.
6. M.Warasawa, A. Kaijo, M. Sugiyama, Thin Solid Films 2012, 520, 2119.
7. L. Cao, L.P. Zhu, J. Jiang, R. Zhao, Z.Z. Ye, B.H. Zhao, Sol. Energy Mater. Sol. Cells
8. 2011, 95, 894.
9. B.N. Pawar, G. Cai, D.K. Ham, R.S. Mane, T. Ganesh, A. Ghule, R. Sharma, K.D.
10. Jadhava, S.H. Han, Sol. Energy Mater. Sol. Cells 2009, 93, 524.

A. Tubtimtae, M.w. Lee, Superlattices Microstruct. 2012, 52, 987.

11. S.C. Chen, C.H. Wang, H. Sun, C.K. Wen, C.F. Lu, C.L. Tsai, Y.K. Fu, T.H. Chuang, Surf. Coat. Technol. 2016, 303, 203.
12. V.K. Jayaraman, A.M. Alvarez, Y.M. Kuwabara, Y. Koudriavstev, M.O. Amador, Mater. Sci. Semicond. Process. 2016, 47, 32.
13. F.H. Wang, C.L. Chang, Appl. Surf. Sci. 2016, 370, 83.

B. Jin, R. Narayan, A. Tiwari, H.H. Zhou, A. Kvit, J. Narayan, Mater. Sci. Eng. B 2005, 117, 348.

14. M. Snure, A. Tiwari, J. Appl. Phys. 2007, 101, 124912.
15. C. Jang, Q.J. Jiang, J.G. Lu, Z.Z. Ye, J. Mater. Sci. Technol. 2015, 31, 1108.
16. Y. Yamada, K. Kadowaki, H. Kikuchi, S.S. Funaki, S. Kubo, Thin Solid Films 2016, 609, 25.
17. J.H. Kim, I.H. Yer, Ceram. Int. 2016, 42, 3304.
18. V. Bhosle, A. Tiwari, J. Narayan, J. Appl. Phys. 2006, 100, 033713.
19. V. Bhosle, A. Tiwari, J. Narayan, Appl. Phys. Lett. 2006, 88, 032106.

20. R. Wendt, K. Ellmer, K. Wiesemann, J. Appl.Phys. 1997, 82, 2115.
21. J. Hu, R.G. Gordon, J. Appl. Phys. 1992, 71, 880.
22. G.A. Hirata, J. McKittrick, T. Cheeks, J.M. Siqueiros, J.A. Diaz, O. Contreras, O.A. Lopez, Thin Solid Films 1996, 288, 29.
23. A. Sanchez-Juareza, A. Tiburcio-Silverb, A. Ortizc, E.P. Zironid, J. Rickards, Thin Solid Films 1998, 333, 196.
24. W. Tang, D.C. Cameron, Thin Solid Films 1994, 238, 83.
25. J. Ma, F. Ji, H.L. Ma, S.Y. Li, Thin Solid Films 1996, 279, 213.
26. H. Kato, M. Sano, K. Miyamoto, T. Yao, J. Cryst. Growth 2012, 538, 237.

4.2 Ga doped ZnO nanostructure with different doping concentrations.

4.2.3 Introduction

Impurity doped ZnO has wide range of applications due to its' enormous properties[1-10]. The doping concentration affects the structure and characteristics of nanostructure. In general, doping level cannot maintain at a higher value due to the increase of lattice distortions[11-18]. Among many deposition methods for developing Ga doped ZnO thin films, advanced spray pyrolysis deposition technique of rotational, pulsed and atomized is play a major role to obtain an excellent nanostructure[19-34].

4.2.2 Experimental

Ga doped ZnO samples were fabricated as described in section 2.2. The sample nomenclature of prepared Ga doped ZnO samples at different doing concentrations is shown in table 4.2. X-ray diffraction patterns, field emission scanning electron microscope images and optical transmittance data were used to characterize the prepared Ga doped ZnO samples as described in section 2.3.

Table 4.2. Sample preparations with different doping concentrations.

Sample	Growth Temperature (ºC)	Ga to Zn Ratio
Ga (400 ºC) 1%	400	1:99
Ga (400 ºC) 2%	400	2:98
Ga (400 ºC) 3%	400	3:97

4.2.3 Results and discussion

Fig. 4.4 shows the obtained XRD patterns of Ga doped ZnO samples prepared at different doping concentrations. Growth of the nanostructure is favoured in (002) direction of hexagonal wurtzite ZnO phase (JCPDS card No. 36-1451), as confirmed by significant peak around 34.37º in all samples. All other peaks are for FTO layer.

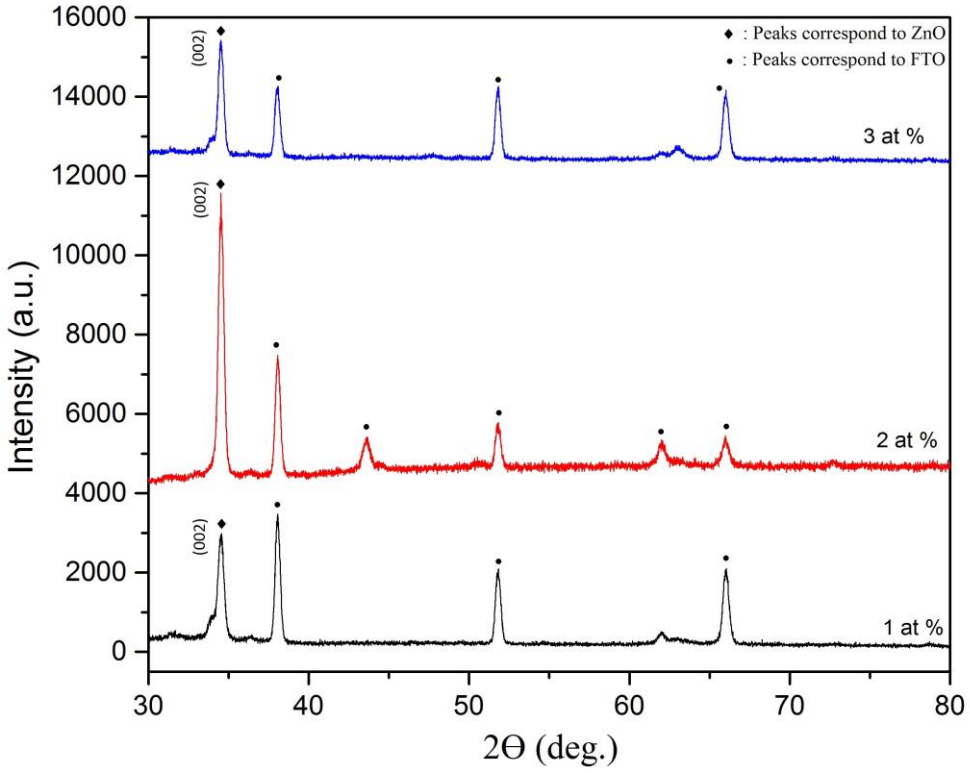

Fig.4.4: X-ray diffraction patterns for the Ga doped ZnO samples at different doping concentrations.

Figure 4.5 shows the FE-SEM image of Ga (400 ºC) 1% sample. The top diameter was around 22.9 nm while the average structure density was 366 per μm^2. However, the structure cannot be confirmed by FE-SEM images. Figure 5.6 shows the FE-SEM image of Ga (400 ºC) 2% sample. There is no significant difference of nanostructure when increasing the doping concentration. However, average top diameter and the average nanostructure density increases up to 37.0 nm and 230.4 per μm^2.

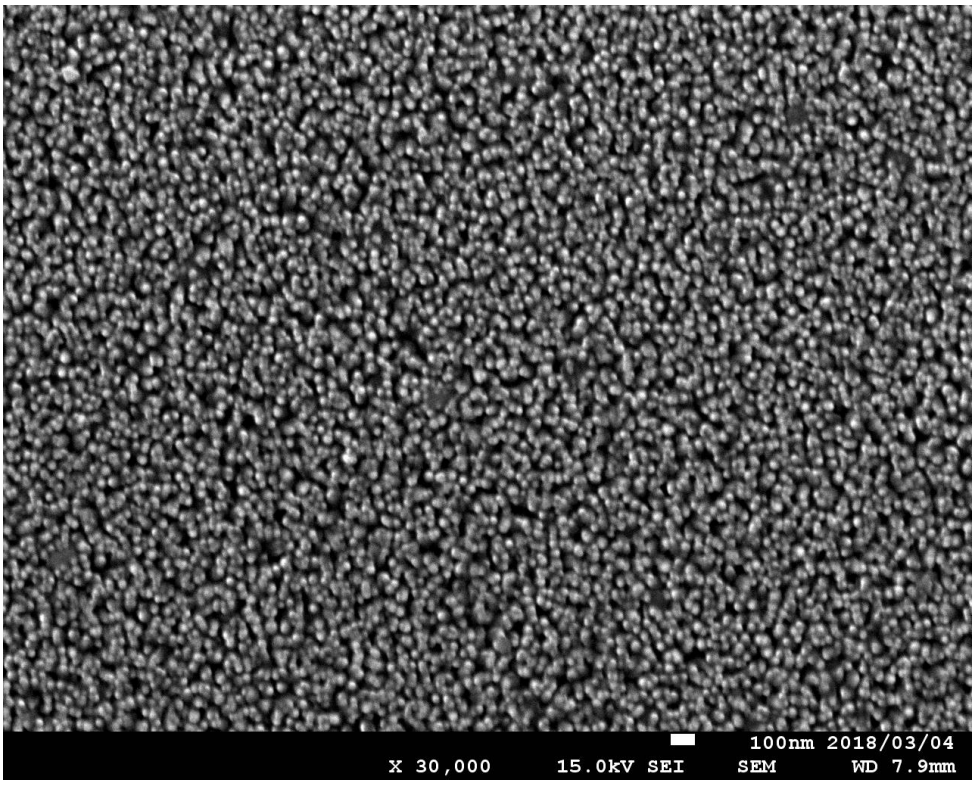

Fig.4.5: FE-SEM image of Ga (400 ºC) 1% sample.

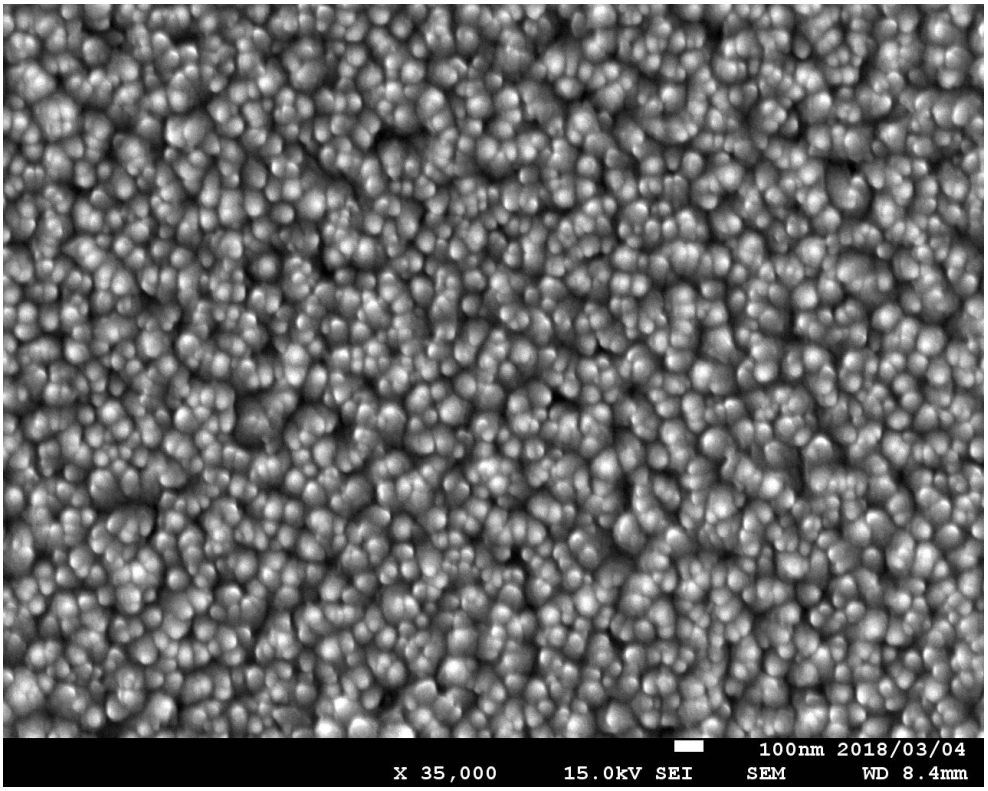

Fig. 4.6: FE-SEM image of Ga (400 ºC) 2% sample.

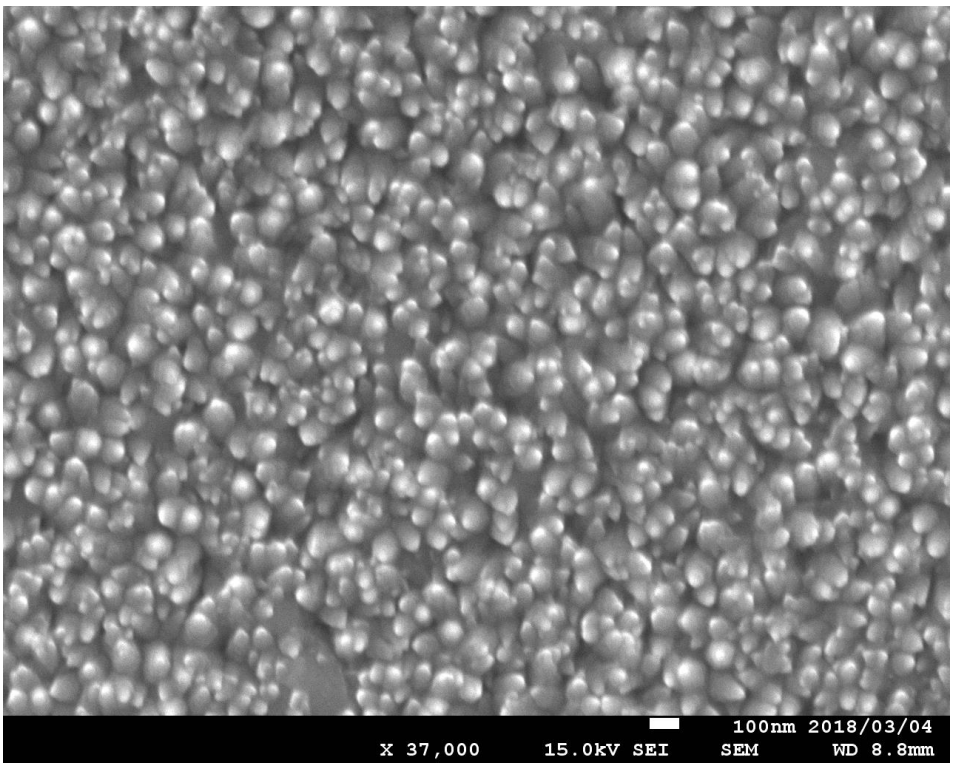

Fig. 4.7: FE-SEM image of Ga (400 ºC) 3% sample.

FE-SEM image of Ga (400 ºC) 3% is shown in fig. 4.7. The structure density further reduced to 143.1 per μm^2. The average top diameter increased up to 50.6 nm. Plate-like structural defects were identified in some regions.

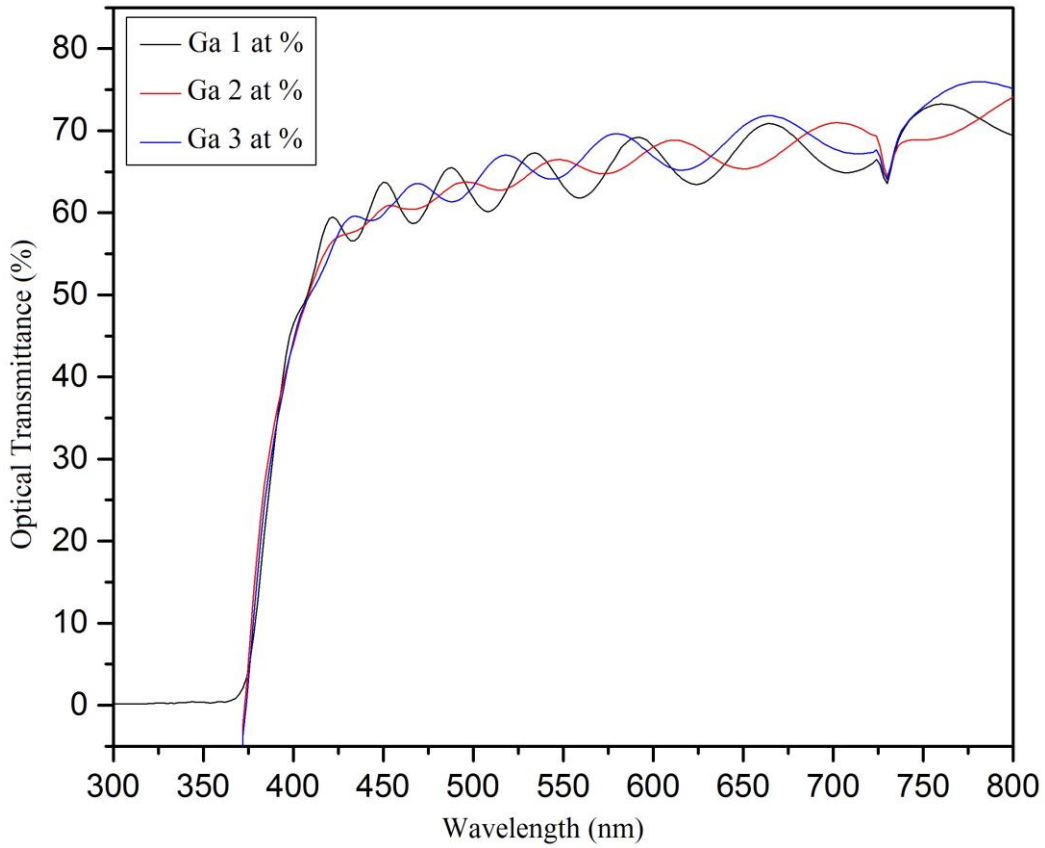

Fig. 4.8: UV- visible spectra of Ga doped ZnO prepared at different Ga to Zn ratio.

Figure 4.8 shows the UV-visible spectra of Ga doped ZnO at all different Ga concentrations. All samples showed moderately high optical transmittance of 70% - 75% in the visible range.

Conclusion

Structural and optical properties vary with the doping concentration. The average top diameter and the average nanostructure density were 22.9 nm and 366 per μm^2, 37.0 nm 230.4 per μm^2, 50.6 nm and 143.1 per μm^2, for Ga doped ZnO samples doped with 1 at %, 2 at % and 3 at %, respectively. However, at higher doping concentrations, structural defects were identified. An excellent nanostructure was found in Ga to Zn ratio of 2:98, with well-separation and low structural defects. All samples show moderately high optical transmittance of 70 %-75 % in the visible range.

References

1. K.J. Kim, Y.R. Park, Journal of Applied Physics 2003, 94, 867.
2. M. Wraback, H. Shen, S. Liang, C.R. Gorla, Y. Lu. Appl. Phys. Lett. 1999, 76, 507.
3. Y. Caglar, S. Ilican, M. Caglar, F. Yakuphanoglu, Journal of Sol–Gel Science and Technology 2010, 53, 372.
4. S.O. Kucheyev, J.E. Bradley, J.S. Williams, C. Jagadish, M.V. Swain, Appl. Phys. Lett. 2002, 80, 956.
5. V.I. Sokolov, A.V. Druzhinin, N.B. Gruzdev, A. Dejneka, O. Churpita, Z. Hubicka, D.M. Bagnall, Y.R. Chen, Z. Zhu, T. Yao, S. Koyama, M.Y. Shen, et al, Appl. Phys. Lett. 1997, 70, 2230.
6. V. Jastrabik Land Trepakov, Physical Review B 2010, 81, 153104.
7. M. Joseph, H. Tabata, T. Kawai. Jap. J. Appl. Phys. 1999, 38, L1205.
8. S. Chattopadhyay, S.K. Neogi, A. Sarkar, M.D. Mukadam, S.M. Yusuf, A. Banerjee, S. Bandyopadhyay, Journal of Magnetism and Magnetic Materials 2011, 323, 363.
9. R.K. Shukla, A.Srivastava, A.Srivastava, K.C.Dubey, J.Cryst.Growth 2006, 294, 427.
10. S. Krishnamoorthy, A.A. Iliadis, A. Inumpudi, S. Choopun, R.D. Vispute, T. Venkatesan, Solid-State Electron 2002, 46, 1631.
11. K.K. Kim, S. Niki, J.Y. Oh, J.O. Song, T.Y. Seong, S.J. Park, et al. J. Appl. Phys. 2005, 97, 066103.
12. H.J. Ko, Y.F. Chen, S.K. Hong, H. Wenisch, T. Yao, D.C. Look, Appl. Phys. Lett. 2000, 77, 3761.
13. S.Y. Bae, C.W. Na, J.H. Kang, J. Park, J. Phys. Chem. B 2005, 109, 2526.
14. P. Sharma, A. Gupta, K.V. Rao, F.J. Owens, R. Sharma, R. Ahuja, J.M. Osorio Gullen, B. Johansson, G.A. Gehring, Nature Material 2003, 2, 673.

15. D.C. Kundaliya, S.B. Ogale, S.E. Lofland, S. Dhar, C.J. Metting, S,R. Shinde, Z. Ma, B. Varughese, K.V. Ramanujachary, L. Salamanca-Riba, T. Venkatesan, Nature Material 2004, 3, 709.
16. C.J. Cong, L. Liao, C.J. Li, L.X. Fan, K.L. Zhang. Nanotechnology 2005, 16, 981.
17. S. Venkataprasad Bhat, F.L. Deepak, Solid State Communications 2005, 135, 345.
18. R. Viswanatha, S. Sapra, S.S. Gupta, B. Satpati, P.V. Satyam, B.N. Dev, D.D. Sarma, J.Phys. Chem. B 2004, 108, 6303.
19. S. Fay, U. Kroll, C. Bucher, E. Vallatsauvain, A. Shah, Sol. Energy Mater. Sol. Cells 2005, 86, 385.
20. M.D. Barankin, E. Gonzalez, A.M. Ladwig, R.F. Hicks, Sol. Energy Mater. Sol. Cells 2007, 91, 924.
21. T. Minami, S. Ida, T. Miyata, Y. Minamino, Thin Solid Films 2003, 445, 268.
22. X.-B. Lou, H.-L. Shen, H. Zhang, B.-B. Li, Trans. Nonferrous Met. Soc. China 2007, 17, s814.
23. S. Ilican, Y. Caglar, M. Caglar, J. Optoelectron. Adv. Mater. 2008, 10, 2578.
24. J.-S. Huang, C.-F. Lin, J. Appl. Phys. 2008, 103, 014304.
25. C. Agashe, O. Kluth, G. Schöpe, H. Siekmann, J. Hüpkes, B. Rech, Thin Solid Films 2003, 442, 167.
26. H. Cezternaskek, Vacuum 2008, 82, 994.
27. C. Li, M. Furuta, T. Matsuda, T. Hiramatsu, H. Furuta, T. Hirao, Thin Solid Films 2009, 517, 3265.
28. T. Hiramatsu, M. Furuta, T. Matsuda, C. Li, T. Hirao, Appl. Surf. Sci. 2011, 257, 5480.
29. D. Wang, T. Narusawa, T. Kawaharamura, M. Furuta, C. Li, J. Vac. Sci. Technol. B 2011, 29, 051205.
30. S. Hou, C. Li, Thin Solid Films 2016, 605, 37.

4.3 Ga doped ZnO nanostructure at different spray angles.

4.3.1 Introduction

A transparent conductive oxide (TCO) material is a semiconductor material with high conductivity and high optical transparency in the visible range. TCO materials have wide range of applications such as smart devices, liquid crystal displays (LCDs), light emitting diodes (LEDs), touch panels, energy efficient windows, as electrodes of photovoltaic cells, as a fire-retardant material, and gas sensors. In general, ITO, SnO_2, Ga_2O_3, In_2O_3 and CdO are abundantly used as TCO material. Among them, ITO is the most established TCO material as it has excellent properties. However, this material is rare and less stable in hydrogen plasma. Therefore, impurity doped ZnO is vastly use as an optional TCO material.[1-6] ZnO is an n-type II-VI semiconductor with unique physical and chemical properties such as direct wide band gap (3.37 eV), large exciting binding energy at room temperature (~60 meV), high thermal stability, radiation hardness, non-toxicity.[7-15] The conductivity of ZnO is attained by ionization of Zn interstitials and O vacancies. The carrier formation by ionization of Zn interstitial is the preponderant mechanism for intrinsic ZnO.[13] In order to enhance the electrical conductivity and optical transparency, ZnO is doped with B, Al, Ga, In, Sn, F, Si, Ge, Y, Sc, Ti, N, P, As and Zr.[4,5,10,13]

Even though Al and Ga attained the dominant attention as dopants of ZnO, Ga is considered as the most preferable dopant due to its similarity of both covalent and ionic radii (0.62 Å and 1.26 Å) with that of Zn (0.74 Å and 1.31 Å).[3] Moreover, covalent bond length of Ga-O (1.92 Å) is comparable with covalent bond length of Zn-O (1.97 Å) regarding that of Al-O (2.7 Å) and In-O (2.1 Å).[17] Because of that, even ZnO is highly doped with Ga, lattice distortion is possessed at a minimal value.[4] With respect to Al, Ga has high electronegativity, high stability

to moisture, less reactivity and less diffusivity.[4,15] It is consider that doped Ga atoms replace Zn host atoms and expand free electron density.

Various methods have been developed to produce ZnO thin films such as pulsed laser deposition, metal-organic chemical vapor deposition (MOCVD), spray pyrolysis, molecular beam epitaxy, sputtering, arc plasma evaporation, sol-gel, dip coating, chemical bath deposition and ion planting.[18-25] Spray pyrolysis deposition technique has several advantages such as, simplicity, low cost, ability for large area deposition, homogeneity and convenience.[26] In this study, we have used advanced spray pyrolysis deposition technique of rotational, pulsed and atomized (RPASP). This deposition technique has numerous advantages over normal SPD technique as we can change the parameters according to the requirement. We have investigated the effect of spray angle for the growth and properties of Ga doped ZnO nanostructured thin films prepared by RPASP deposition technique.

4.3.2 Experimental

Ga doped ZnO samples were fabricated as described in section 2.2. The sample nomenclature of prepared Ga doped ZnO samples at different spraying angles is shown in table 4.3.

Table 4.3. Spray angles of Ga-doped ZnO samples

Sample	Growth Temperature (ºC)	Ga:Zn Ratio	Spraying Angle
Ga (400 ºC/2%) 15º	400	2:98	15º
Ga (400 ºC/2%) 30º	400	2:98	30º
Ga (400 ºC/2%) 45º	400	2:98	45º

X-ray diffraction patterns, field emission scanning electron microscope images and optical transmittance data were used for the characterization of prepared Ga doped ZnO samples as described in section 2.3.

4.3.3 Results and Discussion

Figure 4.9 (a) shows the FE-SEM images of Ga doped ZnO sample, which was prepared at the spraying angle of 45º. Nanostructure was observed clearly with the average top diameter of 38.3 nm and an average structure density of 138.5 per μm^2. Since the plate-like structures formed and it interferes the growth of nanostructure, structure density was minimized at a higher angle. Figure 4.9 (b) shows the FE-SEM image of Ga doped ZnO samples at 30º of spraying angle, which indicates the rice shaped nanostructure.

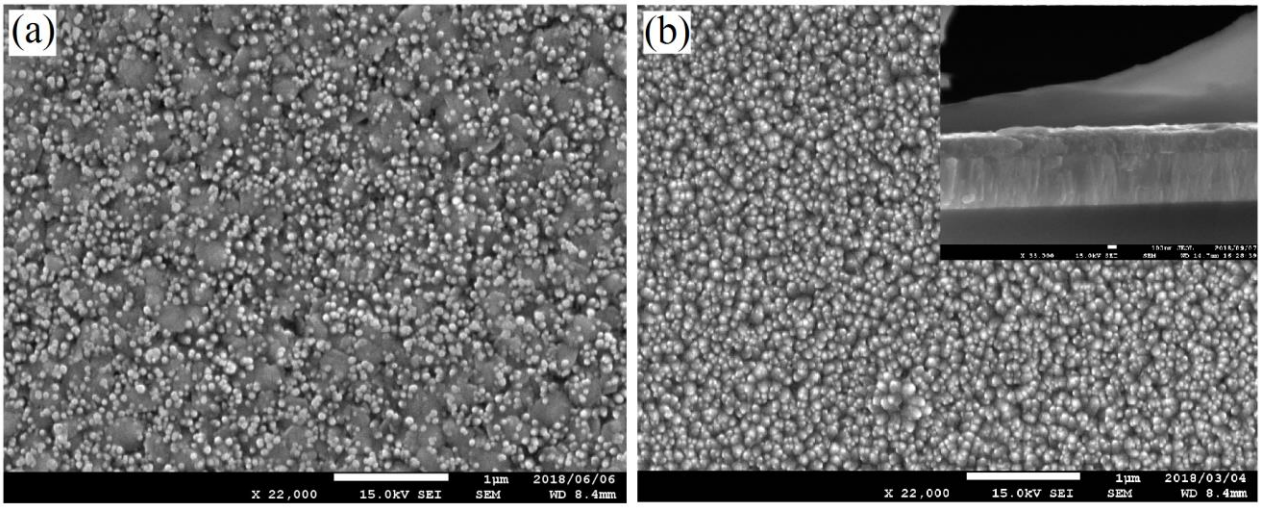

Fig. 4.9. FE-SEM images of, (a) Ga (400 ºC/2%) 45º sample, (b) Ga (400 ºC/2%) 30º sample.

The average top diameter was 36.99 nm, while length was ~230 nm and the average structure density was 230.4 per μm^2. The spray angle should be lower, to obtain good nanostructure by increasing the sweep of the atomized particle along the surface and grow freely. Vertical and horizontal velocities of particles play the major role deciding the nanostructure (see chapter 3.3). High nanostructure density at this spray angle affects the growth and it ends up with rice-shaped and linked nanostructure. Figure 4.10 shows the FE-SEM image of Ga doped ZnO samples at 15º of spraying angle with hexagonal shaped nanostructure. The average top diameter was 22.8 nm and the average structure density was 195.8 per μm^2 and the structure height is ~230 nm.

According to FE-SEM images, the sample prepared at 15º of spray angle, shows much favorable structure with respect to other samples.

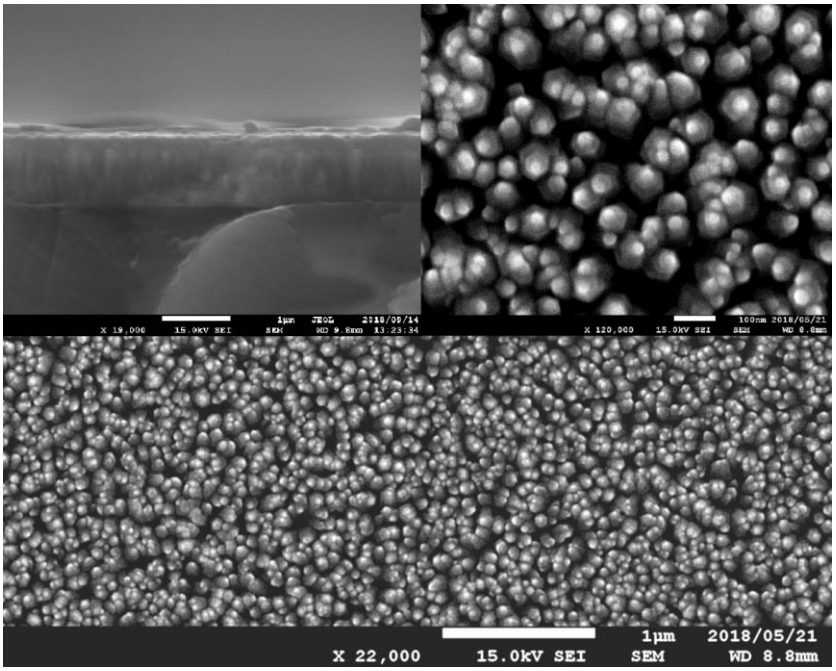

Fig. 4.10. FE-SEM images of Ga (400 ºC/2%) 15º sample.

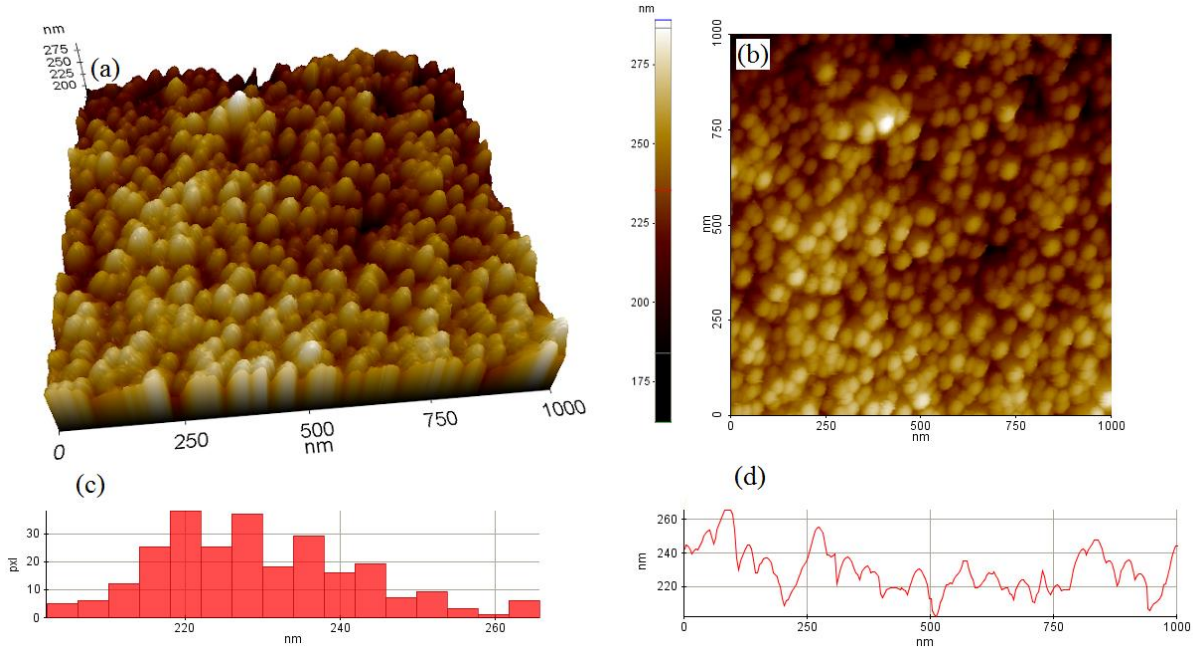

Fig.4.11. (a) 3D image, (b)Topographical image, (c) Line histogram, (d) Line profile, of Ga (400 ºC/2%) 15º sample.

Figure 4.11 shows the AFM images, line histogram and line profile of the Ga doped ZnO sample synthesized at 15º of spraying angle. The surface roughness and mean nanostructure height were obtained as 63.4 nm and 229.3 nm, respectively. Figure 4.12 shows the X-ray diffraction patterns of Ga doped ZnO grown at different spraying angles. Significant peak around 34.37º indicates the crystal structure was favored on (002) direction of hexagonal wurtzite ZnO phase (JCPDS card No. 36-1451) in all three spraying angles. All the other peaks, which are marked with "•" originate from the FTO glass substrate. Crystallite sizes were calculated by equation 1, as 21.6, 21.8 and 21.8 nm and FWHMs are 0.40, 0.39 and 0.39 for Ga (400 ºC/2%) 15º, Ga (400 ºC/2%) 30º and Ga (400 ºC/2%) 45º samples, respectively. There is no coherent change of crystallite size and FWHM values with the spray angles as the solution parameters kept same throughout the process.

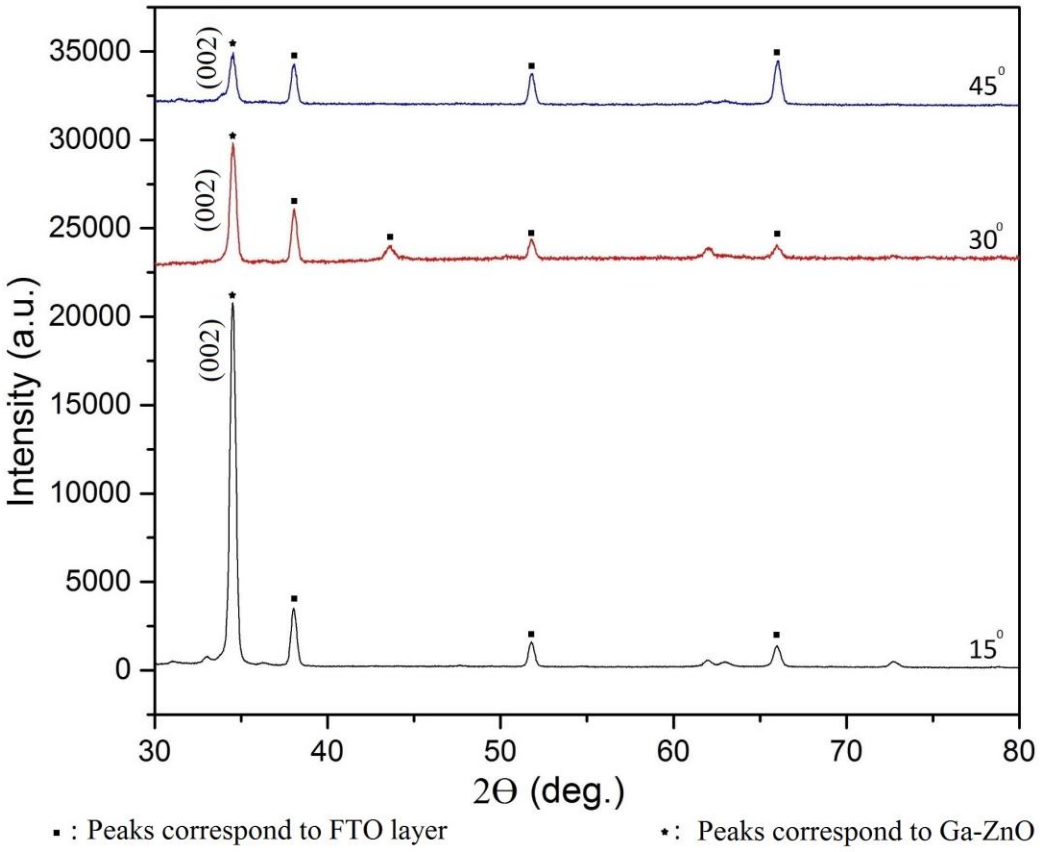

Fig. 4.12. XRD patterns of Ga doped ZnO thin films of each spray angles.

Figure 4.13 shows the obtained UV-visible spectra of Ga doped ZnO samples. The obtained optical transmittance in the visible range were 82%, 81%, and 79% in Ga (400 ºC/2%) 15º, Ga (400 ºC/2%) 30º, and Ga (400 ºC/2%) 45º samples, respectively. All the samples show a transmittance peak around 300 – 340 nm. The optical transmittance in the visible range of Ga (400 ºC/2%) 45º sample was decreased due to plate-like structure, which increased the light scattering. Figure 4.14 shows the Tauc plots which were graphed hv vs $(\alpha hv)^2$. Band gap of Ga (400 ºC/2%) 15º, Ga (400 ºC/2%) 30º and Ga (400 ºC/2%) 45º samples were 3.24 eV, 3.25 eV and 3.25 eV, respectively. The decease of optical transmittance at higher spraying angle might be because of the increase of scattering of photons due to crystal defects, as the optical band gaps are not significantly changed with the spraying angle.

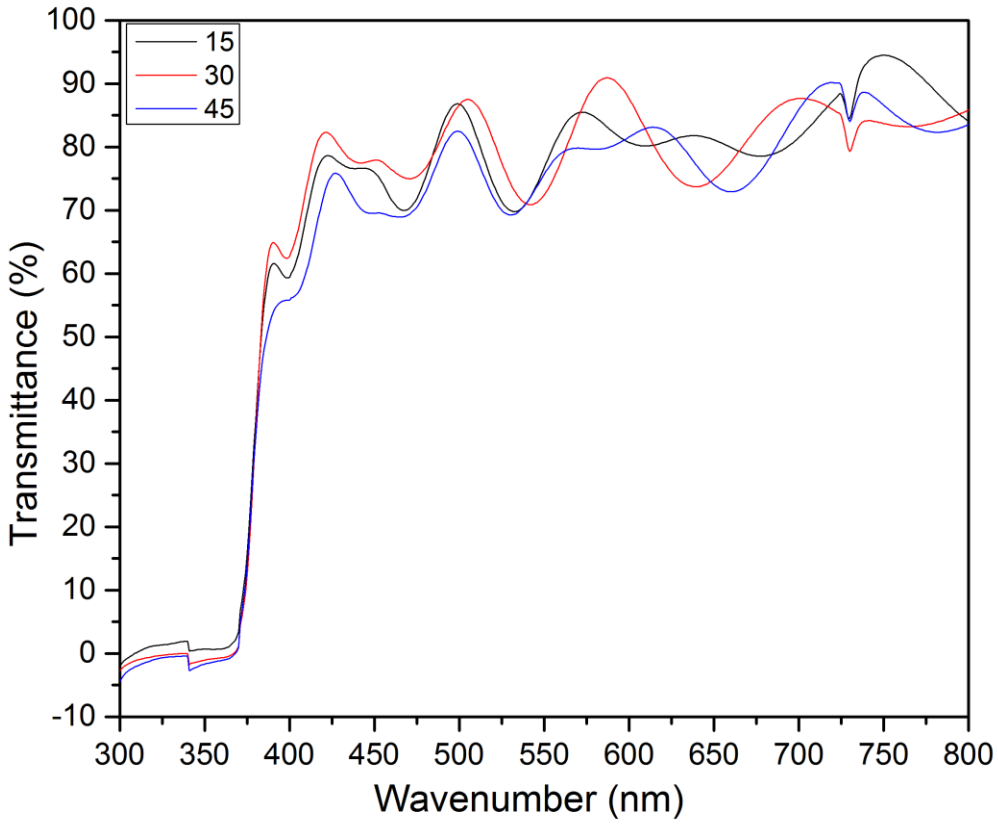

Fig. 4.13. UV-visible spectra of Ga doped ZnO thin films of each spray angle.

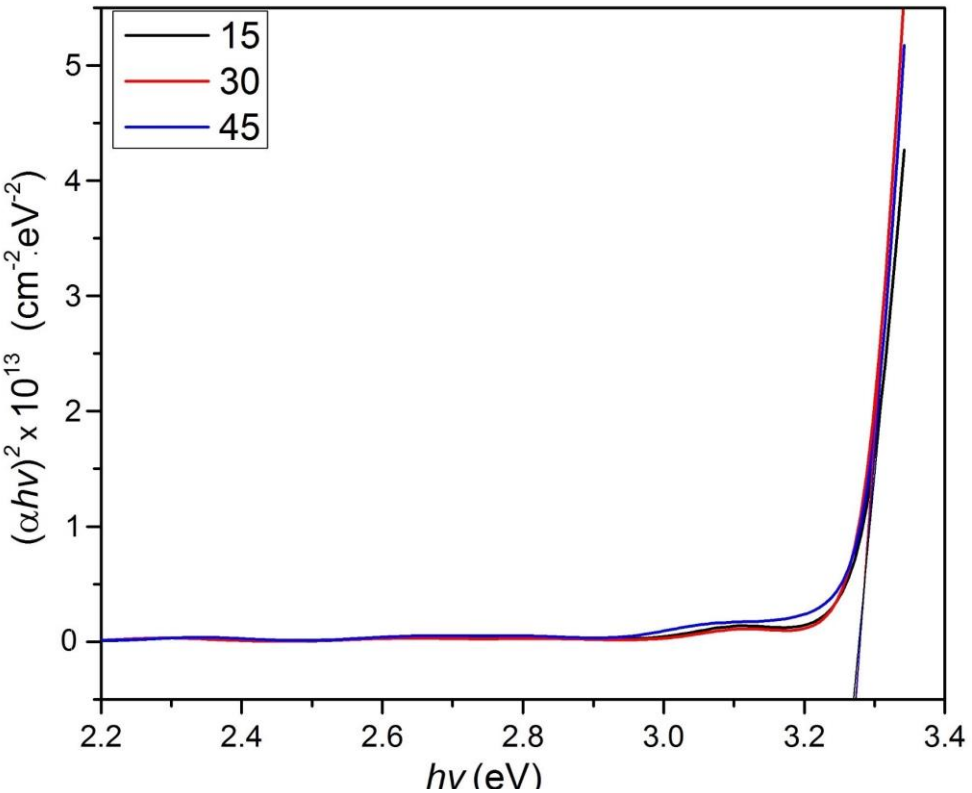

Fig. 4.14. Tauc plots of Ga doped ZnO thin films of each spray angle.

Table 4.4. Calculated crystal size, FWHM and E_g values for Ga doped ZnO thin films.

	Crystallite Size (nm)	FWHM	Optical band gap (eV)
Ga (400 ºC/2%) 15º	21.61	0.4018	3.24
Ga (400 ºC/2%) 30º	21.84	0.3976	3.25
Ga (400 ºC/2%) 45º	21.80	0.3983	3.25

The electrical conductivity of the Ga-doped ZnO samples were measured by using the four-probe method (as described in section 3.3.1). The resistivity values were 3.9×10^{-4}, 4.4×10^{-4}, and 4.2×10^{-4} Ω.cm for Ga (400 ºC/2%) 15º, Ga (400 ºC/2%) 30º, Ga (400 ºC/2%) 45º, samples respectively.

The lowest resistivity was observed by Ga (400 ºC/2%) 15º sample, while the highest resistivity was in Ga (400 ºC/2%) 30º sample. The utmost conductivity of Ga (400 ºC/2%) 15º sample was due to its' better orientation which confirmed by higher (002) peak broadening. On the other hand, Ga (400 ºC/2%) 45º sample showed lower conductivity as its' poor orientation which confirmed by lower (002) peak broadening.

Conclusion

We investigate the Ga doped ZnO thin films with 2 at % Ga doping grown at 400 ºC by using advanced spray pyrolysis deposition technique at different spraying angles. The average top diameter and the average structure density were 22.8 nm and 195.8 per μm^2, 37.0 nm and 230.4 per μm^2, 38.3 nm and 138.5 per μm^2, respectively for 15º, 30º and 45º spraying angles. The sample prepared at lowest spraying angle show, moderately high nanostructure density, low average top diameter and homogeneous structure with lower structural deformations with 63.4 nm of surface roughness. XRD patterns confirmed the growth of nanostructure was along the c-axis, perpendicular to the FTO substrate. The Highest optical transmittance of 81% at visible range was obtained at lower spraying angles. Higher spraying angles decreased the optical transmittance due to their structural defects, which increased the light scattering.

The band gap of samples was not significantly changed with the spray angle. The foremost electrical conductivity of $2.5 \times 10^3\ \Omega^{-1}.cm^{-1}$ as well as optimum optical transparency of 82 % at the visible range were observed at Ga doped ZnO sample, synthesized at 15° of spraying angle.

References

1. K. Park, Deok-Kyou Lee, Byung-Sung Kim, Haseok Jeon, Nae-Eung Lee, Dongmok Whang, Hoo-Jeong Lee, Youn Jea Kim, and Jong-Hyun Ahn, *Adv. Funct. Mater.* ***20***, 3577 (2010).
2. Erki Kärber, Taavi Raadik, Tatjana Dedova, Jüri Krustok, Arvo Mere, Valdek Mikli, Malle Krunks, Nanoscale Res. Lett. **6,** 359 (2011).
3. F.Z. Bediaa, A. Bedia, M. Aillerie, N. Maloufi, F. Genty, B. Benyoucef, Energy procedia **50** 853 (2014).
4. D.C. Look, Mater. Sci. Eng., B **80,** 383 (2001).
5. T. Prasada Rao, M.C. Santhosh Kumar, J ALLOY COMPD **506,** 788 (2010).
6. Chih-Hsiung Hsu and Dong-Hwang Chen, Nanotechnology **21**, 285603 (2010).
7. M. Ajili, N. Jebbari, N. Kamoun Turki, M. Castagné, EPJ Web of Conferences **29**, 2 (2012).
8. El Manouni, F.J. Manjón, M. Mollar, B. Marí, R. Gómezc, M.C. López, J.R. Ramos-Barrado, Superlattices Microstruct. **39**, 185 (2006).
9. R. Karmakar, S.K. Neogi, Aritra Banerjee, S. Bandyopadhyay, Appl Surf Sci. **263,** 671 (2012).
10. Charles Moditswe, Cosmas M. Muiva, Albert Juma, Optik **127**, 8317 (2016).
11. L.J. Mandalapu, F.X. Xiu, Z. Yang, J.L. Liu, Solid-State Elect ron., **51,** 1014 (2007).
12. S.J. Pearton, D.P. Norton, K. Ip, Y.W. Heo, T. Steiner, Prog. Mater. Sci. **50**, 293 (2005).
13. K. Yim, H. W. Kim and C. Lee, MATER SCI TECH-LOND, **23**, 108 (2007).
14. Doyoung Kim, Ilgu Yun, Hyungjun Kim, CURR APPL PHYS **10**, S459 (2010).
15. S. Fernández, J.J. Gandía, Thin Solid Films **520**, 4698 (2012).
16. P. Yang, H. Yang, S. Mao, R. Russo, J. Johnson, R. Saykally, N. Morris, J. Pham, R. He, and Heon-Jin Chang, Adv. Func. Mater. **12** [5], 323 (2002).

17. Hong Quang Le,z Swee Kuan Lim, Gregory Kia Liang Goh, Soo Jin Chua, and JunXiong Ong, J. Electrochem. Soc.**157** [8], H796 (2010).

18. G. A. Hirata et al, Thin Solid Films **288**, 29 (1996).

19. Jianhua Hu, Roy G. Gordon, J. Appl. Phys. **71** [2], 880 (1992).

20. Sanchez-Juareza, A. Tiburcio-Silverb, A. Ortizc, E.P. Zironid, J. Rickards, **333**, 196 (1998).

21. Yefan Chen, D. M. Bagnall, Hang-jun Koh, Ki-tae Park, Kenji Hiraga, Ziqiang Zhu, and Takafumi Yao, J. Appl. Phys. **84** [7], 3912 (1998).

22. R. Wendt, K. Ellmer, K. Wiesemann, J. Appl. Phys. **82** [5], 2115 (1997).

23. Jin Ma, Feng Ji, Hong-lei Ma, Shu-ying Li, Thin Solid Films **279**, 213 (1996).

24. W. Tang, D.C. Cameron, Thin Solid Films **238**, 83 (1994).

25. Shengwen Hou, Chaoyang Li, Thin Solid Films **605**, 37 (2016).

26. A.A. Yadav, M.A. Barote, E.U. Masumdar, SOLID STATE SCI **12,** 1173 (2010).

4.4 Ga doped ZnO nanostructure with using different volumes.

4.4.1 Introduction

Zinc oxide is gained the interest of researchers for many decades due to its' unique properties[1-10]. Doping of gallium into ZnO, helps to increase its' electrical conductivity and optical transparency in visible range[11-16]. In general, many researchers found several structures such as nanoflower, nanoplate, nanonails etc., when ZnO is doping with gallium., which could be used in many applications [16-28]. However, some researches have obtained nanocone structured impurity doped ZnO, due to their high light harvesting properties[29-30]. In this section we have increased the spraying volume of Ga doped ZnO, which was synthesized by using spray pyrolysis, to confirm the growth of terrace-truncated nanocone structure.

4.4.2 Experimental

Ga doped ZnO samples were fabricated as described in section 2.2. The sample nomenclature of prepared Ga doped ZnO samples with different volumes is shown in table 4.5.

Table 4.5. Spray volumes of Ga-doped ZnO samples

Sample	Growth Temperature (ºC)	Ga:Zn Ratio	Spraying Angle	Spraying Volume (ml)
Ga (400 ºC/ 2%/15º) 100	400	2:98	15º	100
Ga (400 ºC/ 2%/15º) 200	400	2:98	30º	200
Ga (400 ºC/ 2%/15º) 400	400	2:98	45º	400

X-ray diffraction patterns, field emission scanning electron microscope images and optical transmittance data were used to characterize the Ga doped ZnO samples as described in section 2.3.

4.4.1 Results and discussion

Figure 4.15 shows the obtained XRD images of Ga doped ZnO samples prepared with different spray volumes. Significant peak around 34.37º in all samples, shows the growth of nanostructure favoured in (002) direction of hexagonal wurtzite ZnO phase (JCPDS card No. 36-1451), which is along the c-axis, perpendicular to the substrate. All other peaks are for FTO layer. Figure 4.16 shows the FE-SEM image of Ga (400 ºC/ 2%/15º) 100 sample, which has hexagonal wurtzite nanostructure. The average top diameter is 22.8 nm and the average structure density was 195.8 per μm^2.

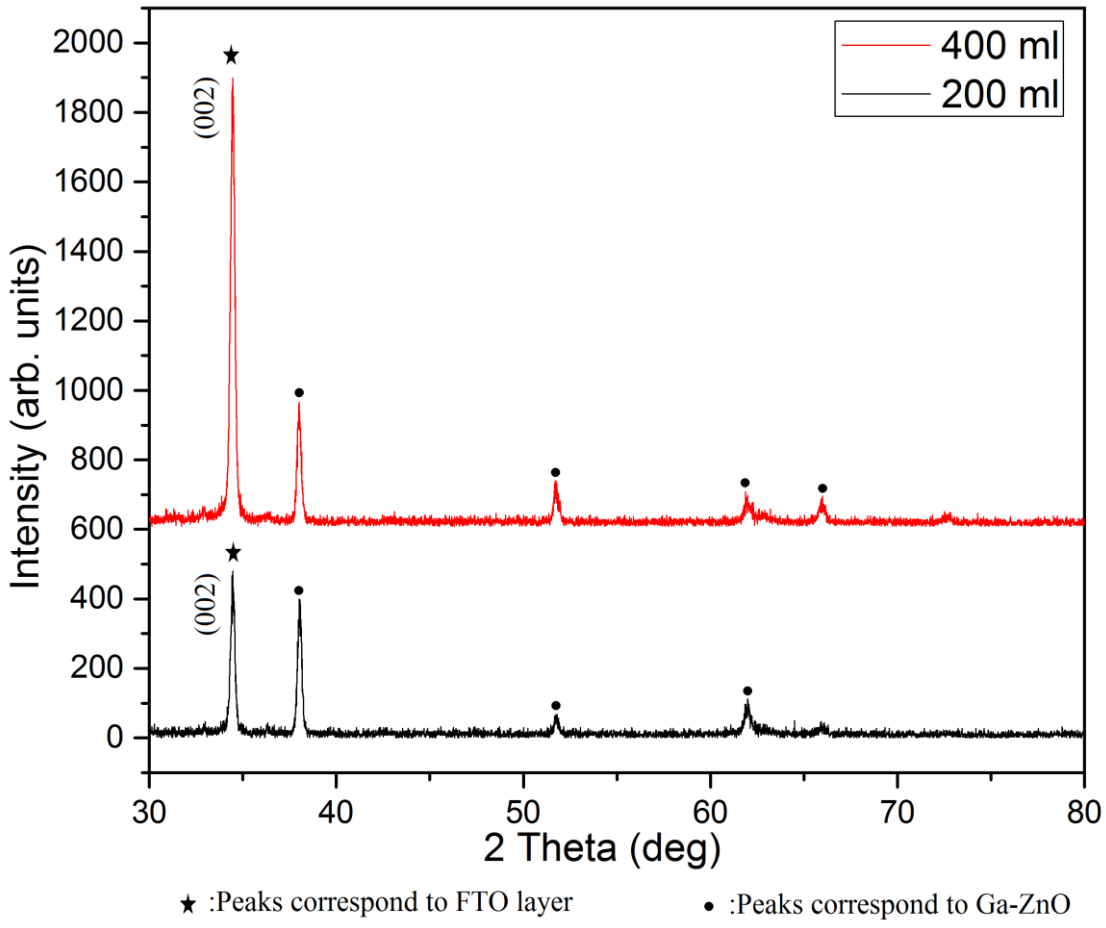

Fig. 4.15: X-ray diffraction pattern for Ga doped ZnO samples with different volumes.

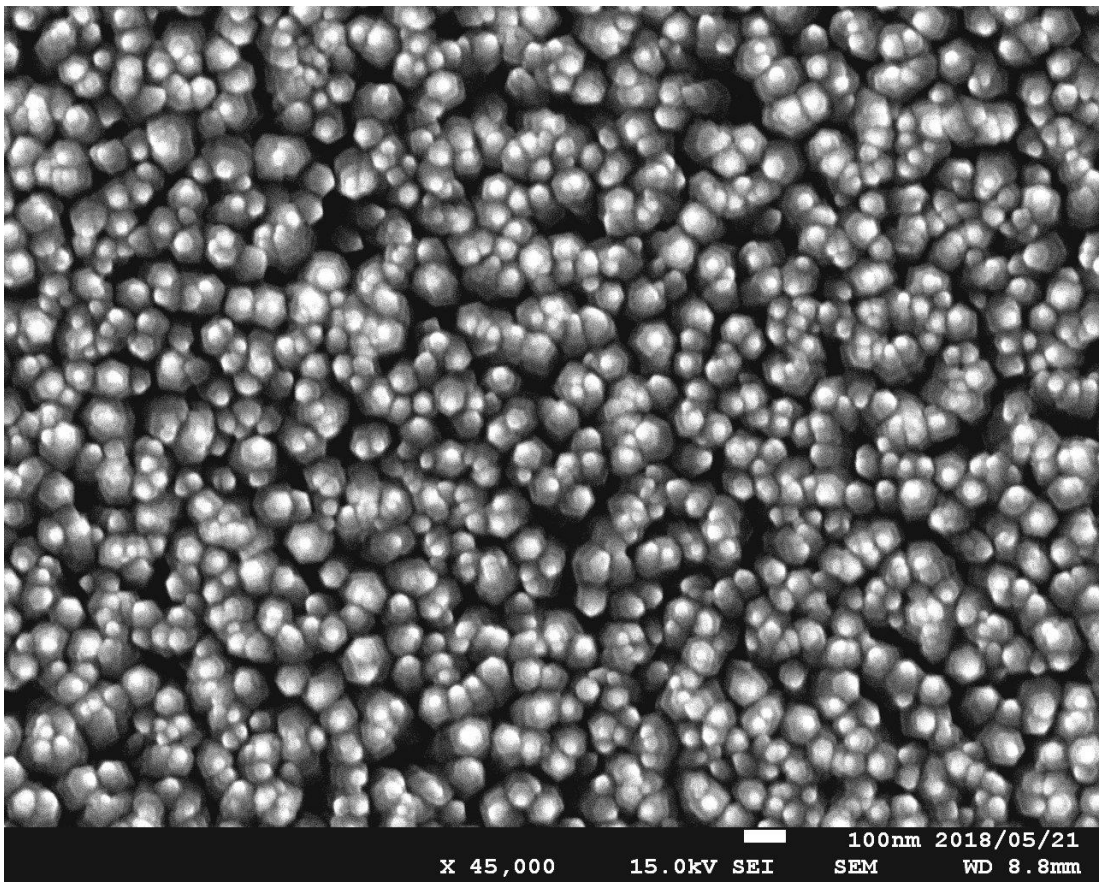

Fig. 4.16: FE-SEM image of Ga (400 ºC/ 2%/15º) 100 sample.

Figure 4.17 shows the FE-SEM image of Ga (400 ºC/ 2%/15º) 200 sample. An excellent nanostructure with average top diameter of 38.6 nm and an average structure density of 67.9 per μm^2 is observed. Obtained structures are well separated. Figure 4.18 shows the FE-SEM image of Ga (400 ºC/ 2%/15º) 400 sample. The average structure density was further reduced to 33.0 per μm^2. Well-aligned and well-separated nanostructure could be observed. The average top diameter was increased up to 58.5 nm.

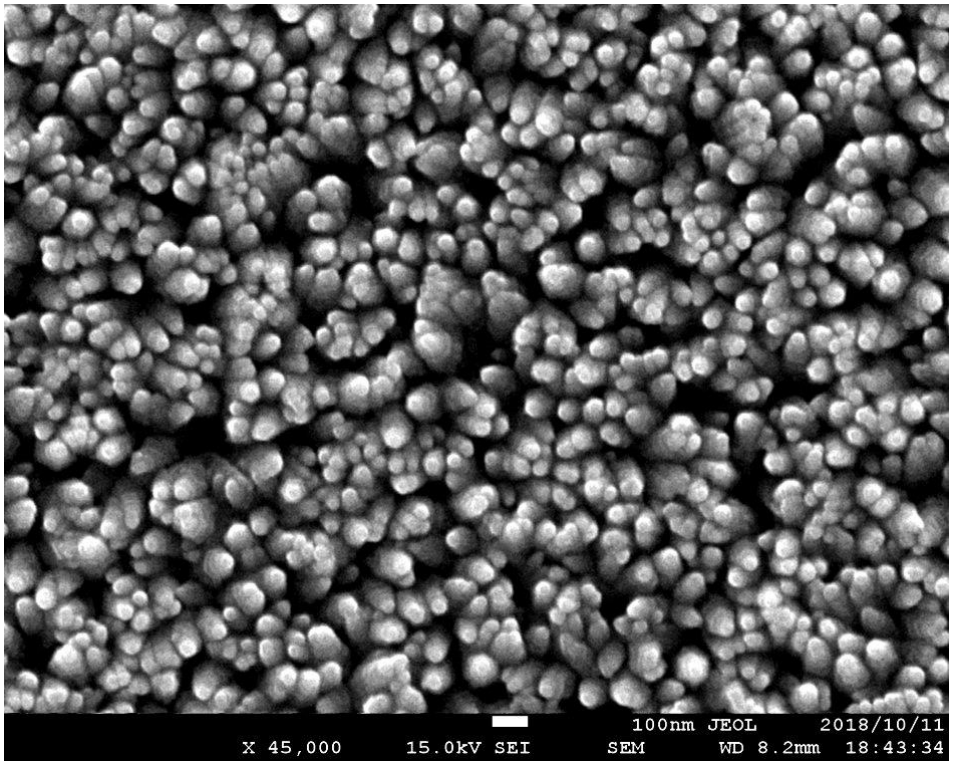

Fig. 4.17: FE-SEM image of Ga (400 ºC/ 2%/15º) 200 sample.

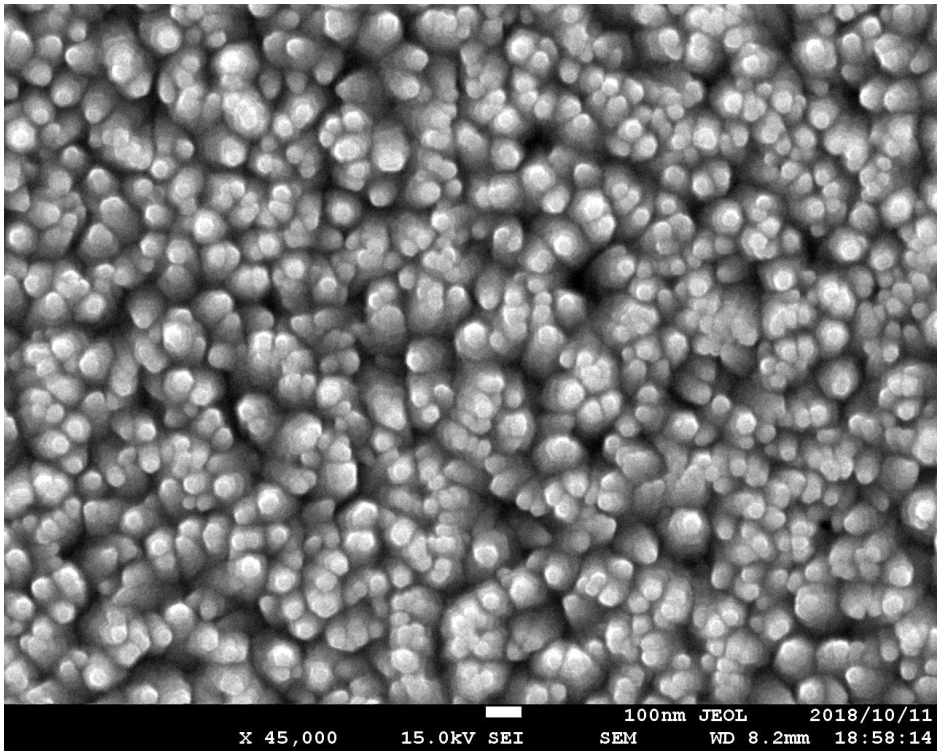

Fig. 4.18: FE-SEM image of Ga (400 ºC/ 2%/15º) 400 sample.

Fig. 4.19 shows the magnified FE-SEM image of Ga (400 ºC/ 2%/15º) 200 sample, which can see the terrace-truncated nanocone structure. As described in chapter 3.4, the high growth rate along the (002) direction leads to high decay rate in the same direction. As a result, Ga doped ZnO nanostructure end up with terrace-truncated nanocone as shown in fig 4.20. The thickness of the structure was 300 nm.

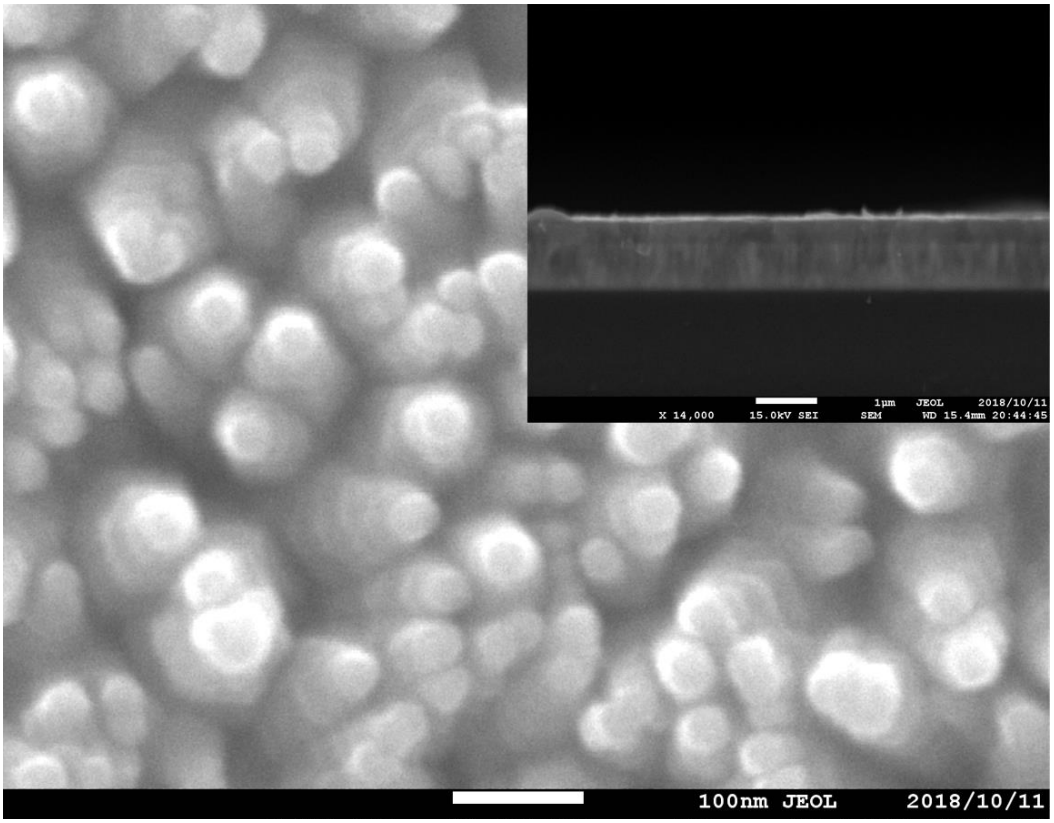

Fig. 4.19: Magnified FE-SEM image of Ga (400 ºC/ 2%/15º) 200 sample.

Fig. 4.20 show the magnified FE-SEM images of Ga (400 ºC/ 2%/15º) 400 sample. The terrace-truncated nanocone structure (*see chapter 3.4*) was identified with the thickness of 700 nm.

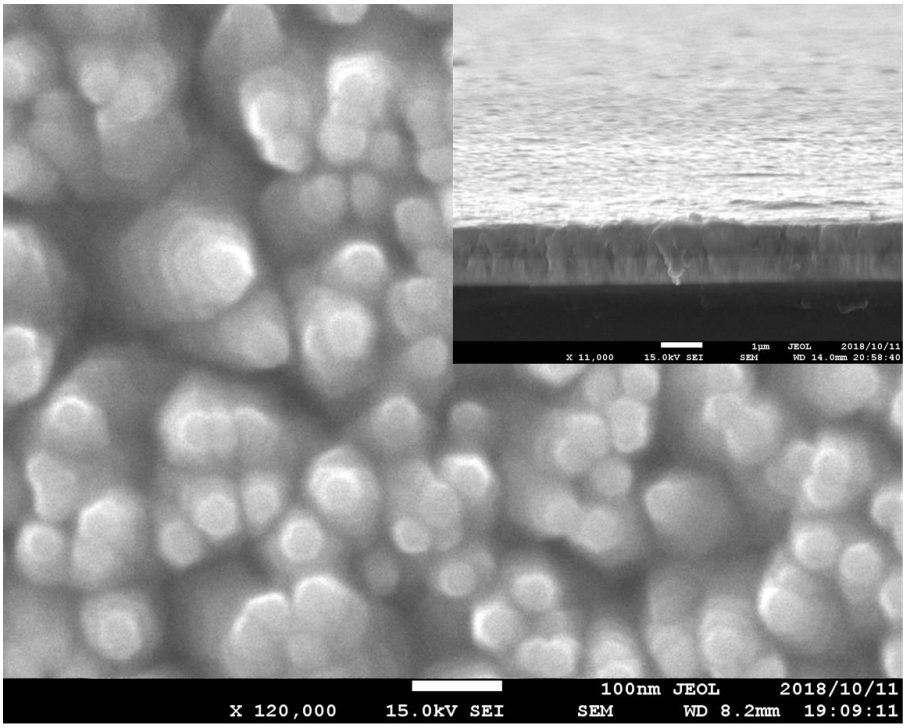

Fig. 4.20: Magnified FE-SEM image of Ga (400 ºC/ 2%/15º) 400 sample.

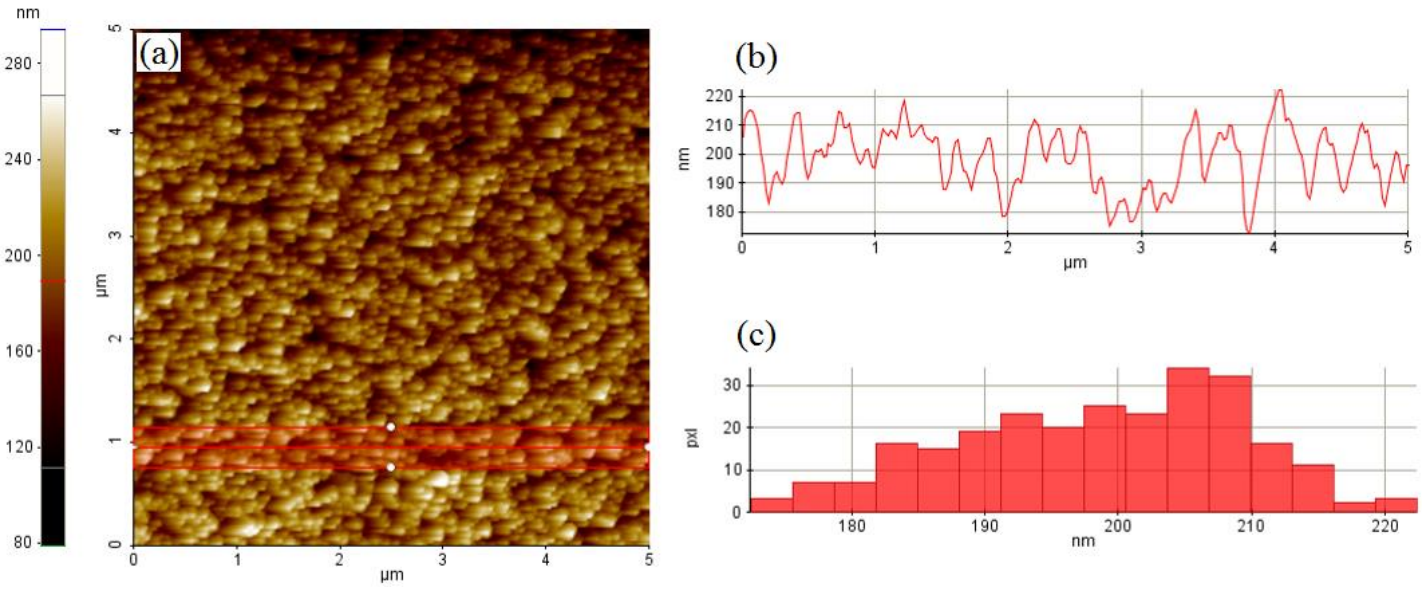

Fig. 4.21: (a) AFM image, (b) Line profile, (c) Line histogram, Ga (400 ºC/ 2%/15º) 200 sample.

The AFM images of Ga (400 ºC/ 2%/15º) 200 sample are shown in fig. 4.21. Surface roughness were 10.4, 8.8 nm for Ga (400 ºC/ 2%/15º) 100, Ga (400 ºC/ 2%/15º) 200, respectively. Figure 4.22 shows the optical transmittance of Ga doped ZnO with different volumes. The optical transmittance of the visible range was 80.5 %, 83.1 % and 82.0 % for Ga (400 ºC/ 2%/15º) 100, Ga (400 ºC/ 2%/15º) 200 and Ga (400 ºC/ 2%/15º) 400 samples, respectively. The light transparency is in the range of a typical transparent conductive oxide material. Optical transmittance can be increased by increasing the vertical alignment of nanostructure as there are few inclined terrace-truncated nanocone structure. The optical transmittance was not high as we expected, due to the two layered structure (FTO layer and the layer of Ga doped ZnO nanocone structure-*see fig. 3.26(a)*), as the photons are tended to scatter while propagating through each layer boundaries

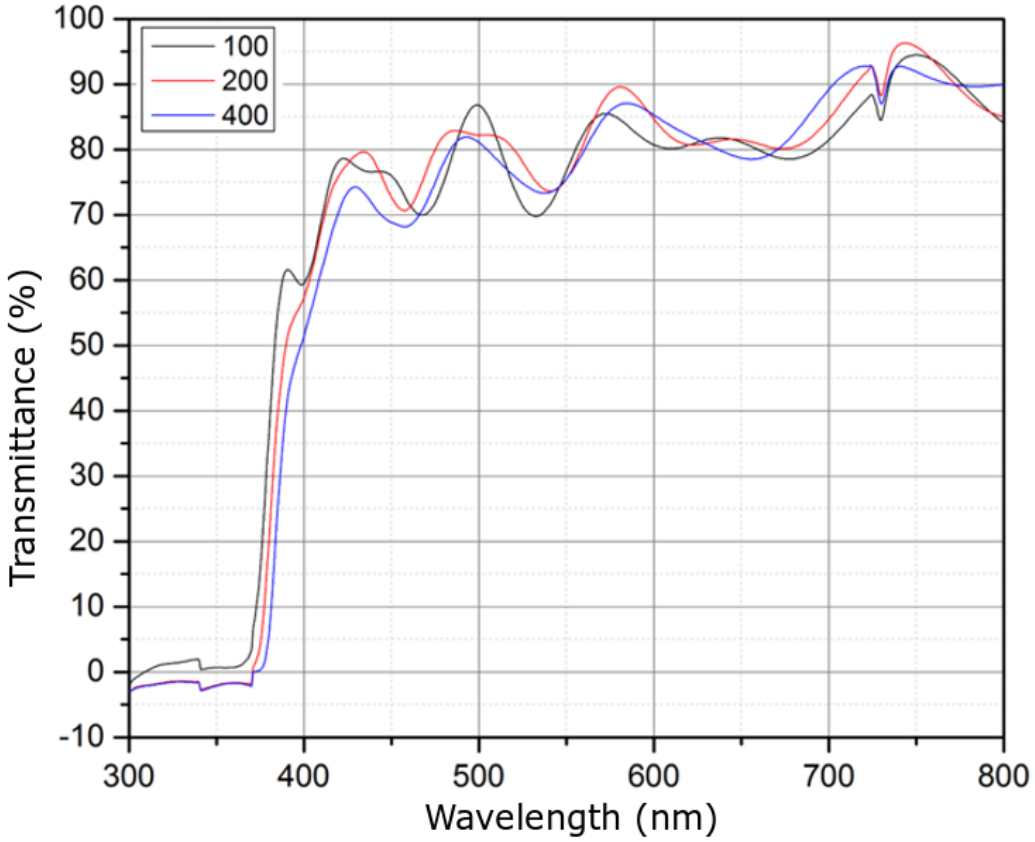

Fig. 4.22: Transmittance of the Ga-doped ZnO samples with different volumes.

Conclusion

Terrace-truncated nanocone structure Ga doped ZnO samples were successfully prepared at different volumes. The average diameter was 29.9, 38.6 and 58.5 nm for al doped ZnO sample with 100 ml, 200 ml and 400 ml, respectively. The average structure density values were decreased due to the reduction of average top diameter from 86.2, 67.9 and 33.0 per μm^2 for Ga doped ZnO samples with 100 ml, 200 ml and 400 ml samples, respectively. Terrace-truncated nanocone structure was formed as confirmed by FE-SEM images. Surface roughness were 10.37 nm, 8.76 nm for Ga doped ZnO samples with 100 ml and 200 ml respectively. The optical transmittance in the visible range were 80.5 %, 83.1 %, and 82.0 % for Ga doped sample with 100 ml, 200 ml and 400 ml, respectively. The optimum transparent conductive oxide properties were shown by Ga doped ZnO sample with volume of 200 ml.

Chapter 5

Conclusion

I have investigated Al doped ZnO and Ga doped ZnO Terrace-truncated nanocone structure by advanced spray pyrolysis deposition technique with rotational, pulsed and atomized functions. The optimum growth temperature for Al doped ZnO was investigated in the range of 300 to 450 ºC. The major structural differences were found when changing the growth temperature. The optimum growth temperature was decided to be 400 ºC for Al doped ZnO nanocone structure with 40 nm and 290.10 per μm^2 of average top diameter and average structure density, respectively. All samples at different growth temperatures showed ~80 % of optical transparency in the visible range. Al doping level was varied under four levels, from 1 at % to 4 at %, and excellent nanostructure with optimum transparency in the visible range and higher electrical properties were obtained at 2 at % of Al doping. The optical transparency was observed ~80% in the visible range. The spray angle is the crucial factor of deciding the properties of nanostructure in spray pyrolysis deposition technique. This value was investigated in three different values ~15º, ~30º and ~45º. An excellent nanostructure with good separation, lowest number of structural defects (agglomerated/plate like structures etc.) was observed at lower spraying angle of 15º. Moreover, the lowest resistivity of 1.05×10^{-4} Ω.cm and the highest optical transparency of 80.3 % in the visible range were observed in Al doped ZnO sample prepared at ~15º of spraying angle. The spraying volume was changed from 100, 200 and 400 ml to confirm the nanostructure. Terrace-truncated nanocone structure was confirmed at this stage of the research. High growth rate along the (002) direction which leads to the high decay rate in same direction and the structure is end up with nanocone structure. The rough edges of the crystal, leads to a terrace nanostructure. And finally ends up with terrace-truncated nanocone structure. The average top diameter and the height was increased when increasing the spraying volume.

In the case of Ga doped ZnO, I have succeeded to grow terrace-truncated nanocone structure by using advanced spray pyrolysis deposition technique. The deposition temperature was changed from 300 to 450 ºC. An excellent nanostructure of Ga doped ZnO was found at 400 ºC of growth temperature with 22.9 nm of diameter and 366 per μm^2 of an average structure density. Ga doping level was varied from 1 to 3 at %. The superior TCO properties was found when sample was doped with 2 at % of Ga doping, the average top diameter and the average structure density were 37 nm and 230.4 per μm^2, respectively. All the Ga doped ZnO samples with varied Ga to Zn ratio showed high optical transmittance in the visible range. The spray angle dependence for the growth of nanostructure and for optimum TCO properties were investigated in three different angles, which are 15º, 30º, and 45º. The ideal transparent conductive oxide properties with 82 % of optical transmittance in the visible range and 3.9×10^{-4} Ω.cm of lower resistivity was achieved at 15º of spraying angle. The average top diameter, the average structure density, and the film thickness were 22.8 nm, 195 per μm^2 and ~200 nm, respectively. Terrace-truncated nanocone structure was confirmed when increasing the spraying volume from 100, 200, and 400 ml. Film thickness was ~200, ~300 and ~700 nm for 100, 200, and 400 ml volumes, respectively. No relationship was found in between the dopant and the terrace-truncated nanocone structure. However, the effect of the dopant material for the growth of terrace-truncated nanocone structure needs further studies.

In this research I have succeeded to grow terrace-truncated nanocone structure of Al doped ZnO and Ga doped ZnO, separately. Moreover, I have proposed the growth mechanism of terrace-truncated nanocone structure as there was no proper study was done. Optimum TCO properties were obtained in the terrace-truncated nanocone structure prepared at 400 °C of temperature, 2:98 of impurity (Al or Ga) to Zn ratio and 15° of spraying angle.

List of Publications

Published Papers

1. Sameera Attanayake, Masuki Okuya, Kenji Murakami-(2019), Synthesis and characterization of Al-doped ZnO terrace-truncated nanocone structure by the advanced spray pyrolysis deposition technique, Japanese Journal of Applied Physics. Volume 58, 080904
2. Sameera Attanayake, Masuki Okuya, Kenji Murakami-(2020), Spray Angle Dependence for the Growth of Terrace-truncated Nanocone Structure of Gallium-doped Zinc Oxide by Advanced Spray Pyrolysis Deposition Technique. International Journal of Technology. Volume 11(1) 81-90
3. Sameera Attanayake, Kenji Murakami, Masayuki Okuya-(2018) Effect of spray angle on the properties of Al-doped ZnO 1-D nanorod array prepared by advanced spray pyrolysis deposition technique. J. chem. biol. phys. sci. 9 [1].

List of Conferences

1) Sameera Attanayake, Masuki Okuya, Kenji Murakami (2017), Synthesis and Characterization of ZnO and Al Doped ZnO Nanostructures by Using Advanced Spray Pyrolysis Deposition Technique, 64th Japan Society of Applied Physics Spring Meeting – Japan.
2) Sameera Attanayake, Masuki Okuya, Kenji Murakami (2017), Synthesis & Characterization of ZnO Nanostructures by Using Advanced Spray Pyrolysis Deposition Technique, International Symposium Toward the Future of Advanced Researches in Shizuoka University.
3) Sameera Attanayake, Masuki Okuya, Kenji Murakami (2017), Properties of ZnO & Al Doped ZnO Nanorod Structures by Using Advanced Spray Pyrolysis Deposition Technique of Rotational, Pulsed & Atomized, 4th International Conference on Nanoscience & Nanotechnology - SRM, India.
4) Sameera Attanayake, Masuki Okuya, Kenji Murakami (2017), Synthesis & Characterization of ZnO and Al Doped ZnO Nanostructures by Using Advanced Spray Pyrolysis Deposition Technique at Different Growth Temperatures, 78th Japan Society of Applied Physics Autumn Meeting – Japan.

5) Sameera Attanayake, Masuki Okuya, Kenji Murakami (2017), Synthesis & Characterization of Al Doped ZnO Nanostructures by Using Advanced Spray Pyrolysis Deposition Technique at Different Annealing Temperatures, The 34th International Japan-Korea seminar on Ceramics – Japan.
6) Sameera Attanayake, Masuki Okuya, Kenji Murakami (2017), Synthesis & Characterization of Al Doped ZnO Nano Rod Arrays by Using Advanced Spray Pyrolysis Method of Rotational, Pulsed and Atomized, The 19th Takayanagi Kenjiro Memorial Symposium – Japan.
7) Sameera Attanayake, Masuki Okuya, Kenji Murakami (2018), Synthesis & Characterization of Ga Doped ZnO Nanostructures by Using Advanced Spray Pyrolysis Deposition Technique of Rotational, Pulsed and Atomized. The 4th International Symposium toward the Future of Advanced Researches in Shizuoka University.
8) Sameera Attanayake, Masuki Okuya, Kenji Murakami (2018), Synthesis & Characterization Ga Doped ZnO 1-D Nanostructures by Using Advanced Spray Pyrolysis Deposition Technique of Rotational, Pulsed and Atomized, 65th Japan Society of Applied Physics Spring Meeting – Japan.
9) Sameera Attanayake, Masuki Okuya, Kenji Murakami (2018), Synthesis & Characterization of Ga Doped ZnO 1-D Nanostructures by Using Advanced Spray Pyrolysis Deposition Technique at Different Spraying Angles, 79th Japan Society of Applied Physics Autumn Meeting – Japan.
10) Sameera Attanayake, Masuki Okuya, Kenji Murakami (2018), Synthesis & Characterization of Impurity Doped ZnO 1-D nanostructure by Using Advanced spray Pyrolysis Deposition Technique of Rotational, Pulsed and Atomized, The International Conference on Global Research & Education Kaunas, Lithuania
11) Sameera Attanayake, Masuki Okuya, Kenji Murakami (2018), Synthesis & Characterization of Ga Doped ZnO Nano Rod Arrays by Using Advanced Spray Pyrolysis Method of Rotational, Pulsed and Atomized, 7th International Symposium on Transparent on Conductive Materials – Crete, Greece.